

1. Report No. FHWA/TX-90+556-2		2. Government Accession No.		3. Recipient's Catalog No.	
4. Title and Subtitle PRESTRESSED CONCRETE PAVEMENT: INSTRUMENTATION, IN-SITU BEHAVIOR, AND ANALYSIS				5. Report Date August 1989	
				6. Performing Organization Code	
7. Author(s) Elliott David Mandel, Ned H. Burns, and B. Frank McCullough				8. Performing Organization Report No. Research Report 556-2	
9. Performing Organization Name and Address Center for Transportation Research The University of Texas at Austin Austin, Texas 78712-1075				10. Work Unit No.	
				11. Contract or Grant No. Research Study 3-10-88/9-556	
				13. Type of Report and Period Covered Interim	
12. Sponsoring Agency Name and Address Texas State Department of Highways and Public Transportation; Transportation Planning Division P. O. Box 5051 Austin, Texas 78763-5051				14. Sponsoring Agency Code	
				15. Supplementary Notes Study conducted in cooperation with the U. S. Department of Transportation, Federal Highway Administration. Research Study Title: "Prestressed Concrete Pavement (PCP) Overlay IH35 in McLennan County"	
16. Abstract The long-term work plan at the initial design phase of the McLennan County prestressed concrete pavement (PCP) overlay consisted of the determination of variables that are relevant to design, the development of models and design procedures, and the study of the effect of environmental factors on PCP slabs. The present study focuses on the evaluation of the performance of PCP, with specific observation of horizontal slab displacements caused by changes in temperature. The behavior of the PCP is characterized by the presentation of a field data analysis. The instrumentation of the PCP slabs is described, graphs of measured displacements of the slabs for daily temperature cycles are presented, and a regression analysis of the slab movements is performed. In addition, a model that predicts both displacements and stresses is presented. The model is calibrated to the field data and is used to analyze stress concentrations in the slabs. Finally, conclusions and recommendations based on the instrumentation program, data analysis, and model are outlined.					
17. Key Words prestressed concrete pavement (PCP), variables, environmental factors, slab, displacements, temperature, stress, data analysis, instrumentation			18. Distribution Statement No restrictions. This document is available to the public through the National Technical Information Service, Springfield, Virginia 22161.		
19. Security Classif. (of this report) Unclassified		20. Security Classif. (of this page) Unclassified		21. No. of Pages 58	22. Price

**PRESTRESSED CONCRETE PAVEMENT:
INSTRUMENTATION, IN-SITU
BEHAVIOR, AND ANALYSIS**

by

Elliott David Mandel
Ned H. Burns
B. Frank McCullough

Research Report Number 556-2

Research Project 3-10-88/9-556

Prestressed Concrete Pavement (PCP) Overlay,
IH-35 in McLennan County

conducted for

**Texas State Department of Highways
and Public Transportation**

in cooperation with the

**U.S. Department of Transportation
Federal Highway Administration**

by the

CENTER FOR TRANSPORTATION RESEARCH

Bureau of Engineering Research
THE UNIVERSITY OF TEXAS AT AUSTIN

August 1989

The contents of this report reflect the views of the authors, who are responsible for the facts and the accuracy of the data presented herein. The contents do not necessarily reflect the official views or policies of the Federal Highway Administration. This report does not constitute a standard, specification, or regulation.

PREFACE

The report presents details of an instrumentation program that was carried out on the experimental PCP section in McLennan County. In addition, an analysis of horizontal slab movements is presented and used to characterize the expansion-contraction behavior of the slabs. Finally, an analytical model is developed and calibrated to the field data. The model is then used to investigate slab stresses.

This work is part of Research Project 556, "Prestressed Concrete Pavement (PCP) Overlay," conducted as a part of the overall research program at the Center for Transportation Research (CTR), Bureau of Engineering Research, The University of Texas at Austin. The work was sponsored by the Texas State Department of Highways and Public Transportation (SDHPT) and the

Federal Highway Administration under an agreement with The University of Texas at Austin and the Texas State Department of Highways and Public Transportation.

Thanks go to Carl Bertrand for assistance with data acquisition, Ken Hankins and Humberto Castedo for assistance with planning, and Jose A. Tena-Colunga for his help with data collection. Further thanks are extended to Dr. Luis M. Vargas-Lolá, Dr. John S. Tassoulas, and Mounir E. El-Mabsoot for their assistance with model development. Final thanks go to Lyn Gabbert for word processing and to Mary Mooney for assistance with graphics.

Elliott D. Mandel
Ned H. Burns
B. Frank McCullough

LIST OF REPORTS

Report No. 556-1, "Performance Tests on a Prestressed Concrete Pavement—Presentation of Data," by Elliott Mandel, Jose Tena-Colunga, and Kenneth Hankins, presents information found in the literature search, reviews the past parent project, and presents the volumetric, thermal, and deflection data collected in the subject project. November 1989.

Report No. 556-2, "Prestressed Concrete Pavement: Instrumentation, In-Situ Behavior, and Analysis," by

Elliott David Mandel, Ned H. Burns, and B. Frank McCullough, presents the instrumentation techniques used to collect field data, presents the final results of the horizontal displacement data, and addresses the accuracy and consistency of the data. The report then presents an analytical model for horizontal displacements and stresses, describes the calibration of the model, and shows the results of a parametric study using the model. August 1989.

ABSTRACT

The long-term work plan at the initial design phase of the McLennan County prestressed concrete pavement (PCP) overlay consisted of the determination of variables that are relevant to design, the development of models and design procedures, and the study of the effect of environmental factors on PCP slabs. The present study focuses on the evaluation of the performance of PCP, with specific observation of horizontal slab displacements caused by changes in temperature. The behavior of the PCP is characterized by the presentation of a field data analysis. The

instrumentation of the PCP slabs is described, graphs of measured displacements of the slabs for daily temperature cycles are presented, and a regression analysis of the slab movements is performed. In addition, a model that predicts both displacements and stresses is presented. The model is calibrated to the field data and is used to analyze stress concentrations in the slabs. Finally, conclusions and recommendations based on the instrumentation program, data analysis, and model are outlined.

SUMMARY

This report describes the instrumentation program for the McLennan County PCP in detail. The instrumentation techniques used to collect field data are presented. The objectives of the instrumentation program are outlined along with constraints on the method of data collection. The data collection equipment and methods of data acquisition are described. In addition, variables that affected the accuracy of the data and methods of error prevention are presented.

An analysis of the horizontal displacement data is performed. Final results of the horizontal displacement data are presented through average horizontal displacement curves. Results of a regression analysis of horizontal displacements are outlined and discussed. The consistency and accuracy of the data are then addressed.

An analytical model for the horizontal displacements of PCP slabs is developed. The background and theory of the model is described. Then, the computational operation of the model is outlined. The use of the model is presented along with user guidelines. The model is implemented in three studies: a study of internal accuracy of the model, calibration of the model to the collected field data, and a study of stress concentrations in the PCP slabs. Results and conclusions of the studies are presented.

Finally, conclusions are presented, followed by recommendations based on the instrumentation program and the field data analysis, and the model studies are outlined.

IMPLEMENTATION STATEMENT

This report describes the instrumentation program used for the McLennan County PCP. A field data analysis and the development and use of an analytical model for PCP are also presented. Maximum and minimum joint spacings for a wide range of temperatures are reported.

Rates of slab expansion and contraction are determined through analysis of the field data. The analytical model is used to analyze stress conditions in the slab.

The method of collection of field data was quite successful. The information presented in this report can be used as a guideline for future instrumentation programs. Field measurements that can be used for the design of

expansion joints for concrete pavements constructed on a polyethylene surface or for the calibration of other mathematical models are provided. The measurements indicate that the entire slab is moving for both 240 and 440-foot joint spacings. Therefore data for these two joint spacings may be interpolated or extrapolated for other joint spacings (assuming that the data are used for slabs where initial shrinkage and creep movements have already occurred). The computer program PCPFEL1 may be used to study special conditions such as blockouts or tendon anchor areas.

TABLE OF CONTENTS

PREFACE	iii
LIST OF REPORTS	iii
ABSTRACT	iii
SUMMARY	iv
IMPLEMENTATION STATEMENT.....	iv
 CHAPTER 1. INTRODUCTION	
Background.....	1
General Behavior.....	1
Volumetric Movement	1
Curling Movement.....	2
Previous Research.....	2
Objectives	3
Scope.....	3
 CHAPTER 2. INSTRUMENTATION	
Layout of the PCP.....	4
Previous Instrumentation.....	4
Current Instrumentation	5
Objectives and Scope.....	5
Field Visits.....	5
Limitations.....	6
Instrumentation Set-up	7
Measurement.....	7
Prevention of Error.....	9
 CHAPTER 3. DATA ANALYSIS	
Data Reduction.....	13
Behavior Analysis.....	13
Regression Analysis of Horizontal Displacements.....	15
Analysis of Joint Widths.....	17
Seasonal Slab Operation.....	18
Consistency and Error Analysis	18
Consistency Analysis.....	18
Error Analysis	19
Summary.....	22
Analysis.....	22
Design	22

CHAPTER 4. ANALYTICAL MODELLING	
Background.....	24
Model Development.....	25
Material Stiffness	25
The Finite Element Method for PCP	27
Program Operation.....	28
CHAPTER 5. MODEL IMPLEMENTATION	
Program PCPFEL1.....	31
User Interface	31
User Guidelines.....	31
Studies Using Program PCPFEL1	32
Mesh Fineness	32
Program Calibration.....	33
Stress Concentrations.....	34
Summary.....	35
CHAPTER 6. CONCLUSIONS AND RECOMMENDATIONS	
Instrumentation	39
Data Analysis.....	39
Modelling.....	40
REFERENCES.....	42
APPENDIX A. TABLE OF AVERAGE HORIZONTAL SLAB DISPLACEMENTS	43
APPENDIX B. GRAPHICS OF HORIZONTAL DISPLACEMENT VERSUS CONCRETE TEMPERATURE.....	46
APPENDIX C. DERIVATION OF MODEL FORMULATION.....	49

CHAPTER 1. INTRODUCTION

BACKGROUND

Prestressed Concrete Pavement (PCP) takes advantage of the high compressive strength of concrete in order to prevent or decrease tensile stresses during service. When a permanent horizontal compressive stress is introduced to a pavement slab during construction, its capacity to withstand traffic and environmental loads is increased. This compression of concrete slabs results in a potentially cost-efficient alternative to traditional pavements or pavement overlays.

The advantage of PCP over conventional concrete pavement is two-fold. First, it allows for the more efficient use of construction materials since the pavement thickness can be reduced due to increased flexural strength. It also allows for longer pavement slab lengths, therefore requiring fewer joints and less probability of cracking and reducing maintenance requirements. However, PCP also has disadvantages which are related to both construction and design. Most paving contractors are unfamiliar with prestressed concrete. Therefore bids for PCP construction are likely to be inflated in order to cover the cost of inexperience. Additionally, PCP is inherently more complex than traditional concrete pavement. Special friction reducing membranes and special grouting and jacking for prestress operations are generally required. Also, special joint hardware between PCP slabs is required in order to accommodate comparatively large thermal slab movements that result from the use of longer slab lengths. Finally, the application of pavement theory requires modification due to prestress and long slab lengths.

This study addresses applications of pavement theory by reporting the analysis of data collected from in situ PCP slabs. The data are used to characterize the behavior of the slabs due to environmental loads and to calibrate a model that predicts the behavior of PCP. The results of this study are offered as input to an ongoing process of understanding PCP for the purpose of refining the design process for its wider implementation.

General Behavior

All concrete pavements are subject to constant fluctuations in temperature due to daily and seasonal thermal cycles. These temperature changes cause individual pavement slabs to undergo two types of movements: volumetric and curling. Motion that is subjected to restraint at boundaries or gravity loads causes stress to develop in the concrete. The magnitudes of displacement and stress determine the behavior and ultimate serviceability of a pavement.

Volumetric Movement. Since PCP slabs are much longer than they are wide or thick, longitudinal expansion

and contraction are the most significant volumetric movements. Thermal expansion and contraction of pavement are restrained by frictional forces imparted by the subbase onto the bottom surface of a slab. When the slab expands, it is subjected to compressive stresses caused by the frictional resistance of the subbase. Similarly, when a slab contracts, it is subjected to tensile stresses. Because the inherent material properties of plain concrete provide high compressive strength but low tensile strength, contraction of a slab dictates whether it will crack due to a tensile stress that exceeds its tensile capacity. For slab movements that are symmetrical with respect to the longitudinal centerline, a long slab experiences a higher magnitude of tensile stress upon contraction than a short slab, since the stress accumulates from the ends of a slab to the middle. The amount of stress accumulation also depends on the frictional characteristics of the subbase; a smooth interface between the slab and the subbase provides less resistance than a rough one does, resulting in an increase in magnitude of longitudinal movement and a decrease in tensile stress. In PCP, the slabs are pre-compressed so that they can have longer lengths without suffering damage from tensile stresses. Figure 1.1 illustrates the effect of

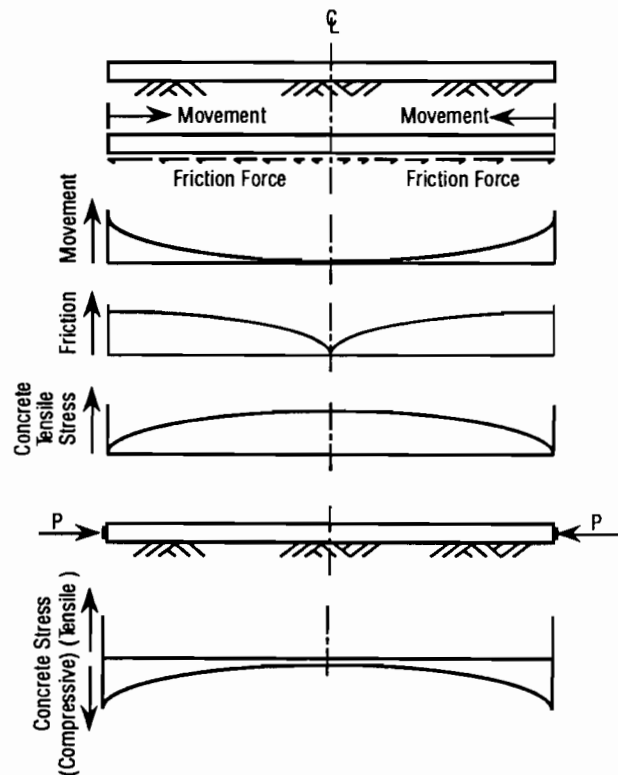


Fig 1.1. The effect of subbase frictional restraint on the stress in a concrete slab for a temperature decrease and the additional effect of pre-compression by force P.

subbase frictional restraint on the tensile stress in a pavement slab, and the combined effect of friction and pre-compression on slab stresses.

The characterization of expansion and contraction displacements of PCP slabs allows for the formulation of some important design limits. For a specific slab length and subbase frictional medium, horizontal displacements will always fluctuate within the limits defined by extreme ambient temperatures. It is important to determine these limits so that joints between PCP slabs will not become too wide (affecting the riding quality of the pavement) and so that joints will not ever completely close (preventing expansion, possibly causing compression failure of the concrete, buckling of the slab, or damage to joint hardware). It is also important to determine the characteristics of daily slab displacement cycles in order to verify and calibrate design and analysis models used to predict the slab movements.

Curling Movement. Temperature gradients across the thickness of the pavement resulting from a time-lag effect of heat transfer from the top surface to lower regions in the slabs cause curling movements. When the ambient temperature increases, the top region of a slab experiences a more rapid increase in temperature than the bottom region. This effect causes the top region to undergo a more rapid volumetric increase than the bottom region. Similarly, when the ambient temperature decreases, the top region experiences a more rapid volumetric decrease than the bottom region. The differential in volumetric deformation through the thickness of the pavement causes the slabs to curl vertically. This movement of the slabs fluctuates constantly as the temperature gradient across the thickness of the slab changes, reversing the direction of induced curling movement.

The stresses that result from curling movements are caused by flexural forces developed from slab weight. The stresses occur in regions where the curling causes the most vertical movement, which, for a normal slab on-grade, is near the corners. When the slab curls up at the corners, moments due to the self-weight of the slab (or due to any superimposed load) cause tensile stress in the top of the slab. Similarly, when the slab curls down at the corners, tensile stress develops in the bottom of the slab. If the tensile stress in either case is greater than the tensile capacity of the concrete, a corner-break will occur. For long pavement slabs, curling movements can be large, causing significant tensile stress in the concrete. In addition, large curling movements can cause the slab to pull away from the subbase; if enough separation occurs, repetitive traffic loads can cause pumping of material from beneath the slab, resulting in large voids under the pavement.

Previous Research

The present study on the behavior of PCP is an extension of previous research conducted at The University of Texas at Austin from 1984 to 1987. A series of conceptual and experimental investigations into the design and implementation of PCP were carried out during that time. These studies examined several separate aspects of PCP, including the application of special prestressing techniques, the evaluation of projected in-situ parameters, and the formulation of design procedures. The research provided information required for the design, construction, and early-life instrumentation of a one-mile experimental prototype section of a PCP overlay located in McLennan County, on the southbound lane of Interstate Highway 35, about 15 miles north of Waco. The following paragraphs review the general results of the investigations.

A literature review was performed along with an evaluation of concept and performance of several previous prestressed pavement projects sponsored by the Federal Highway Administration. The collected information was used to develop design and construction details and procedures for the experimental pavement near Waco. In addition, several new PCP construction concepts were introduced which addressed problems encountered on previous projects and were intended to improve constructability and performance on future projects (Ref 4).

An investigation into very early post-tensioning of concrete was conducted to examine the possibility of preventing temperature and shrinkage cracks in long PCP slabs during the first night after placement. Experiments on the capacity of the anchorage zone in slabs were performed considering slab thickness, tendon spacing, anchor size, and time from placement as test variables. Results of the tests indicated that partial post-tensioning can be applied to concrete pavement within 12 to 24 hours of placement. A recommended post-tensioning table was presented along with design aids (Ref 3). The later use of the recommendations for the actual construction of the McLennan County overlay was quite successful.

Experiments were performed to determine the amount of initial prestressing that is lost along the length of unbonded tendons. Prestress losses were measured for different arrangements of tendons and were used to predict losses in actual PCP. The experimental losses were then compared to actual losses that were experienced in the McLennan County overlay (Ref 8).

An experimental study was carried out to evaluate the effectiveness of using polyethylene sheeting in reducing friction at the interface of a concrete overlay on an asphalt base. The maximum coefficient of friction for single and double layers of the sheeting was determined through

push-off tests carried out over a one-year period in varying seasonal conditions. Conclusions of the study indicated that a single layer of sheeting is adequate for reducing base friction enough to prevent detrimental tensile stress in PCP slabs (Ref 7).

An instrumentation program was conducted for the McLennan County overlay for the purpose of measuring early-life behavior of the PCP slabs. The program included the continuous measurement of ambient and concrete temperatures, horizontal slab movements, slab curling movements, concrete strains, and joint widths. Additional data were collected on tendon elongation, very early concrete strength and modulus of elasticity, and slab cracking (Ref 6).

A design methodology for PCP that incorporates procedures for determining slab thickness, prestress level, and slab length was presented. In addition, a computer model that uses a finite difference procedure to focus on slab length changes and longitudinal stresses in PCP as a result of changes in concrete temperature and base-friction was developed. The information generated by the computer model was then compared to measured short-term responses from the McLennan County PCP overlay (Ref 5).

A series of regression analyses carried out on data from both the Portland Cement Association and from The University of Texas at Austin test program on fatigue of prestressed concrete beams were performed. Investigations included studies of the effect of prestress on the fatigue life of concrete, the interaction of prestress and stress due to vehicular loading, the effect of prestress in delaying microcracking in concrete, and the effect of prestress on elasto-plastic behavior of prestressed concrete. General conclusions of the study address whether current fatigue design procedure is appropriate for prestressed concrete and whether the superposition of prestress and stress due to vehicular loads is valid (Ref 9).

OBJECTIVES

This report describes part of the field work performed on the McLennan County PCP overlay from July 1988 to February 1989, as well as analytical work performed subsequently. The goals of the work were

- (1) to determine the displacement characteristics of the McLennan County PCP slabs through the collection of field data,
- (2) to use the collected field data to calibrate an analytical model, and
- (3) to formulate design recommendations for PCP based on the collected data and results obtained from the analytical model.

SCOPE

This report describes the instrumentation techniques used to collect field data, presents the final results of the horizontal displacement data, and addresses the accuracy and consistency of the data. It then presents an analytical model for horizontal displacements and stresses, describes the calibration of the model to the collected field data, and shows the results of a study using the model. Finally, recommendations for design based on the data and the study are presented. A compilation of all field data collected, an analysis of vertical displacement data, a mechanistic analysis of the McLennan County PCP, and a description of the calibration of previous PCP models are not covered in this report, but a complete presentation of these topics can be found in Refs 1 and 2.

The order of presentation of the topics covered in this report is as follows:

- (1) **Chapter 2.** The general layout of the McLennan County PCP is presented, and previous instrumentation of the slabs is described. The objectives of the instrumentation program carried out for this study are outlined along with constraints on the methods of data collection. The data collection equipment and methods of data acquisition are described. Finally, variables that affected the accuracy of the data and methods of error prevention are presented.
- (2) **Chapter 3.** Average horizontal displacement curves for the PCP are presented. Results of a regression analysis of horizontal displacements are outlined and discussed. The consistency and accuracy of the data are then addressed.
- (3) **Chapter 4.** The background and theory of an analytical model for PCP is described. Features of the model that reflect specific aspects of the construction of the McLennan County PCP overlay are presented. The computational operation of the model is then outlined.
- (4) **Chapter 5.** The use of the model presented in Chapter 4 is described, along with user guidelines. The model is implemented in three studies. Results and conclusions of the studies are presented.
- (5) **Chapter 6.** Conclusions of this report are presented. Finally, recommendations based on the instrumentation program, the field data, and the results of the studies in Chapter 5 are outlined.

the data was recorded manually. In general, the instrumentation scheme was successful, despite an unfortunate loss of one segment of data due to an error in the acquisition system. All methods of measurement, except for the use of strain gages to measure daily cyclic changes in concrete strain or to measure transverse strains due to transverse post-tensioning, were determined to be successful.

CURRENT INSTRUMENTATION

A second instrumentation program for the McLennan County PCP was carried out in order to monitor movements of the slabs after changes in the material properties of the concrete had stabilized and after shrinkage and creep effects were essentially complete. Information collected in this instrumentation program was to be used to characterize the long-term behavior of the PCP. The descriptive information in the following sections is based on Refs 15, 16, and 17.

Objectives and Scope

The purpose of the present instrumentation program was to evaluate the response of the McLennan County PCP to daily temperature cycles for a variety of extreme seasonal conditions. Information about daily horizontal and vertical slab movements was used to calibrate both the computer model presented in this document and the model presented in Ref 5. Information collected during extreme seasonal conditions was used to compare the behavior of the slabs under different moisture conditions, and to establish boundaries on the joint movements of the slabs for a large range of temperatures.

The following points outline the basic objectives of the instrumentation program:

- (1) to determine the magnitude of longitudinal slab movements due to daily temperature cycles, for different moisture conditions, and to correlate them with the mid-depth temperature of the slabs;
- (2) to determine the magnitude of curling slab movements due to daily temperature cycles, for different moisture conditions, and to correlate them with the change in temperature gradient across the slabs' thickness; and
- (3) to determine the magnitude of changes in joint opening between slabs for a maximum range of mid-depth slab temperatures.

Several differences exist between this instrumentation program and the previous instrumentation program. The present program took place several years after construction of the pavement. Therefore,

data collection for the purpose of evaluating phenomena that are active only during the construction or the early-life phase of the pavement is not applicable. This precludes the collection of tendon stressing data (the tendons are inaccessible) and creep and shrinkage data (assuming that most creep and shrinkage movements of the slabs have already occurred). Furthermore, the measurement of concrete strains for the present instrumentation program was considered to be unnecessary since slab displacements rather than concrete strains are a primary design criterion for PCP. In addition, the computer models give slab displacements as output and, therefore, were to be calibrated with measured displacements.

Field Visits

Work performed at the McLennan County PCP site included site surveys, preliminary measurements, installation of instrumentation equipment, and data collection. Data collection took place from July 1988 to February 1989. During that time span, a total of 6 field visits to the PCP were made. The field visits took place under different conditions of moisture and ambient temperature: three during hot and dry conditions, one during mild and dry conditions, and two during cold and wet conditions. Also, one additional trip to the PCP was made during extremely cold conditions for the purpose of measuring maximum joint openings. Table 2.1 outlines the data collection field visits and the additional trip. A site survey (Ref 1) was conducted during the first field visit, so it is not included on the table. The duration of all data collection periods was 24 hours, with the exception of the sixth field visit, which lasted 48 hours.

This array of weather conditions covers a maximum range of temperatures that occur at the site. It is difficult to evaluate whether the wet moisture conditions can be considered as the extreme conditions; 1988 was a drought year with almost no precipitation from July to December. The conditions described as "wet" in Table 2.1 were moist from rains that occurred one to two days prior to data collection.

TABLE 2.1. DATA COLLECTION FIELD VISITS

Field Visit	Date	Maximum Ambient Temperature (°F)	Minimum Ambient Temperature (°F)	Weather Condition
2	July 26, 1988	107.13	74.80	Hot, Dry
3	August 6, 1988	104.00	75.85	Hot, Dry
4	August 26, 1988	107.87	71.28	Hot, Dry
5	November 5, 1988	84.00	41.72	Mild, Dry
6	January 21, 1989	64.22	27.39	Cold, Wet
Additional	February 4, 1989	—	17.60	Cold
7	February 9, 1989	62.87	30.90	Cold, Wet

Limitations

Since calibration of the computer models was to be one of the primary outcomes of the present instrumentation program, it was important to establish the best statistical base for data collection. This meant that the maximum number of slabs possible had to be instrumented and that there had to be consistency in the types of measurements taken for each data collection period. Several constraints limited the number of slabs that could be instrumented. Other constraints limited the method in which data could be collected. The following points outline the constraints that had an effect on devising an instrumentation program:

- (1) Economic constraints did not allow for traffic control for all data-collection field visits. Therefore, all instrumentation had to be conducted at the edge of the slabs.
- (2) The maximum LVDT cable length that could be used without introducing electrical resistance errors, or without using pre-amplified circuitry, was 100 feet. Since the length of the PCP slabs is either 240 feet or 440 feet, it was impossible to instrument more than one joint with LVDT's at any one time.
- (3) An automatic data acquisition system was used to collect both magnitudes of slab movement from LVDT's, as well as slab temperatures from thermocouples (drilled and grouted into the PCP slabs). Due to the cable length restriction mentioned in (2), the joint that was to be instrumented with LVDT's had to be the same for all field visits, since the locations of the thermocouples were fixed.
- (4) The number of LVDT's available for data collection was 6. Therefore, dial gages were used in addition to LVDT's. The number of dial gages available for each data collection period was 26.
- (5) Manpower was limited to two or three personnel for each field visit. This affected the number and proximity of slabs that could be instrumented with dial gages, since data collected from these slabs had to be continuously collected manually.

In response to (1), slab movements were measured from the edge of the outside shoulder of the pavement. Concrete "dead-man" anchors were buried and used to support dial gages or LVDT's. Steel angles were fixed to the sides of the slabs to act as a reaction-stop for dial gage or LVDT plunger-pins measuring longitudinal slab movements. Plastic receptacles were attached to the tops of the slabs to act as a reaction-stop for dial gage or LVDT plunger-pins measuring vertical curling slab movements. A more complete description of the equipment can be found in the section on instrumentation set-up.

In response to (2) and (3), Joint 10 (Fig 2.1) was chosen to be instrumented with LVDT's so that data could be collected automatically from one end of a 240-foot and a 440-foot slab simultaneously. Thermocouples were drilled and grouted into the slab adjacent to Joint 10

on the south side, about 15 feet south of the joint and about 5 feet from the west edge of the slab. Figure 2.2 shows the thermocouples inserted into the pavement, and Fig 2.3 shows the locations and depths of the thermocouples. An additional thermocouple was placed in the shade to measure the ambient temperature.

In response to (4) and (5), slabs that were symmetrically adjacent to Joint 10 were chosen for instrumentation. This was considered to be an acceptable approach from an experimental standpoint since it had been previously determined that all slabs of each length, 240 feet and 440 feet, in the entire experimental section had generally similar expansion and contraction characteristics. Therefore, these characteristics would not have to be considered as criteria for the selection of slabs to be instrumented (Ref 1). Dial gages were manually read every two

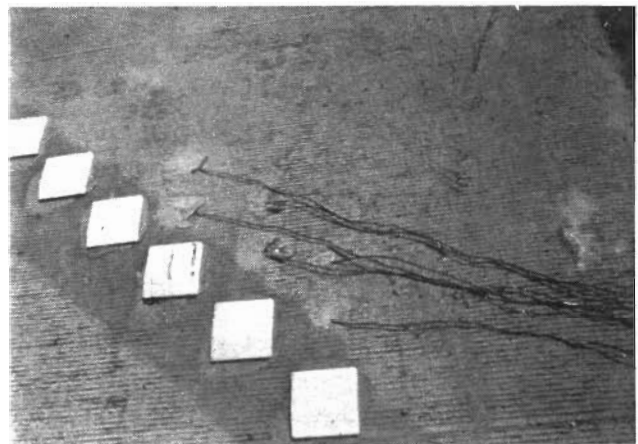


Fig 2.2. Thermocouples inserted into the pavement near Joint 10.

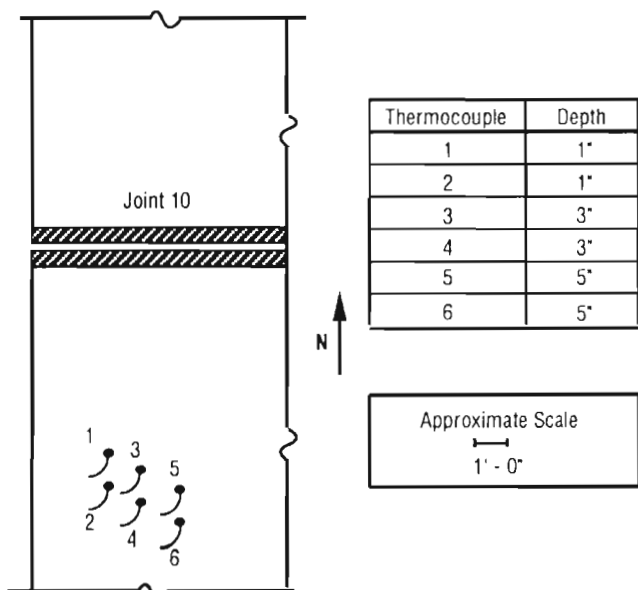


Fig 2.3. Thermocouple locations at Joint 10.

hours (this time interval was adequate to determine the necessary trends in the data and to calibrate the computer models). Furthermore, the maximum number of adjacent slabs from which data could be collected by one person in a two-hour period was six. This was because, in every two-hour period, all dial gages were read (and adjusted if necessary), joint widths were measured, the tank of a gasoline generator that powered the data acquisition system was filled, and the engine of the supply vehicle was run in order to recharge its battery (warning lights were run off this battery at night). In addition, with the given availability of dial gages, six was the maximum number of slabs that could be adequately instrumented. The locations and details of the six slabs selected are described in the section on measurement.

Instrumentation Set-up

Concrete “dead-man” anchors were used to support dial gages and LVDT’s. The anchors consisted of typical 6-inch x 12-inch concrete cylinders with embedded threaded inserts that receive 7/8-inch threaded dowels. Two inserts were installed just in case one failed to function. Rubber stoppers were used to protect the inserts when they were not in use. Figure 2.4 shows the construction of the dead-man anchors in detail. The anchors were inserted into the soil, levelled, and secured into place with concrete about 18 inches from the west edge of the slabs. Then, for each field visit, a vertical dowel with a threaded end was screwed into each anchor, and horizontal dowels, onto which dial gages or LVDT’s were secured, were attached to the verticals with 90° dowel clamps. This type of set-up allowed for the temporary fabrication of instrumentation supports at the work site and for their removal after data collection was completed for each field visit.

Steel angles (3 inches x 3 inches x 3/8 inch) were bolted onto lead inserts that were drilled and epoxied onto the edges of the slabs; as mentioned earlier, the angles served as reaction-stops for the dial gage or LVDT plunger-pins. Plastic receptacles were used to provide smooth and level surfaces for the plunger-pins of the dial gages or LVDT’s that were measuring curling slab movements. Each receptacle consisted of a 3-inch x 3/8-inch x 3/4-inch polyvinylchloride pipe that was epoxied to the top surface of the slab and filled with hot (liquid) sulphur mortar. The liquid was allowed to cool and solidify, creating a level top surface, onto which a 1-1/2 inch x 1-1/2 inch x 1/4-inch plastic square was epoxied. The typical set-up of the instrumentation is shown in Fig 2.5. Components of the instrumentation set-up are labelled in Fig 2.6 (this figure shows dial gages, but the set-up for LVDT’s is identical).

Measurement

As previously mentioned, the number of locations on the slabs that could be instrumented simultaneously was

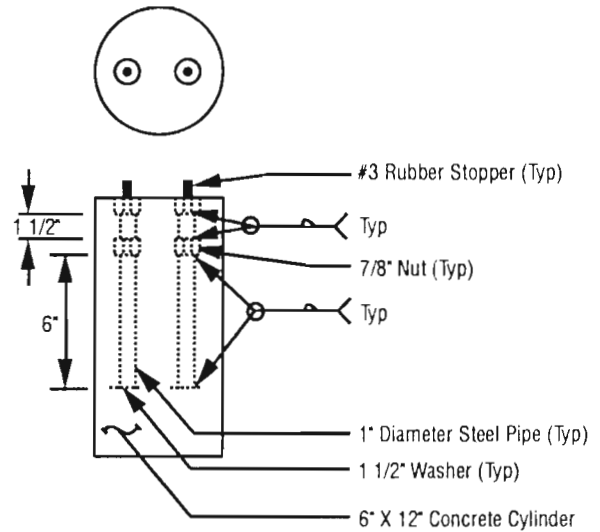


Fig 2.4. Details of concrete anchor for dowel supports.

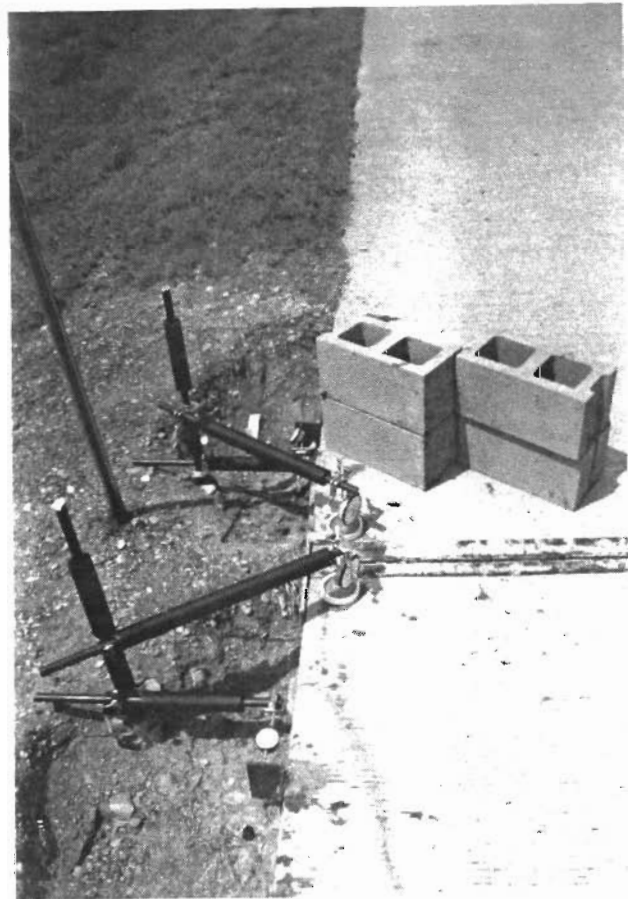


Fig 2.5. Instrumentation set-up.

limited by the number of available dial gages. Figure 2.7 shows a plan view of the slabs that were instrumented for this project, along with instrumentation locations. Instrument action locations labelled with “/3” or “/6” respectively indicate third or sixth points along the slab length. Figure 2.8 shows a more detailed plan of instrumentation

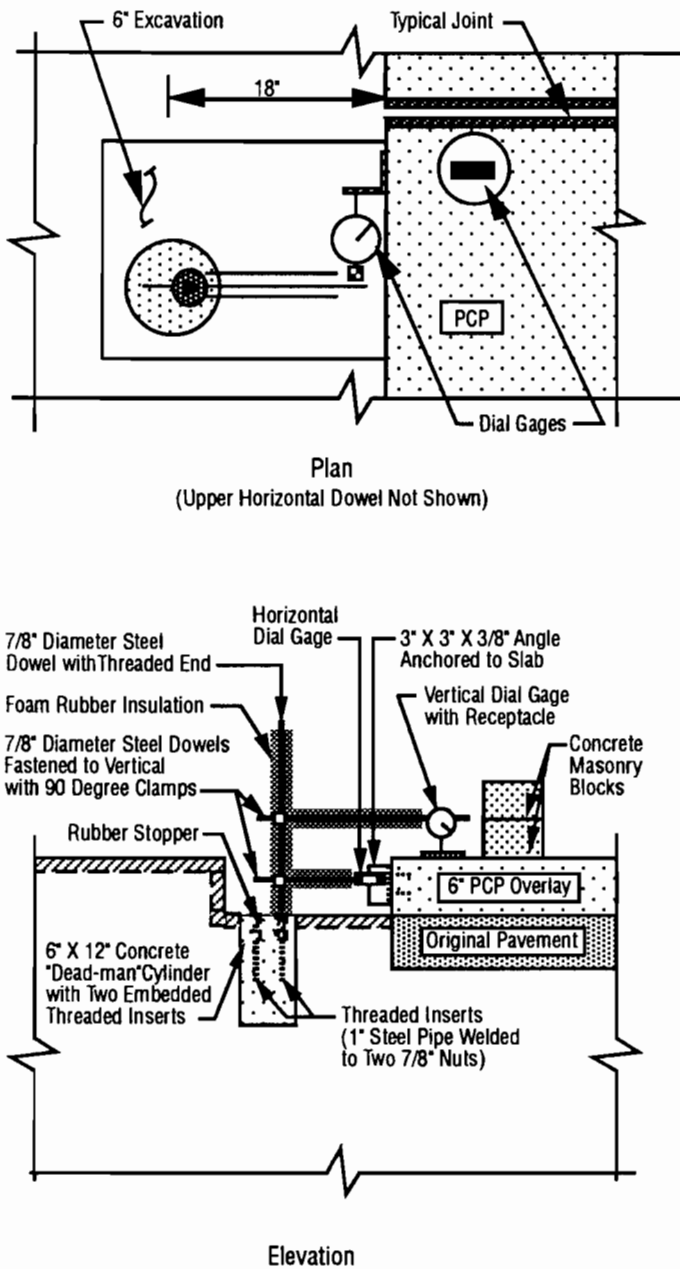


Fig 2.6. Components of instrumentation set-up.

locations for slabs that were instrumented along their length as well as at their ends. During the first three data collection periods, data were collected only from joint locations so that joint displacement data could be based on the largest possible sample for a portion of the field visits. For the remainder of the data collection periods, displacement data were collected at locations along slab lengths so that the computer models could be calibrated to displacements of the entire slabs. Table 2.2 shows a compilation of the instrumentation schemes that were carried out for each field visit. It outlines the type of instrument used at each instrumentation location for the measurement of

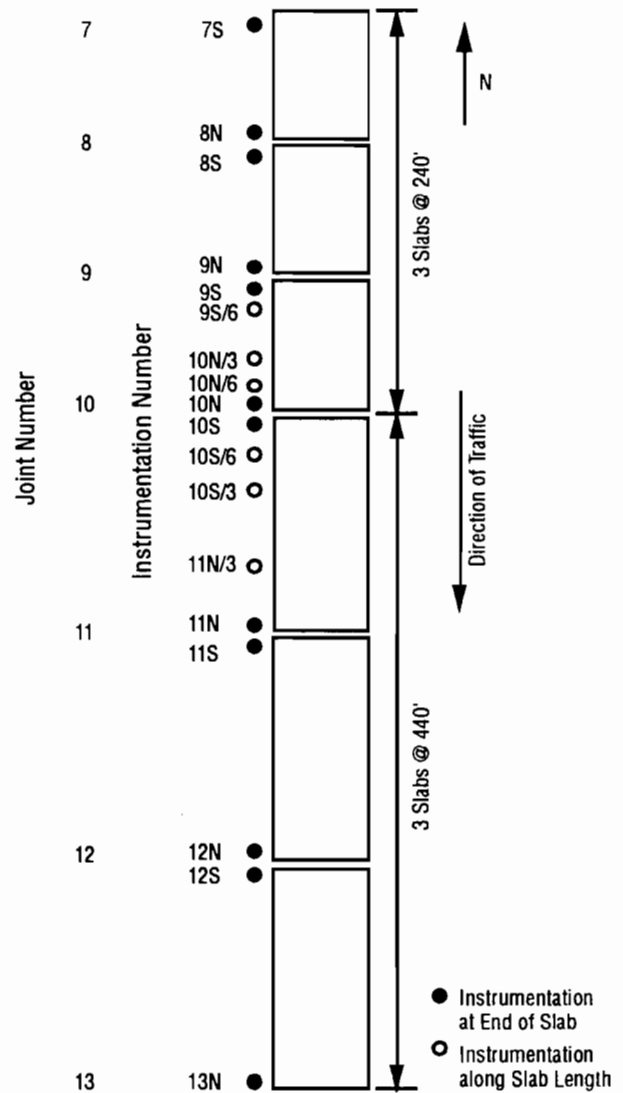


Fig 2.7. Instrumented slabs and instrumentation locations.

both horizontal and vertical slab movements. The dial gages had an accuracy of 0.001 inch and the LVDT's had an accuracy of 0.0001 inch. As mentioned in the section on limitations, Joint 10 was the only joint instrumented with LVDT's. The redundant readings of horizontal movements at locations 10S and 10N provided for a verification of data readings. Figure 2.9 shows the set-up of the combined dial-gage/LVDT instrumentation.

The instrumentation set-up allowed for the relative measurement of horizontal and vertical slab movements with respect to an arbitrary datum. The collected data for these movements give displacements measured from the

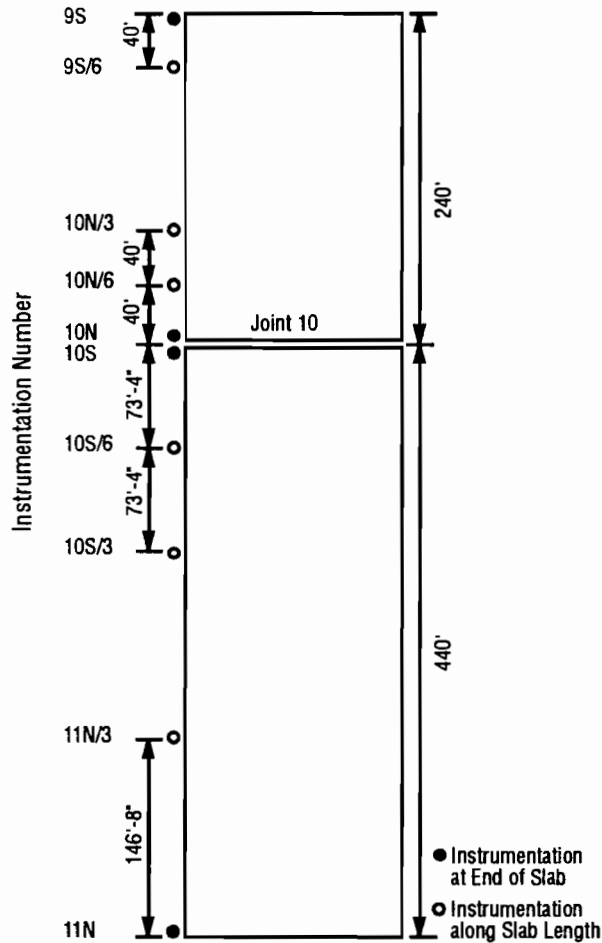


Fig 2.8. Instrumentation locations between Joints 9 and 11.

first data reading at each location for each field visit. The displacements for a daily temperature cycle determined in this manner are in direct parallel with the displacement output from the computer models.

Joint widths were measured with a dial-caliper by inserting the legs of the caliper into the joint, flush with the joint edges. Measurements took place at scribe marks on the joint hardware so that readings would reflect joint movements at one location for each joint. The method of joint width measurement is shown in Fig 2.10.

Data were collected both manually and automatically. Dial gage data and joint width readings were recorded manually onto data sheets at two-hour intervals. LVDT measurements and thermocouple readings were recorded automatically every 10 minutes by a programmed data acquisition system. A schematic diagram of the data acquisition system is shown in Fig 2.11 (Ref 16).

Prevention of Error

Several methods of avoiding error in final versions of data were employed. These methods include redundant

readings, internal checking of data, prevention of thermal movements of instrumentation supports, protection from wind gusts due to traffic, and monitoring of thermal movements of instrumentation supports.

Several redundant data readings were taken. Two slab temperature readings were taken at each of the three depths, 1 inch, 3 inches, and 5 inches. At Joint 10, horizontal slab movements were measured with both dial gages and LVDT's for the purpose of redundancy and comparison. All joint opening measurements were accompanied by a measurement of opening between scribe marks that were parallel to the joint; these marks could be used to determine changes in joint movement if a joint opening measurement was in error. Also, the measurements of horizontal slab movements could be internally checked since the sum of the movements measured by dial gages or LVDT's at the ends of the slabs should add up to the change in joint opening measured with dial calipers. The results of this check are presented in Chapter 3.

Significant gusts from truck traffic occurred throughout every field visit. The gusts had the potential to rotate the upper horizontal dowels on the instrumentation set-up. In order to prevent this movement, concrete masonry blocks were used as wind screens at every instrumentation location.

Insulation was placed around all support dowels to prevent warping due to uneven expansion from radiant solar heat. This prevented vertical movements of horizontal dowels, and horizontal movements of vertical dowels. It did not, however, prevent longitudinal movements of the dowels. Longitudinal movements of horizontal dowels would not introduce any error since this movement was not in the same direction as the slab movements being measured. Longitudinal movements of the vertical dowels, however, were in the direction of vertical slab movements and had the potential of introducing error to curling measurements.

In order to correct errors in measurement of vertical slab displacements due to expansion and contraction of the vertical support dowels, a monitor was used to determine the magnitude of the longitudinal movements of the dowel. The monitor consisted of an insulated dowel with 90° dowel clamps attached in the same locations as on the vertical support dowels. The monitor dowel was supported on a wooden frame that allowed for one end of the dowel to be fixed and the other end to have a roller support. An LVDT was mounted so that it could measure movements of a portion of the monitor dowel that was of the same length as the portion of the actual vertical support dowels that would cause error. An additional LVDT was mounted on the monitor with the plunger-pin set against a fixed block of wood for the purpose of measuring error that might occur due to thermal movements in the LVDT's themselves. The monitor was set in the field so that it could experience the same

TABLE 2.2. SUMMARY OF INSTRUMENTATION SCHEMES FOR EACH FIELD VISIT

Location	Field Visit 2 7/26/88		Field Visit 3 8/6/88		Field Visit 4 8/26/88		Field Visit 5 11/5/88		Field Visit 6 1/21/89		Field Visit 7 2/9/89	
	Horiz	Vert	Horiz	Vert	Horiz	Vert	Horiz	Vert	Horiz	Vert	Horiz	Vert
7S	Dial Gage	Dial Gage	Dial Gage	Dial Gage	Dial Gage	Dial Gage						
8N	Dial Gage	Dial Gage	Dial Gage	Dial Gage	Dial Gage	Dial Gage						
8S	Dial Gage	Dial Gage	Dial Gage	Dial Gage	Dial Gage	Dial Gage	Dial Gage	Dial Gage	Dial Gage	Dial Gage	Dial Gage	Dial Gage
9N	Dial Gage	Dial Gage	Dial Gage	Dial Gage	Dial Gage	Dial Gage	Dial Gage	Dial Gage	Dial Gage	Dial Gage	Dial Gage	Dial Gage
9S	Dial Gage	Dial Gage	Dial Gage	Dial Gage	Dial Gage	Dial Gage	Dial Gage	Dial Gage	Dial Gage	Dial Gage	Dial Gage	Dial Gage
9S/6							Dial Gage	Dial Gage	Dial Gage	Dial Gage	Dial Gage	Dial Gage
10N/3							Dial Gage	Dial Gage	Dial Gage	Dial Gage	Dial Gage	Dial Gage
10N/6							Dial Gage	Dial Gage	Dial Gage	Dial Gage	Dial Gage	Dial Gage
10N	LVDT & Dial Gage	LVDT	LVDT & Dial Gage	LVDT	LVDT & Dial Gage	LVDT	LVDT & Dial Gage	LVDT	LVDT & Dial Gage	LVDT	LVDT & Dial Gage	LVDT
10S	LVDT & Dial Gage	LVDT	LVDT & Dial Gage	LVDT	LVDT & Dial Gage	LVDT	LVDT & Dial Gage	LVDT	LVDT & Dial Gage	LVDT	LVDT & Dial Gage	LVDT
10S/6							Dial Gage	Dial Gage	Dial Gage	Dial Gage	Dial Gage	Dial Gage
10S/3							Dial Gage	Dial Gage	Dial Gage	Dial Gage	Dial Gage	Dial Gage
11N/3							Dial Gage	Dial Gage	Dial Gage	Dial Gage	Dial Gage	Dial Gage
11N	Dial Gage	Dial Gage	Dial Gage	Dial Gage	Dial Gage	Dial Gage	Dial Gage	Dial Gage	Dial Gage	Dial Gage	Dial Gage	Dial Gage
11S	Dial Gage	Dial Gage	Dial Gage	Dial Gage	Dial Gage	Dial Gage	Dial Gage	Dial Gage	Dial Gage	Dial Gage	Dial Gage	Dial Gage
12N	Dial Gage	Dial Gage	Dial Gage	Dial Gage	Dial Gage	Dial Gage	Dial Gage	Dial Gage	Dial Gage	Dial Gage	Dial Gage	Dial Gage
12S	Dial Gage	Dial Gage	Dial Gage	Dial Gage	Dial Gage	Dial Gage						
13N	Dial Gage	Dial Gage	Dial Gage	Dial Gage	Dial Gage	Dial Gage						

temperature changes that the actual instrumentation supports were experiencing. Thermocouples were mounted on both the monitor dowel and the vertical and horizontal support dowels at location 10S for the purpose of verification of parallel temperatures between the two. Figure 2.12 shows the set-up of the complete dowel monitor, and Fig 2.13 shows labelled components of the monitor (it was determined, upon inspection of the data

recovered from the monitor, that dowel movements were negligible and could be ignored).

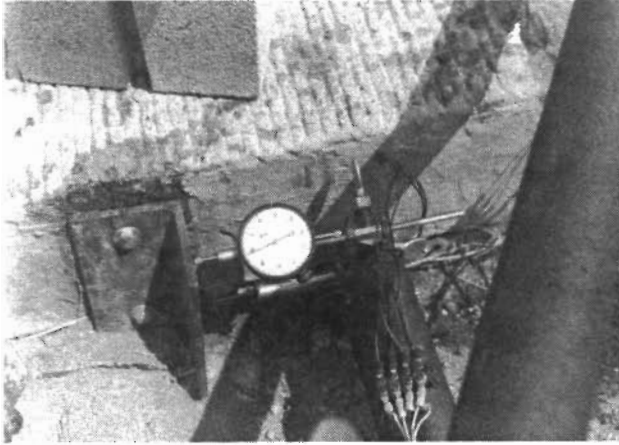


Fig 2.9. Combined dial-gage and LVDT instrumentation.



Fig 2.10. Joint width measurement using dial-caliper.

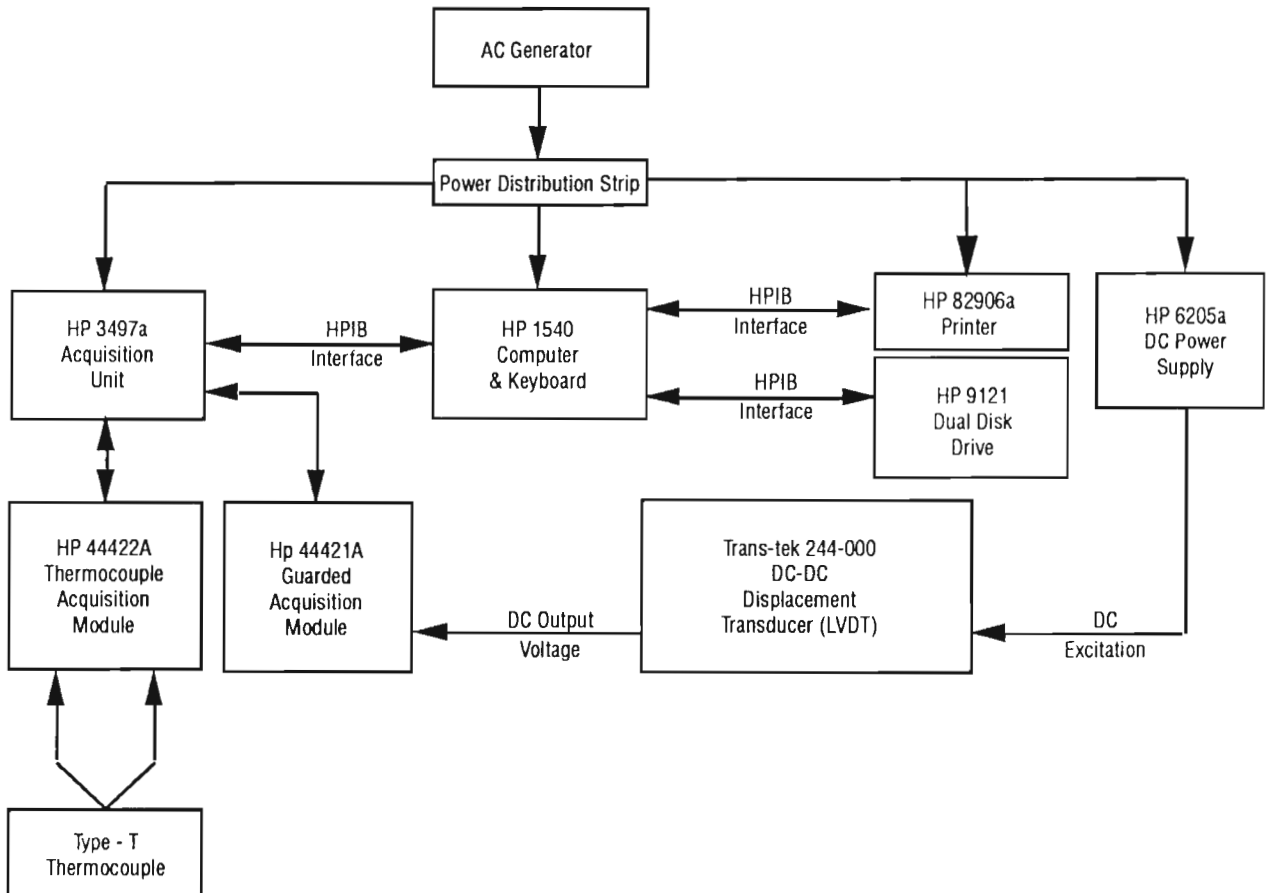


Fig 2.11. Schematic diagram of the data acquisition system.

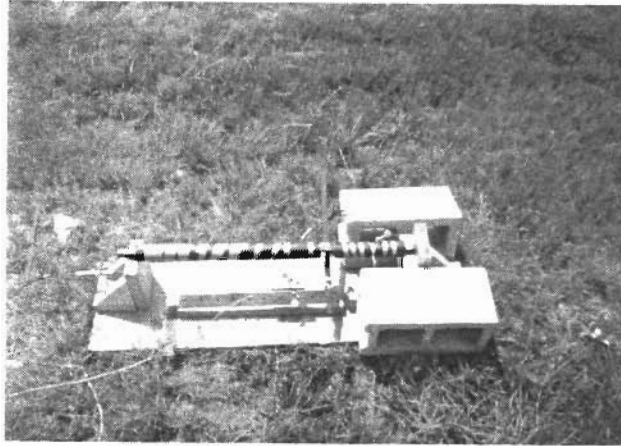


Fig 2.12. Dowel monitor used to measure longitudinal movements of a dowel and thermal movements of an LVDT.

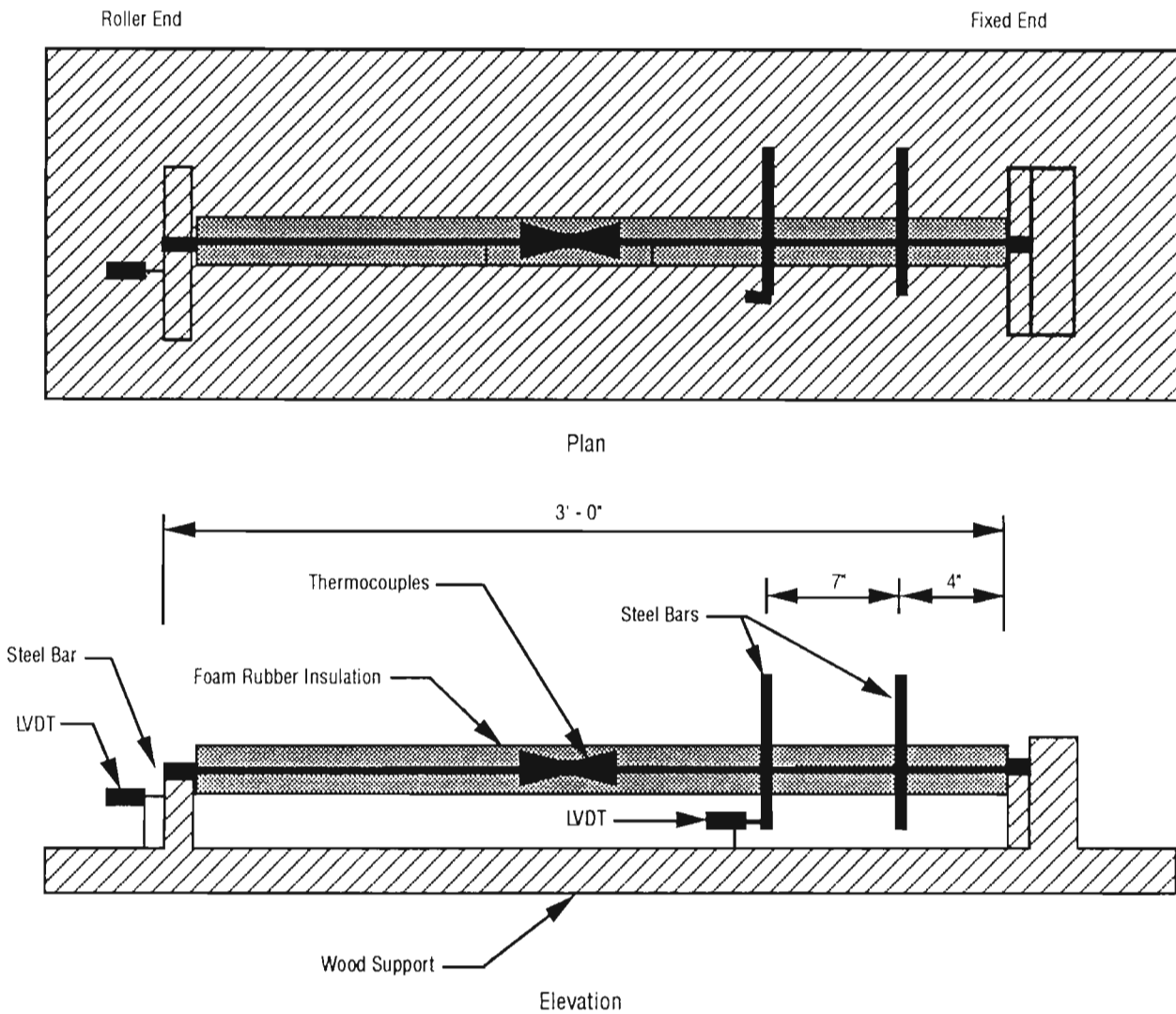


Fig 2.13. Components of the dowel monitor.

CHAPTER 3. DATA ANALYSIS

This chapter describes the treatment of the field data collected at the McLennan County PCP. The data include measurements of horizontal and vertical slab displacements, joint widths, ambient temperatures, and concrete temperatures at three depths in the pavement. Only the analysis of horizontal displacements and their corresponding concrete temperatures at mid-depth in the slabs is included in this report. Vertical displacement data are analyzed in Ref 2. Reference 1 contains a complete listing and graphical presentation of all data.

In the following sections, the reduction of the field data is first described. Next, the behavioral trends of the horizontal movements are analyzed. The last section covers the consistency of the data and an error analysis.

DATA REDUCTION

In order to effectively use the data collected in the field, a data reduction process was designed and performed. This process had the purpose of transforming numbers recorded from the instrumentation into numbers that could be used to characterize the behavior of the PCP in a concise manner and that would also be efficient for calibrating the model presented in Chapter 4. Data reduction was accomplished through

- (1) normalizing displacement data to a common axis;
- (2) "smoothing" data that were in obvious error by using a redundant reading, or by back-calculating from a closure measurement (explained later in this chapter);
- (3) organizing the data by field visit, slab type, and type of instrumentation location; and
- (4) performing a statistical reduction of the data.

Normalization was performed using computer spreadsheets to perform a simple subtraction of the first data value in a series of readings at each slab location from all values in that series. The result was that the first reading was equal to 0.0 for all displacement data. Normalization of data allowed for the direct numerical comparison of all data for a field visit, as well as for easy visual comparison of plotted values.

The smoothing of data was carried out (if necessary) in two ways. First, since horizontal displacements at Joint 10 were measured using both dial gages and LVDT's (Table 2.2), one reading could be used to correct the other. Since only two LVDT's were used to measure horizontal movements, but a large number of dial gages were used, dial gage data were used for the final versions of the data at Joint 10; if values had to be corrected or modified, the LVDT data were used to modify the dial gage data. Second, since the sum of horizontal movements measured at a joint should be equal to the change in joint width, a

horizontal movement reading could be corrected by calculating the difference between the change in joint opening and the horizontal displacement of the end of the adjacent slab at the joint. This phenomenon also allowed for the internal check of horizontal displacement measurements (explained later in this chapter). Both the normalization and smoothing processes were documented using coded files; details on the method of coding, as well as further explanation of the particulars of the sequence of this segment of the data reduction process, can be found in Ref 1.

The reduced form of the horizontal displacement data was organized by field visit, slab type, and type of instrumentation location. The data from each field visit represent slab movements under one particular condition of environmental input. Therefore, each field visit provided one set of calibration curves for the computer model presented in Chapter 4. For every field visit, the 240-foot and 440-foot slab data were treated separately, yielding two distinct groups of data. Furthermore, for each slab length, data were subdivided into measurement groups of the same slab geometry; measurements taken at the joints, the sixth points, and the third points each provided a data set that was used to calibrate parallel locations on the computer model (further explanation in Chapter 5).

The final usable version of the horizontal displacement data consists of the average movement at a specific slab location, for either a 240-foot or a 440-foot slab, for a particular field visit. For example, for the third field visit, all displacements measured at the ends of 240-foot slabs between 14:00 and 16:00 hours were averaged, all between 16:00 and 18:00 hours were averaged, and so on for the total 24-hour measurement period. The same was done for all field visits, for all slab locations. The final results of the average displacements for all field visits are presented in tabular form in Appendix A. The resulting six calibration curves from each field visit are shown in Figs 3.1 through 3.6. These curves reflect logical trends in magnitudes of slab displacement: 440-foot slabs have a wider range of movement than 240-foot slabs, and, for each, the range decreases from the joints, to the sixth points, to the third points.

BEHAVIOR ANALYSIS

The design of a PCP involves the evaluation of two major aspects of the horizontal slab movements: the character of slab activity during temperature changes and the range of joint widths between slabs. The former is of interest because stresses in the slab are a direct function of displacements. The latter affects the placement of slabs (where the design criteria are meant to avoid extremely wide joint widths, or complete closure of the joints). Of course, slab activity affects the range of joint widths, that

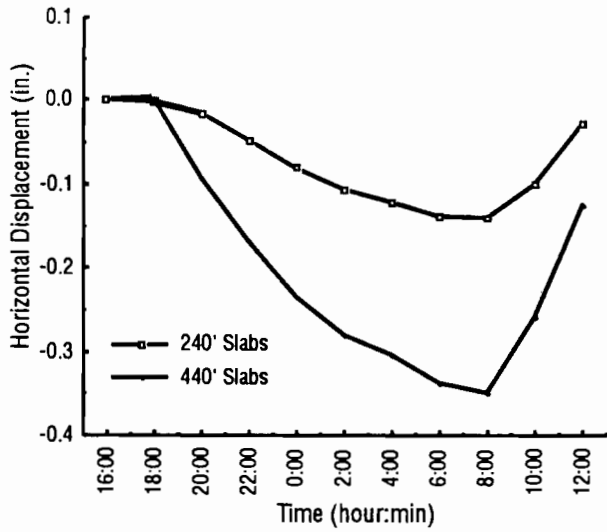


Fig 3.1. Average horizontal slab displacements for field visit 2.

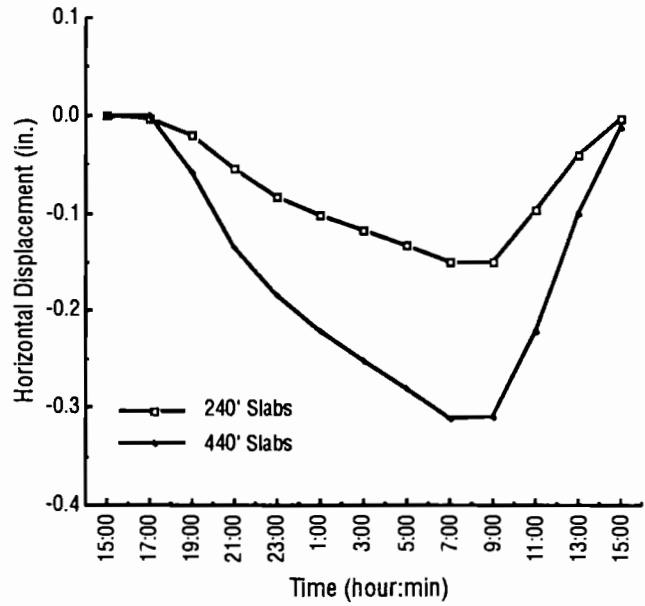


Fig 3.3. Average horizontal slab displacements for field visit 4.

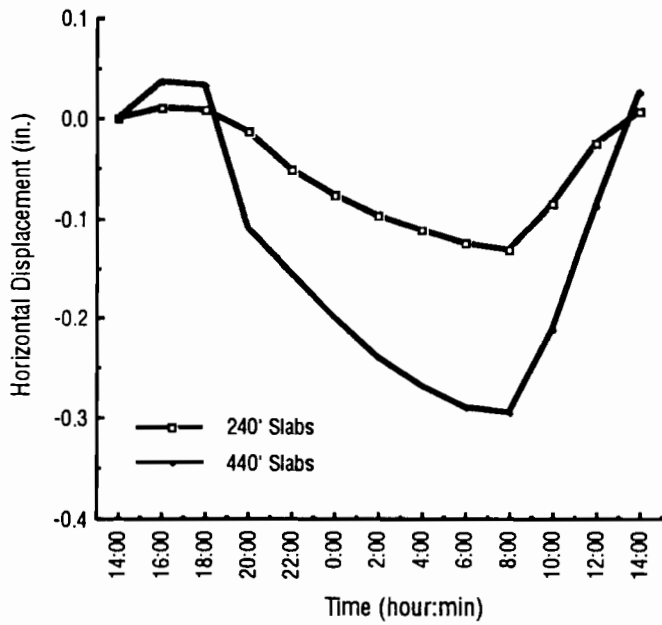


Fig 3.2. Average horizontal slab displacements for field visit 3.

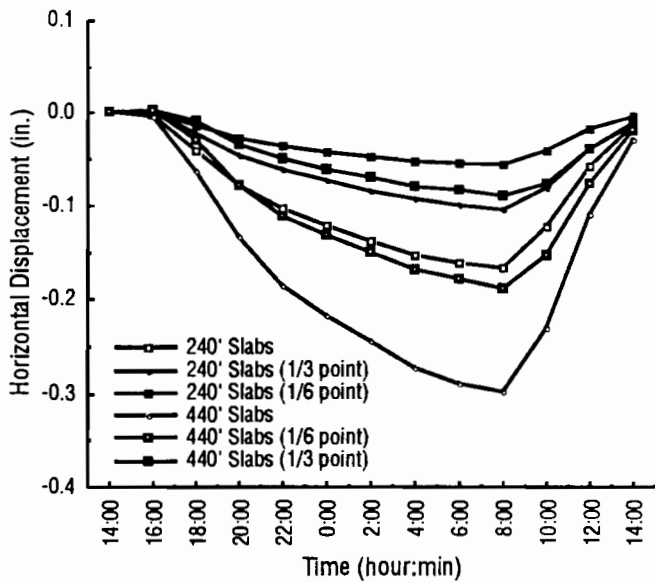


Fig 3.4. Average horizontal slab displacements for field visit 5.

is, slabs with more active horizontal movements will cause a larger range of joint widths.

Regression Analysis of Horizontal Displacements

Analysis of slab activity for temperature changes was performed by calculating a series of regression equations for horizontal displacements. Graphs of slab displacements as a function of decreasing and increasing temperature for all instrumentation locations are presented in Appendix B (Figs B.1 through B.12). The equations are linear, where the abscissa, T , is the concrete temperature at mid-depth of a slab in degrees Fahrenheit, and the ordinate, Y , is the horizontal displacement from the initial data reading for a field visit. Table 3.1 shows a compilation of the regression equations for all field visits, along with the coefficient of partial determination statistic, R^2 . The R^2 value indicates how well the data fit the regression equation, where a value of 1.0 is a perfect fit.

All R^2 values are high; two-thirds of the equations are greater than 0.95, and the lowest value is 0.854. This indicates that the linear equations can predict horizontal displacements with a high degree of accuracy. This regression analysis does not indicate, however, whether stresses in the slab can be predicted with a linear model; stresses are a function of the accumulation of frictional forces under a slab, and any nonlinear behavior of the subbase frictional restraint could cause stress magnitudes to vary nonlinearly. The nature of the frictional restraint under a rigid slab is discussed more completely in Chapter 4.

As expected, the slopes (coefficients of the abscissas) in the equations increase for the longer slabs. The ratio of slab lengths between the 440-foot and the 240-foot slabs is 1.835, and the ratio between the average values of the slopes in the equations for the slabs is 2.024, 10.31 percent higher. This suggests that the increase in horizontal activity with increased slab length is not linear.

The slopes follow logical trends for the different measurement locations. The average slopes for displacements at the joints are 5.890×10^{-3} and 1.193×10^{-2} inch/ $^{\circ}$ F for the 240-foot and 440-foot slabs respectively. At the sixth points, the average slopes are 3.883×10^{-3} and 6.977×10^{-3} inch/ $^{\circ}$ F, 65.93 percent and 58.48 percent of the slopes at the joints. At the third points the average slopes are 1.990×10^{-3} and 3.237×10^{-3} inch/ $^{\circ}$ F, 33.78 percent and 27.13 percent of the slopes at the joints, and 51.25 percent and 46.40 percent of the slopes at the sixth points. The horizontal activity varies approximately linearly with respect to the geometry of the slabs. In addition, it appears that for both 240 and 440-foot lengths, almost the entire slab is moving. Figure 3.7 shows a graph of the slopes of the regression equations as a function of the distance from the centerlines of the slabs. The coefficient of thermal expansion is indicated by the slopes of the equations in Fig 3.7. When converted to inch units, the coefficients of

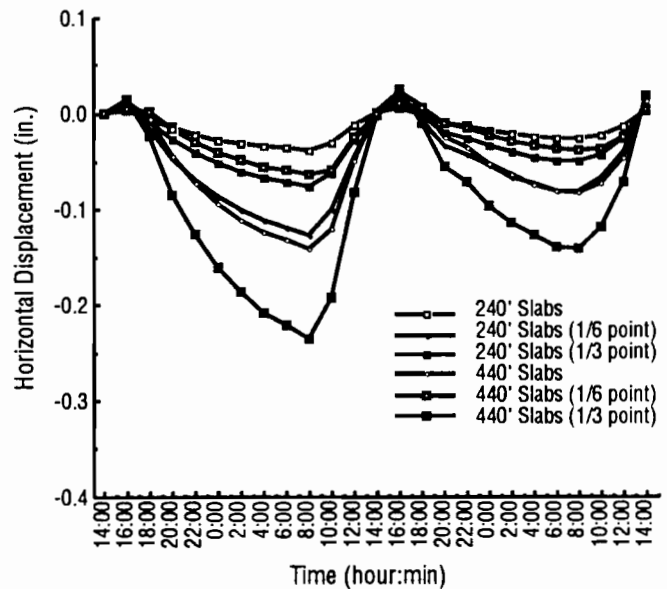


Fig 3.5. Average horizontal slab displacements for field visit 6.

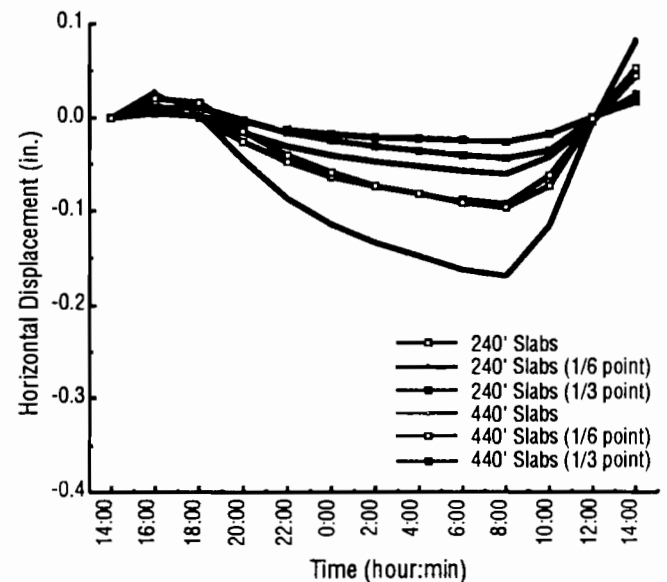


Fig 3.6. Average horizontal slab displacements for field visit 7.

thermal expansion are 4.8×10^{-6} inch/inch/ $^{\circ}$ F for the 240-foot and 440-foot slabs, respectively.

The regression equations do not show a strong trend for different moisture levels. Field visits 6 and 7 took place under moist conditions; the 440-foot slabs have slightly smaller slopes for these visits, and there is no definitive trend for the 240-foot slabs. One explanation for there not being large differences for field visits 6 and 7 is that the slabs might not have been completely saturated, and therefore expansion and contraction characteristics of the slabs would not have changed enough to

TABLE 3.1. REGRESSION EQUATIONS FOR HORIZONTAL DISPLACEMENTS

Field Visit	Measurement Location	Regression Equation	Coefficient of Partial Determination
2	240' Slab (Joint)	$Y = (5.374 \times 10^{-3}) T - 0.586$	$R^2 = 0.854$
	440' Slab (Joint)	$Y = (1.281 \times 10^{-2}) T - 1.422$	$R^2 = 0.951$
3	240' Slab (Joint)	$Y = (5.148 \times 10^{-3}) T - 0.558$	$R^2 = 0.884$
	440' Slab (Joint)	$Y = (1.212 \times 10^{-2}) T - 1.323$	$R^2 = 0.970$
4	240' Slab (Joint)	$Y = (6.076 \times 10^{-3}) T - 0.653$	$R^2 = 0.931$
	440' Slab (Joint)	$Y = (1.270 \times 10^{-2}) T - 1.371$	$R^2 = 0.854$
5	240' Slab (Joint)	$Y = (6.792 \times 10^{-3}) T - 0.542$	$R^2 = 0.991$
	240' Slab (Sixth Point)	$Y = (4.206 \times 10^{-2}) T - 0.335$	$R^2 = 0.982$
	240' Slab (Third Point)	$Y = (2.344 \times 10^{-3}) T - 0.186$	$R^2 = 0.993$
	440' Slab (Joint)	$Y = (1.217 \times 10^{-2}) T - 0.970$	$R^2 = 0.983$
	440' Slab (Sixth Point)	$Y = (7.697 \times 10^{-3}) T - 0.611$	$R^2 = 0.970$
6	440' Slab (Third Point)	$Y = (3.717 \times 10^{-3}) T - 0.295$	$R^2 = 0.932$
	240' Slab (Joint)	$Y = (6.089 \times 10^{-3}) T - 0.358$	$R^2 = 0.991$
	240' Slab (Sixth Point)	$Y = (3.738 \times 10^{-3}) T - 0.219$	$R^2 = 0.971$
	240' Slab (Third Point)	$Y = (1.887 \times 10^{-3}) T - 0.112$	$R^2 = 0.988$
	440' Slab (Joint)	$Y = (1.106 \times 10^{-2}) T - 0.649$	$R^2 = 0.980$
7	440' Slab (Sixth Point)	$Y = (6.948 \times 10^{-3}) T - 0.402$	$R^2 = 0.964$
	440' Slab (Third Point)	$Y = (3.138 \times 10^{-3}) T - 0.182$	$R^2 = 0.920$
	240' Slab (Joint)	$Y = (5.864 \times 10^{-3}) T - 0.542$	$R^2 = 0.985$
	240' Slab (Sixth Point)	$Y = (3.706 \times 10^{-3}) T - 0.335$	$R^2 = 0.966$
	240' Slab (Third Point)	$Y = (1.738 \times 10^{-3}) T - 0.186$	$R^2 = 0.984$
	440' Slab (Joint)	$Y = (1.074 \times 10^{-2}) T - 0.970$	$R^2 = 0.981$
	440' Slab (Sixth Point)	$Y = (6.287 \times 10^{-3}) T - 0.611$	$R^2 = 0.947$
	440' Slab (Third Point)	$Y = (2.855 \times 10^{-3}) T - 0.295$	$R^2 = 0.904$

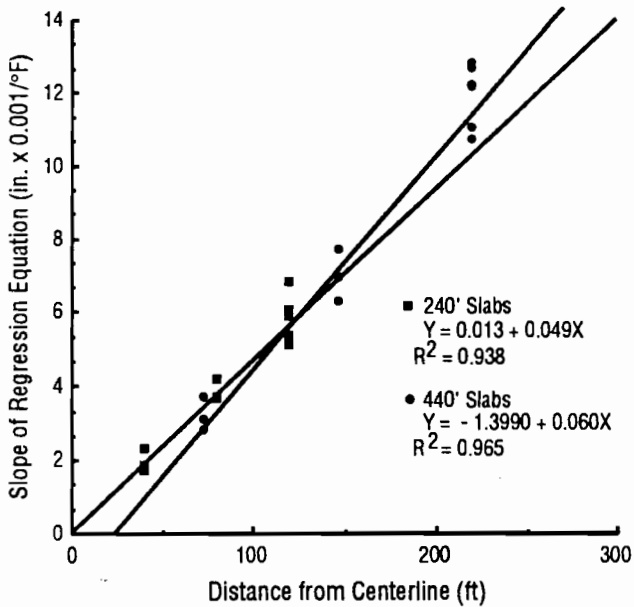


Fig 3.7. Slopes of the regression equations in Table 3.1 as a function of distance from slab centerline.

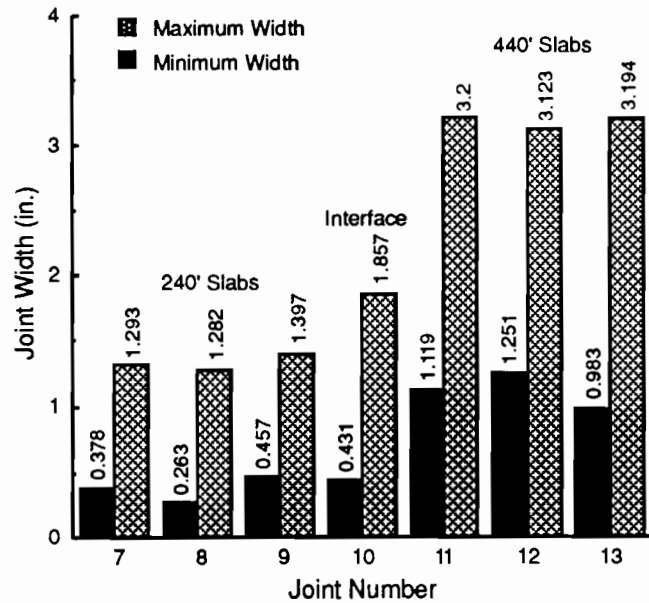


Fig 3.8. Maximum and minimum joint widths for all field visits.

show up in the data. Another explanation is that the horizontal activity is not very sensitive to changes in moisture levels. The reason for this would be that the regression equations are relative since they relate horizontal movements to the concrete temperature at mid-depth of the slabs. The moisture level might affect the lag time between changes in ambient temperature and changes in concrete temperature, but the expansion and contraction characteristics of the slab would not necessarily change appreciably for the same concrete temperatures.

Figures B.1 through B.12 reveal that horizontal displacements, while behaving almost perfectly linearly in most instances, show a small amount of nonlinearity in others. The displacements for the 440-foot slabs during field visits 5 and 7 (Figs B.8 and B.12) clearly exhibit nonlinear variation of displacements with respect to concrete temperature. The nonlinearity of the displacements observed in these two visits is probably due either to changes in the rate of heating of the concrete (due to differences in the rate of absorption of solar radiant heat by the concrete caused by differences in atmospheric filtering of radiation) or to a pronounced effect of hysteresis (energy absorbing capacity) in the force-displacement behavior of the subbase frictional restraint. It is not possible to draw an exact conclusion for the cause of this effect, but previous research has indicated that the nonlinear behavior of the subbase friction should be considered in the analysis of horizontal displacements of rigid pavement slabs (Ref 5).

Analysis of Joint Widths

The determination of an initial joint width for construction of PCP depends on the following factors:

- (1) the projected amount of creep and shrinkage that will occur during the early life of the pavement,
- (2) the projected amount of elastic shortening a slab will undergo during stressing operations,
- (3) the width requirements for inserting a protective neoprene seal into the joint, and
- (4) the expected range of temperatures and subsequent horizontal displacements that the slabs will experience throughout their service life.

For the current study, a sample range of maximum and minimum joint widths was determined; Fig 3.8 summarizes the results. These maximums and minimums represent a range of ambient temperatures from 17.6°F to 107.13°F.

The joint widths were measured at scribe marks on the joint hardware so that the readings could be compared consistently. The joint edges are not perfectly parallel, so the reported maximum and minimum widths are not necessarily the absolute maximum and minimum widths for the entire length of a joint. In fact, several of the joints between 240-foot slabs were observed to be completely

closed during hot weather measurements. This is demonstrated by the flattening of the upper portion of the curves in Figs B.1, B.3, and B.5. A completely closed joint between 240-foot slabs is shown in Fig 3.9, and a wide open joint between 440-foot slabs is shown in Fig 3.10. In addition, debris in the joints between these slabs often prevented slab movement for temperature increases during

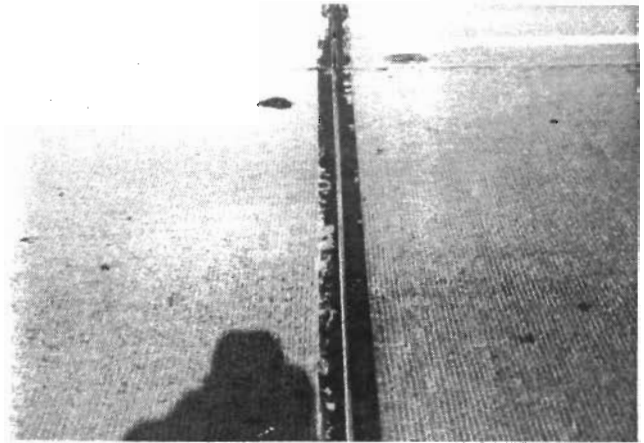


Fig 3.9. Closed joint between 240-foot slabs.



Fig 3.10. Open joint between 440-foot slabs.

hot weather. Figure 3.11 shows the joint for which slab movement was prevented by debris. Joints between 440-foot slabs never completely closed.

Regression equations were calculated for the joint width data for joints between the slabs. The equations describe the joint width behavior (abscissa, X) as a function of concrete temperature at mid-depth of a slab in degrees Fahrenheit (ordinate, Y). Figures 3.12 and 3.13 show graphs of the joint width data for the two slab lengths along with the corresponding regression equations.

Seasonal Slab Operation

Overall seasonal behavior of horizontal movements of the slabs is a function of daily temperature cycles

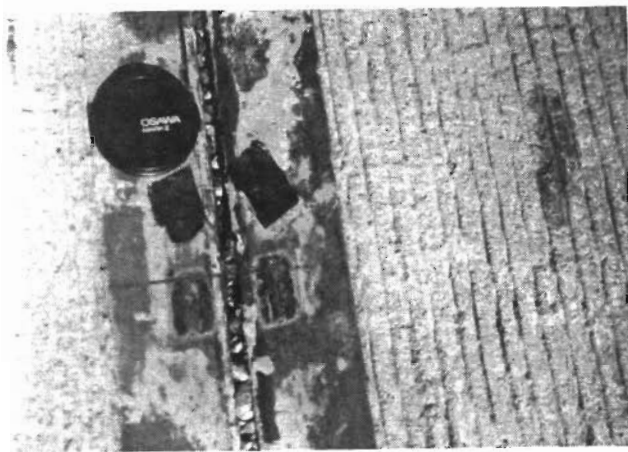


Fig 3.11. Joint expansion prevented by debris.

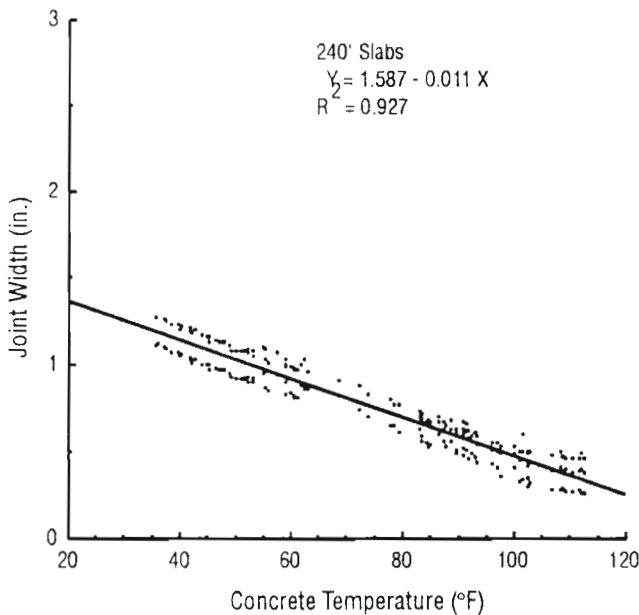


Fig 3.12. Regression equation for joint widths between 240-foot slabs.

superimposed over seasonal temperature cycles. This superposition causes slabs to operate, on a daily basis, at different seasonal datum values. During the summer season, the joint widths are small; horizontal displacements occur over a range of small joint widths. Similarly, during the winter season, horizontal displacements occur over a range of wide joint widths. Figure 3.14 shows the ambient and concrete temperatures that were measured for all field visits.

Figure 3.15 shows the average horizontal displacements for the 240-foot and 440-foot slabs superimposed over a curve of the first joint width measurement for each field visit. This plot illustrates the actual measured seasonal operation of slab movements.

CONSISTENCY AND ERROR ANALYSIS

Consistency Analysis

The consistency of horizontal displacements gives an indication of how reliable the measurements are. High consistency in the data would indicate a high degree of reliability in analysis and recommendations, whereas wide scatter in the data would indicate that any analysis of the data, or any recommendation based on the data, would not be as well founded.

The PCP slabs were keyed and dowelled to the sub-base at their centerlines so that the middle section of the slabs would not shift from horizontal movements. Therefore, the slabs were expected to expand and contract symmetrically about their centerlines. Consistency analysis of horizontal displacement data was performed by comparing the maximum change in horizontal movement divided

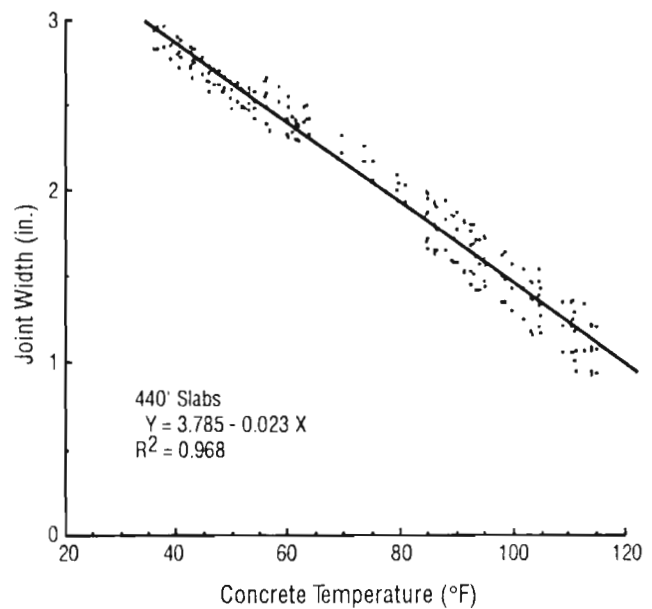


Fig 3.13. Regression equation for joint widths between 440-foot slabs.

by the corresponding change in concrete temperature for all instrumentation locations and all field visits. Figure 3.16 shows plots of these values for slab displacements at joints by instrumentation location for all field visits. Figure 3.17 shows the same values for slab displacements at sixth and third points. Table 3.2 lists the plotted values by field visit, along with mean values, standard deviations, and coefficient of variations (standard deviations divided by the mean values) for all field visits. Table 3.3 lists mean values for each size of slab by field visit, along with mean values, standard errors, and coefficients of variation of the means for all field visits. In both Tables 3.2 and 3.3, dashes indicate data that were not collected for the particular field visit.

The slab movements generally show good consistency; the standard deviation for instrumentation locations is 1.22×10^{-3} inch/ $^{\circ}$ F. The standard errors for all 240-foot and 440-foot slabs for joint instrumentation locations are 0.646×10^{-3} and 0.621×10^{-3} inch/ $^{\circ}$ F, respectively. It is not a coincidence that the average values for each slab in Table 3.3 are very close to the average slopes in regression equations reported earlier in this chapter (5.73×10^{-3} versus 5.890×10^{-3} ; 3.87×10^{-3} versus 3.883×10^{-3} ; and 1.96×10^{-3} versus 1.990×10^{-3} for joint location, sixth point and third point, respectively, for the 240-foot slabs; and 11.56×10^{-3} versus 11.93×10^{-3} ; 6.91×10^{-3} versus 6.977×10^{-3} ; and 3.17×10^{-3} versus 3.237×10^{-3} for joint location, sixth point, and third point respectively, for the 440-foot slabs). The former values represent movement per degree temperature change based on minimum and maximum values, whereas the latter values represent movement per degree temperature change based on all values. The small difference between the values results because the relationship between temperature change and slab displacement is generally very linear.

Inspection of Fig 3.16 shows that the consistency of slab movements per degree of temperature is generally high. The legend codes refer to instrumentation locations shown in Fig 2.7. Location 10N shows the most activity of the 240-foot slabs for the first three field visits, and 9S shows the least. Location 11N generally shows the most activity for the 440-foot slabs. The magnitude of daily slab activity for a particular change in temperature depends upon many factors, including the amount of radiant solar heat that penetrates the atmosphere, coefficient of thermal expansion of the concrete, thermal transmissivity of the concrete, moisture levels, and local deviations in subbase frictional restraint. It is not possible, with the given data, to pinpoint the reasons for more or less slab activity at a particular location or for a particular field visit.

Error Analysis

Error in horizontal measurements can be checked for internal closure. The sum of the displacements of slabs at

a joint should be equal to the change in joint width. Therefore, a closure check was made by comparing the maximum horizontal slab displacement at each joint for a field visit with the corresponding change in joint width. Figure 3.18 illustrates the basis for this comparison.

Table 3.4 shows the values of the sum of horizontal displacements, change in joint width, difference between the two, and percent difference for every measured joint for each field visit. The percent differences are generally low, except for four instances where the error is greater than 10 percent. The magnitude of the greatest error is 0.056 inch. It is most probable that any error in this analysis is due to faulty joint width measurements, since this was done manually. Furthermore, any error does not imply that a series of measurements are in error, but rather that the one measurement that was chosen for this analysis is in error. In effect, this analysis is a spot-check of closure values.

As a final check, the values of the sum of horizontal displacements and the change in joint width were plotted

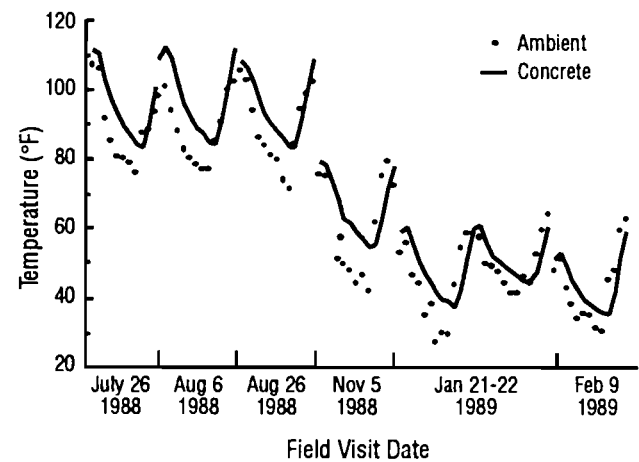


Fig 3.14. Seasonal variation of ambient and concrete temperatures for all field visits.

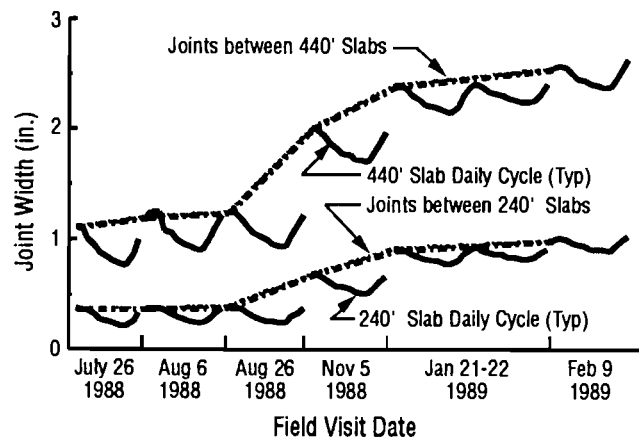


Fig 3.15. Seasonal variation of joint widths with horizontal slab displacements superimposed.

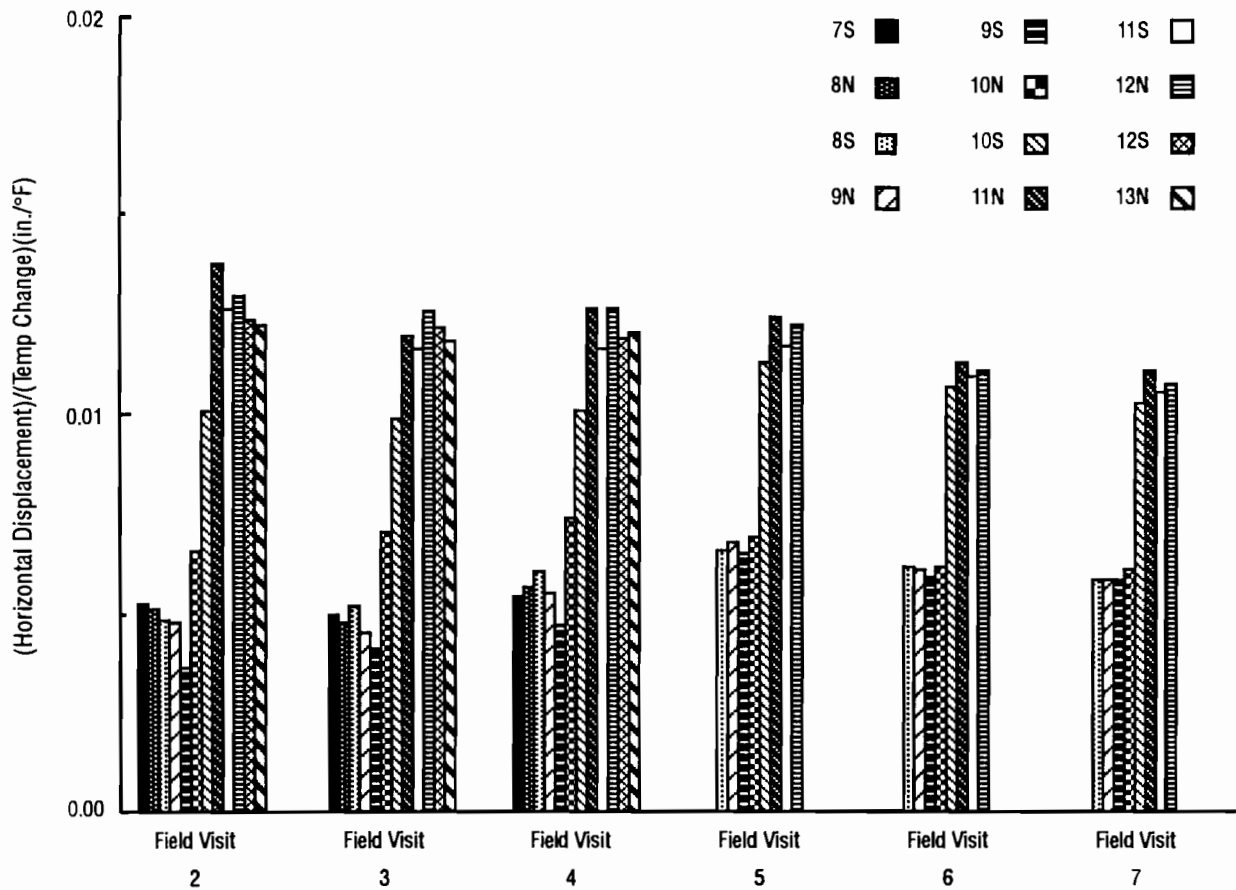


Fig 3.16. Consistency of horizontal slab displacements per degree of change in concrete temperature for all joint locations.

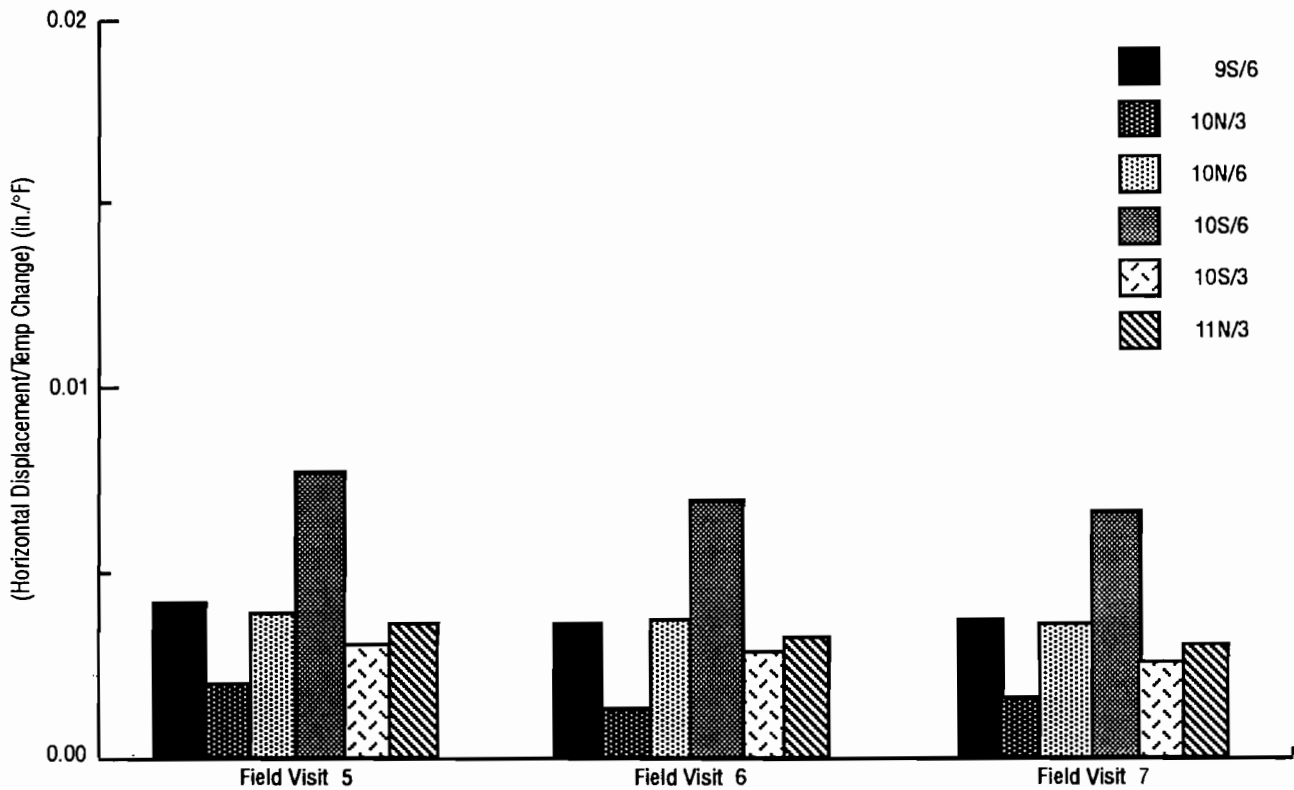


Fig 3.17. Consistency of horizontal slab displacements per degree of change in concrete temperature for all locations along slab length.

TABLE 3.2. VALUES OF (HORIZONTAL DISPLACEMENT) / (TEMPERATURE CHANGE) (X1013) PER INSTRUMENTATION LOCATION AND FIELD VISIT

Field Visits	Instrumentation Location (in./°F)																	
	7S	8N	8S	9N	9S	9S/6	10N/3	10N/6	10N	10S	10S/6	10S/3	11N/3	11N	11S	12N	12S	13N
2	5.21	5.03	4.86	4.72	3.52	-	-	-	6.55	10.00	-	-	-	13.77	12.57	12.92	12.39	12.25
3	4.98	4.80	5.16	4.58	3.92	-	-	-	6.94	9.85	-	-	-	11.92	11.70	12.57	12.10	11.85
4	5.48	5.63	5.99	5.48	4.59	-	-	-	6.97	10.17	-	-	-	12.65	11.66	12.65	11.86	11.98
5	-	-	6.61	6.78	6.53	4.15	2.26	4.07	6.86	11.33	7.39	3.28	3.61	12.44	11.66	12.20	-	-
6	-	-	6.18	6.05	6.05	3.76	1.86	3.93	6.13	10.70	7.02	3.05	3.30	11.25	10.95	11.00	-	-
7	-	-	5.85	5.85	5.85	3.67	1.75	3.67	5.90	10.30	6.32	2.73	3.03	11.02	10.55	10.77	-	-
Average (x 10 ⁻³)	5.22	5.16	5.77	5.57	5.09	3.86	1.96	3.89	6.55	10.39	6.91	3.02	3.32	12.17	11.52	12.02	12.12	12.02
Standard Deviation (x 10 ⁻³)	0.250	0.432	0.653	0.834	1.22	0.251	0.267	0.199	0.453	0.545	0.542	0.276	0.291	1.01	0.698	0.912	0.267	0.207
COV	0.048	0.084	0.113	0.150	0.241	0.065	0.136	0.051	0.069	0.053	0.079	0.091	0.087	0.083	0.061	0.076	0.022	0.017

in Fig 3.19. A regression equation was calculated (shown on the graph) which shows that the slope of the regression line is 0.98, the Y-intercept is small, and the coefficient of partial determination, R^2 , is 0.99. A value of 1.0 for the slope and the R^2 value would indicate a perfect closure for all measurements; thus, overall the error in measurement is small.

SUMMARY

Analysis

Slab movements are significant. Measurements indicate that entire slabs are moving (Fig 3.7). Resulting maximum joint widths range from about 1.5 inches to 3 inches (Fig 3.5). Additionally, slab movements correlate well with concrete temperatures at mid-depth of the slabs (see Table 3.1 and Appendix B). The techniques used for measuring slab movements work well. This is indicated by small cross-check errors.

This study investigated slab movements that occur after shrinkage and creep of the concrete have already occurred. The regression equations that result from these movements are basically the same for all data samples. Regression equations for the 240-foot slabs have flatter slopes than those for the 440-foot slabs. When the slab

temperature rises above about 107°F, joints between 240-foot slabs may close. This is illustrated in Figs B.1, B.3, and B.5, where the curves flatten in the upper regions.

Design

General design equations for predicting slab movements have been developed. For the McLennan County PCP, joint movements can be predicted by

$$\Delta X_{j,T} = \Delta X_o + (-2.8 + 0.06 L)(T_i - T_o)$$

where

- $\Delta X_{j,T}$ = net joint width at any temperature, T_i , inch;
- ΔX_o = joint width at reference temperature, inch;
- L = slab length, feet;
- T_o = reference concrete temperature, °F; and
- T_i = concrete temperature at time L.

For any portland cement concrete pavement placed on a polyethylene sheet, the general equation is

$$\Delta X_{j,T} = \Delta X_o + (-257 + 11L) \alpha_c (T_i - T_o)$$

where

- α_c = thermal coefficient of expansion of concrete, inch/inch/°F.

TABLE 3.3. MEAN, STANDARD DEVIATION, AND COEFFICIENT OF VARIATION OF (HORIZONTAL DISPLACEMENT) / (TEMPERATURE CHANGE) PER SLAB

Slab Length (ft)	Field Visit	Joint			Sixth Point			Third Point		
		\bar{x} ($\times 10^{-3}$) (in./°F)	S ($\times 10^{-3}$) (in./°F)	COV	\bar{x} ($\times 10^{-3}$) (in./°F)	S ($\times 10^{-3}$) (in./°F)	COV	\bar{x} ($\times 10^{-3}$) (in./°F)	S ($\times 10^{-3}$) (in./°F)	COV
240	2	4.98	0.973	0.195	-	-	-	-	-	-
	3	5.06	1.013	0.200	-	-	-	-	-	-
	4	5.71	0.753	0.132	-	-	-	-	-	-
	5	6.69	0.150	0.022	4.11	0.058	0.014	2.26	-	-
	6	6.10	0.063	0.010	3.85	0.120	0.031	1.86	-	-
	7	5.86	0.021	0.004	3.67	0.000	0.000	1.75	-	-
	Average ($\times 10^{-3}$)		5.73			3.87			1.96	
Standard Error ($\times 10^{-3}$)		0.646			0.217			0.267		
COV		0.113			0.056			0.136		
440	2	12.32	1.258	0.102	-	-	-	-	-	-
	3	11.66	0.940	0.081	-	-	-	-	-	-
	4	11.83	0.912	0.077	-	-	-	-	-	-
	5	11.91	0.503	0.042	7.39	-	-	3.45	0.232	0.067
	6	10.97	0.225	0.021	7.02	-	-	3.17	0.179	0.057
	7	10.66	0.309	0.029	6.32	-	-	2.88	0.211	0.073
	Average ($\times 10^{-3}$)		11.56			6.91			3.17	
Standard Error ($\times 10^{-3}$)		0.621			0.543			0.283		
COV		0.054			0.079			0.089		

\bar{x} = Mean
 S = Standard Deviation
 COV = Coefficient of Variance

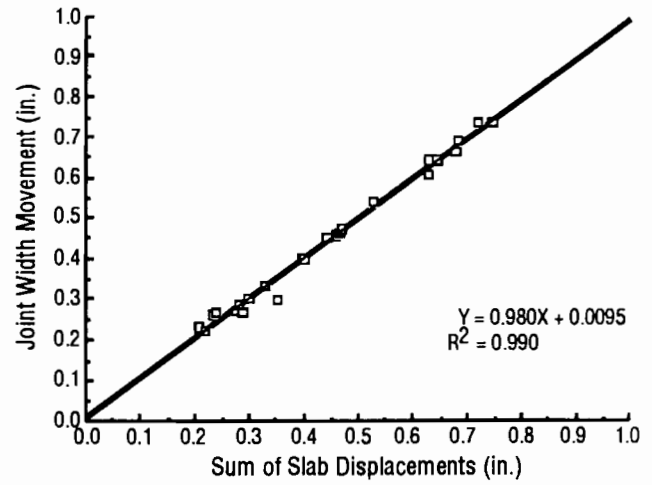
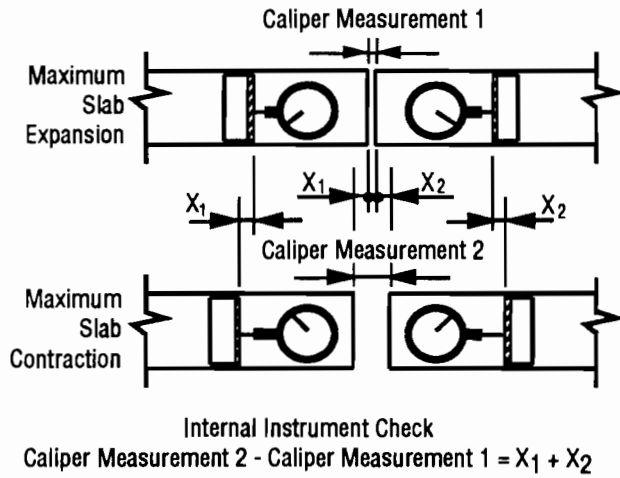


Fig 3.18. Internal check of measurements of horizontal displacements; the sum of slab movements is checked against the corresponding change in joint width.

Fig 3.19. Regression equation relating sum of slab displacements and the corresponding joint width movements for all joints and all field visits.

TABLE 3.4. ERROR IN HORIZONTAL DISPLACEMENT MEASUREMENTS

Field Visit	Joint	Sum of Horizontal Displacements, (in.)	Change in Joint Width, (in.)	Difference, (in.)	Percent Differences
2	8	0.281	0.287	0.006	2.14
	9	0.234	0.260	0.026	11.11
	10	0.470	0.473	0.003	0.64
	11	0.748	0.734	0.014	1.87
	12	0.719	0.732	0.013	1.87
3	8	0.276	0.272	0.004	1.45
	9	0.208	0.229	0.021	10.10
	10	0.458	0.457	0.001	0.22
	11	0.677	0.664	0.013	1.92
	12	0.683	0.688	0.005	0.73
4	8	0.353	0.297	0.056	15.86
	9	0.238	0.267	0.029	12.18
	10	0.442	0.449	0.007	1.58
	11	0.645	0.642	0.003	0.47
	12	0.630	0.642	0.012	1.90
5	9	0.328	0.334	0.006	1.83
	10	0.466	0.460	0.006	1.29
	11	0.629	0.605	0.024	3.82
6	9	0.286	0.265	0.021	7.34
	10	0.398	0.402	0.004	1.01
	11	0.526	0.541	0.015	2.85
7	9	0.219	0.222	0.003	1.37
	10	0.300	0.305	0.005	1.67
	11	0.401	0.399	0.002	0.50

CHAPTER 4. ANALYTICAL MODELLING

A finite element model for PCP that gives horizontal slab displacements and resulting principal stresses for any set of specified changes in slab temperature has been developed. This chapter describes the purpose of the model, and then gives a qualitative description of the function of the model. The information presented is supplemented by that in Appendix C, where the technical theory behind the model is outlined.

BACKGROUND

Although the most significant horizontal displacements for the McLennan County PCP occur in the longitudinal direction, there are several indications that thermal stresses in both the longitudinal and transverse directions are important parameters for the characterization of the behavior of the pavement.

Prestressing of the PCP was applied in both the longitudinal and transverse directions. Figure 4.1 shows the actual locations of longitudinal and transverse tendons for a typical 240 and a 440-foot slab. The major purpose of the longitudinal prestress, as explained in Chapter 1, was to prevent cracking of the pavement slabs due to tensile stress caused by friction forces. Transverse prestress was applied primarily to prevent longitudinal cracking caused by flexural action resulting from wheel loads. Regardless

of the role of the transverse stressing, however, the state of stress in the pavement as a result of thermal movements becomes complex if the transverse force components are considered. The orientation of principal planes (planes of stress in which pure tension or compression exists with no shear stress) could change from transverse to diagonal. This would result in different magnitudes of maximum tensile stress from those when precompression was applied in the longitudinal direction only.

Furthermore, the prestressing method used for the PCP produces a two-dimensional state of stress in the slabs. The technique involved the stressing of tendons from internal locations in the slabs. When the slabs were constructed, tendons were anchored near the joints while blockouts were used to form empty pockets around the ends of the tendons (in the middle region of the slabs) while concrete was placed. As the concrete gained strength, the tendons were stressed from the pocket locations in two stages. The first stage of stressing was applied before the concrete could crack during the first cooling cycle, which occurred during the first night after concrete placement. After the concrete developed its design strength, a second stage of stressing completed final tensioning of the tendons. Several days later, the pockets were filled with concrete. Figure 4.1 shows the locations

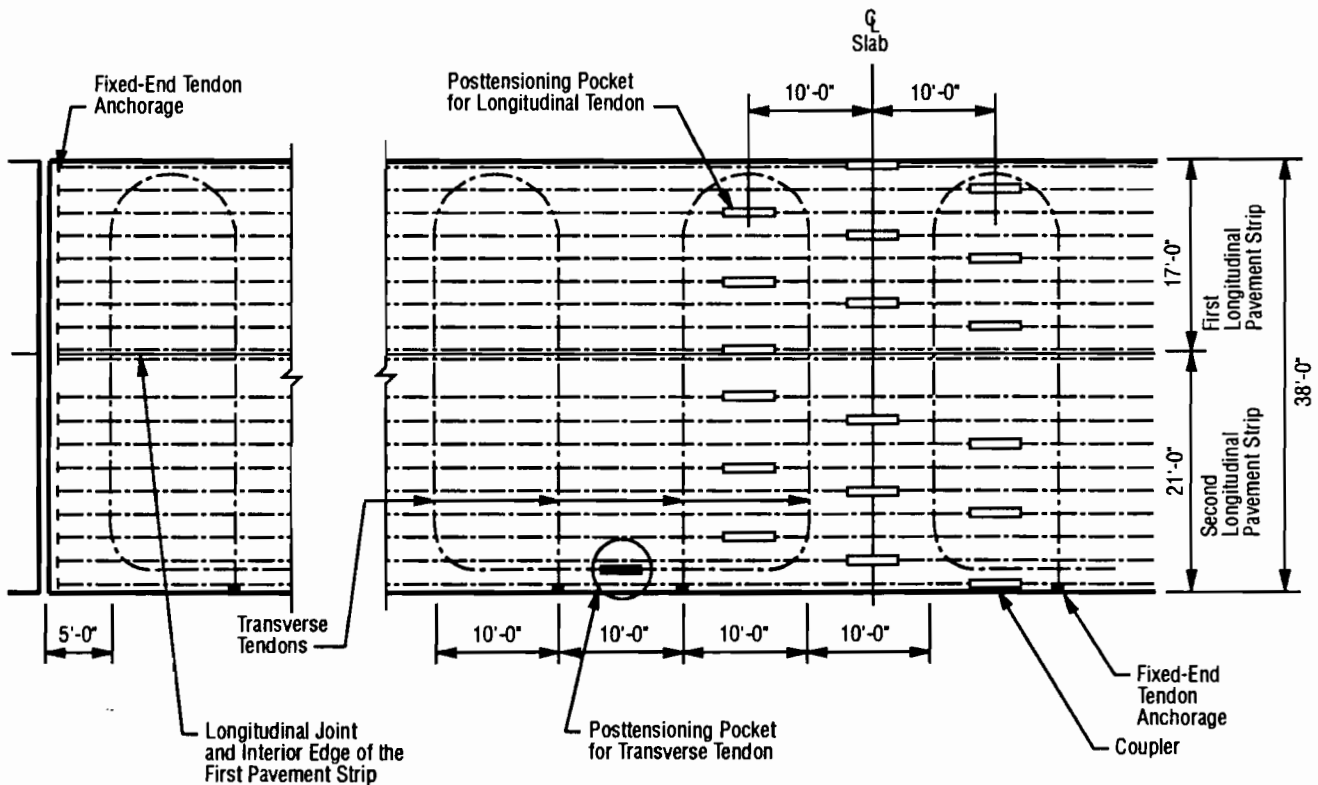


Fig 4.1. Layout of a typical PCP slab.

of the pockets for typical 240 and 440-foot slabs. The significance of the pockets in terms of two-dimensional states of stress is indicated by the presence of cracks in the slabs (Ref 1). Typical cracks were observed to propagate from the corners of the pockets in diagonal directions (Chapter 5 contains a more complete discussion on the cracking patterns in the slabs). Apparently, the pockets caused the maximum tensile stress (the principal stress) to occur on principal planes that were not transverse. This state of stress warrants an investigation of slab behavior that considers two-dimensional effects.

The finite element method was chosen for analysis of the PCP. This method is performed through the discretization of a continuum into connected elements to which material and geometric properties are given. The overall operation of the continuum is accomplished by the transfer of material action from one element to another through connecting nodes. If correct material and geometric properties are assigned to the elements, the method can simulate true two-dimensional prototype behavior with a high degree of accuracy. The finite element model developed in this chapter incorporates the most important material actions of the PCP into a format that is useful for the analysis of specialized problems. The model has a wide range of capabilities for the application of special problems associated with PCP because elements can have different geometric orientations and different material properties and because tendon forces can be applied at many locations in varying magnitudes and directions. In addition, the model is versatile in that a variety of effects not presently included can be easily adapted to it.

The model presented in this report is not intended to be a design model; the input-output aspects of the computer code for the model require that the user be extremely meticulous in order to avoid time-consuming errors. The model presented in Ref 5 is better for use in a design setting. That model has an excellent treatment of the early life behavior of PCP and gives the basic results that are necessary for the routine design of PCP. It is a uni-axial model, however, and cannot simulate all special problems associated with PCP. The model presented in this report is intended for the specialized analysis of complex problems that may occur with PCP.

MODEL DEVELOPMENT

The model developed for PCP is based on a stiffness formulation. Stiffness can be defined as the ability to resist deformation. This concept is best illustrated by a linear-elastic spring mechanism. Spring action is described by the equation $F = kx$, where k is the stiffness of the spring, F is the force exerted on the spring, and x is the resulting displacement of the spring. The same basic relationship also applies to PCP. The stiffness equation is more complex for the pavement than that for a spring, however, because, for PCP, several forces are applied

simultaneously on a body that has several materials and therefore several components of stiffness. Furthermore, the forces are applied on several boundaries, both in discrete and continuous manners.

In order to develop a finite element model for PCP, it was first necessary to characterize the stiffnesses of all of the material components that make up the pavement. This was done by establishing the force-deformation relationship that exists in concrete, in prestressing tendons, and, in subbase friction, under a rigid slab.

Material Stiffnesses

The force-deformation characteristics of concrete are based on curves that result from breaking typical 6-inch by 12-inch cylinders. A typical concrete stress-strain curve is shown in Fig 4.2. If concrete deformations are considered to be completely linear and elastic, the modulus of elasticity, E_c , (material stiffness) of concrete for highway pavements constructed in Texas can be estimated by the equation $E_c = A(2 \cdot e^{-BT} - e^{-CT})$, where A , B and C are experimentally determined coefficients and T is the age of the concrete in days (Ref 10). The shear modulus of the concrete, G , quantifies resistance to shear deformations and is equal to $E_c/2(1+\nu)$, where ν is the Poisson's ratio for concrete (about 0.2). The stress-strain curve of a typical prestressing tendon is shown in Fig 4.3. The tendons in PCP remain in the linear elastic range of deformation. The modulus of elasticity (E_s) of the tendons used in the McLennan County PCP is 28,000,000 psi (Ref 11). The axial stiffness of a tendon is $E_s A_s/L$, where A_s is the cross sectional area of a tendon and L is the tendon length.

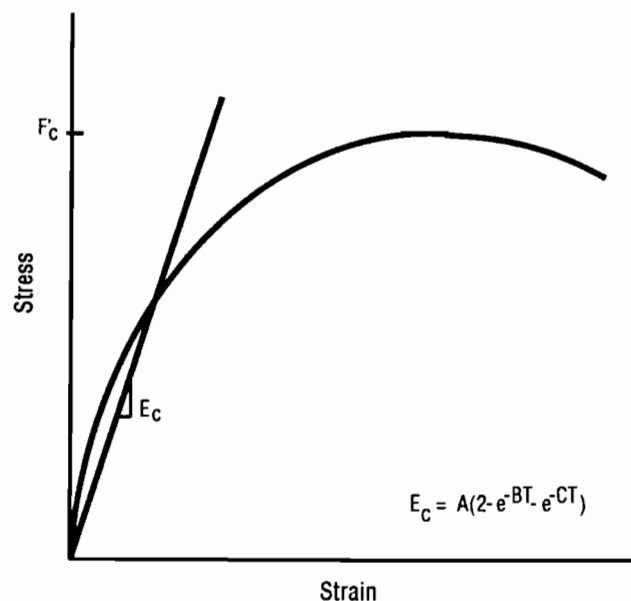


Fig 4.2. Typical stress-strain curves for concrete.

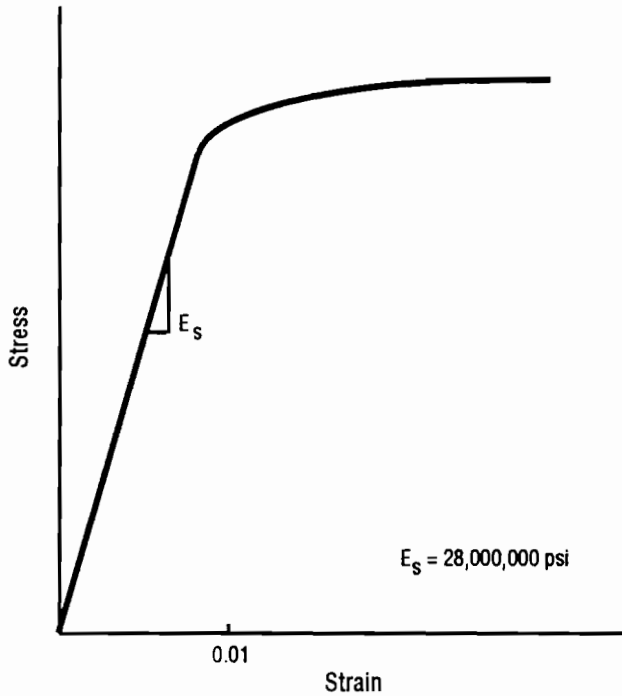


Fig 4.3. Typical stress-strain curve for a prestressing tendon.

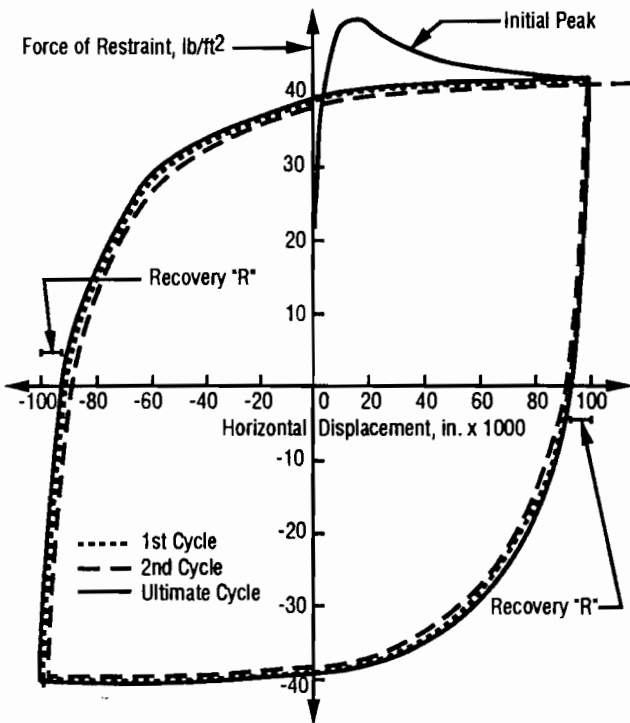


Fig 4.4. Force displacement behavior for subbase friction determined by Stott (Ref 12).

The force-deformation characteristics of subbase friction under a rigid slab have been determined to follow a non-linear hysteretic function. This has been reported by Stott as a result of a comprehensive experimental investigation of the frictional behavior of several materials under a slab (Ref 12). A typical force-deformation curve obtained in the study is shown in Fig 4.4 (from Ref 5). This figure shows how, for one location on a long pavement slab, the curve is steep when a movement reversal first occurs but gradually becomes more shallow as the magnitude of displacement increases. This behavior has been simplified for the finite element model in this study. The frictional behavior has been assumed to follow a bilinear function, as shown in Fig 4.5. This pattern of the force-displacement characteristics for subbase friction divides the type of restraint into two types: elastic friction, as represented by the steep portions of the curve in Fig 4.5, and inelastic friction, as represented by the flat portions of the curve. The elastic limit of force and displacement shown in Fig 4.5 corresponds with results of experiments performed at The University of Texas at Austin in 1986, in which the frictional force-displacement characteristics of a rigid slab on several friction-reducing mediums were determined (Ref 7).

One layer of polyethylene sheeting was used as the friction-reducing medium for the McLennan County PCP. As a slab expands and contracts, every point on the slab cycles through a characteristic friction curve, such as the curve in Fig 4.5. Slab locations that are far from the centerline go through a larger displacement with inelastic friction than do locations that are closer to the centerline. The cyclic behavior of subbase friction for different locations on a slab is shown in Fig 4.6. One daily temperature cycle is shown in 7 steps. These steps are indicated on the force-displacement curve for three different slab locations. The point closest to the centerline (point A) goes through a cycle of elastic displacements, whereas points B and C experience increasing amounts of inelastic behavior.

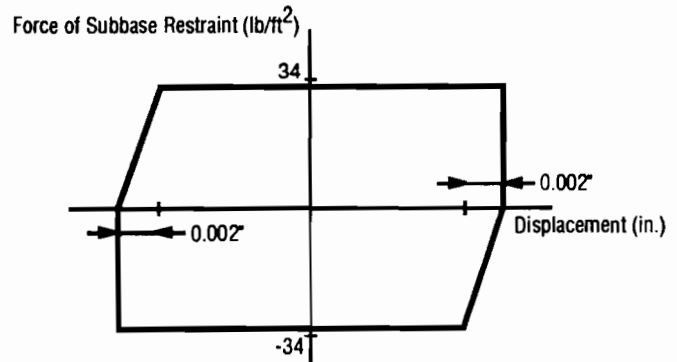


Fig 4.5. Simplified force displacement behavior for subbase friction assumed for this study.

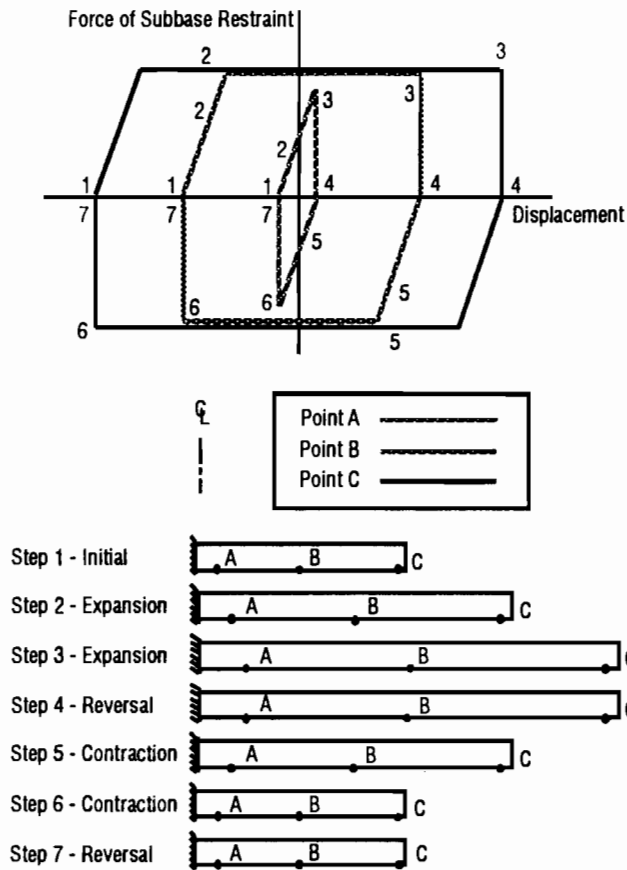


Fig 4.6. Cyclic behavior of subbase friction for different locations on a slab. The numbers on diagram refer to the different steps in the cyclic movements.

The Finite Element Method for PCP

The application of the finite element method to PCP involves the separation of the pavement into elements that are connected by nodes. The element used for the PCP model is isoparametric and has 8 nodes and 9 integration points. An isoparametric element is one in which the functions that describe the geometry of the element describe displacements as well. Because these functions are the same, the element can be distorted to assume any octolateral shape (as long as the general length to general width ratio of the elements does not exceed a value of about 1.75). The 8-node isoparametric element is a common element that is known to give accurate results for elastic problems (although there is inelastic friction in the PCP problem, the elements themselves always remain elastic; friction is applied as an external force). Figure 4.7 shows the element used for this study.

The element's nodes perform several functions: they define the geometry of the elements, they connect the elements, and they serve as readout points for displacements and stresses. The element's integration points allow for the numerical integration of properties

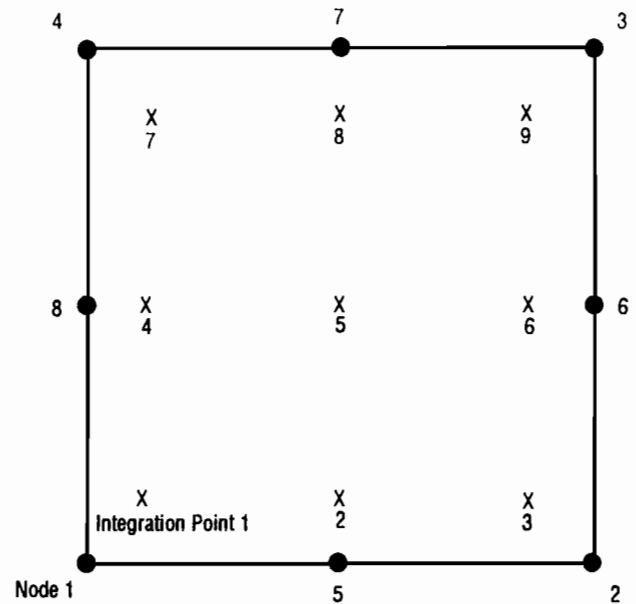


Fig 4.7. Typical 8-node isoparametric element with 9 integration points.

through the element. Each integration point is weighted according to its location in the element; when the numerical integration is carried out, the whole element assumes the property in a continuous manner. The integration points allow the elements to assume the properties of a continuum and to maintain the properties for any geometric orientation.

Stiffnesses and loads for the PCP must be applied at the proper boundaries in the finite element model in order for the behavior of the model to simulate prototype behavior. The concrete stiffness is a function of E_c and ν . This stiffness is applied at the integration points so that the body of elements has the stiffness of concrete. The tendon stiffnesses and forces are applied as discrete forces at nodes that correspond with tendon anchor locations in the prototype. Since the tendons are unbonded, all of the tendon stiffness is applied at the node. The subbase frictional stiffnesses and frictional forces are applied at the integration points. This insures that the friction is "felt" by the elements as if they were in surface contact with the subbase. Finally, temperature changes are applied at the integration points. This allows each element to undergo a volumetric change that corresponds with the coefficient of thermal expansion of the concrete, α , and the geometry of the element. In this manner, slab displacements in the model due to changes in temperature are a function of the accumulation of the volumetric changes of all elements.

Once stiffnesses and forces are given to the model, a stiffness relationship similar to that for the linear spring, $kx=F$, can be formed. Equation 4.1 describes the total stiffness relationship for PCP.

$$([K_c]_{ip} + [K_s]_{ip} + [K_p]_n)[U] = \{[P_s]_{ip} + [P_p]_n + [P_{\Delta T}]_{ip}\} \quad (4.1)$$

where

$[K_c]_{ip}$ = concrete stiffness applied at the integration points, ksi;

$[K_s]_{ip}$ = subbase frictional stiffness applied at the integration points, ksi/inch;

$[K_p]_n$ = tendon stiffness applied at nodes corresponding to anchor points, ksi;

$[P_s]_{ip}$ = subbase frictional forces applied at the integration points, k;

$[P_p]_n$ = tendon forces applied at nodes corresponding to anchor points, k;

$[P_{\Delta T}]_{ip}$ = force corresponding to temperature change applied at the integration points (actually a change in strain, applied on the right-hand side of the equation), k; and

$[U]$ = displacements of nodes, inch.

This equation is the basis for the implementation of the finite element procedure into a computer code. A more detailed derivation of the relationships described by Eq 4.1 is presented in Appendix C. The derivation is based on energy methods and includes all algebraic relationships necessary to write the computer program. Figure 4.8 shows the physical system described by Eq 4.1. The tendon forces and stiffnesses are represented by springs at the right end of the model; these springs are applied at discrete points and are governed by the force-displacement characteristics described by the elastic portion of the curve in Fig 4.3. The subbase stiffness and forces are represented by a bed of horizontal springs; the effects of these springs are integrated over the surface of every element and are governed by the force-displacement characteristics described by the curve in Fig 4.5. Concrete stiffness is applied at the integration points of all elements and is governed by the force-displacement characteristics of the elastic behavior of concrete illustrated in Fig 4.2. The basic procedure of the program is to form all stiffnesses, apply all loads, and solve for displacements, $[U]$. Then, the displacements are used to calculate strains, $\epsilon = B[U]$, where B is the strain displacement matrix as defined in Ref 13; and, with strains, stresses, $\sigma = D\epsilon$, where D represents a matrix of material properties for concrete, are calculated. Appendix C presents a more specific description of the calculations.

The boundary conditions for the model can be specified to allow displacements in either the longitudinal or transverse direction, or to completely fix displacements. The conditions are applied by assigning a displacement equal to 0.0 at specified nodes in the longitudinal or transverse direction, or in both directions. If the geometry of a PCP slab is symmetrical, boundary conditions can be applied so that only a fraction of the prototype is modelled.

This saves both computation time and user effort. Typical boundary conditions are shown in Fig 4.8, at the left side of the body. They are applied at the centerline since the actual slabs are anchored at their centerlines and, therefore, behave symmetrically. The uppermost symbol represents a completely fixed condition and the lower symbols represents fixed longitudinal displacements, but free transverse displacements.

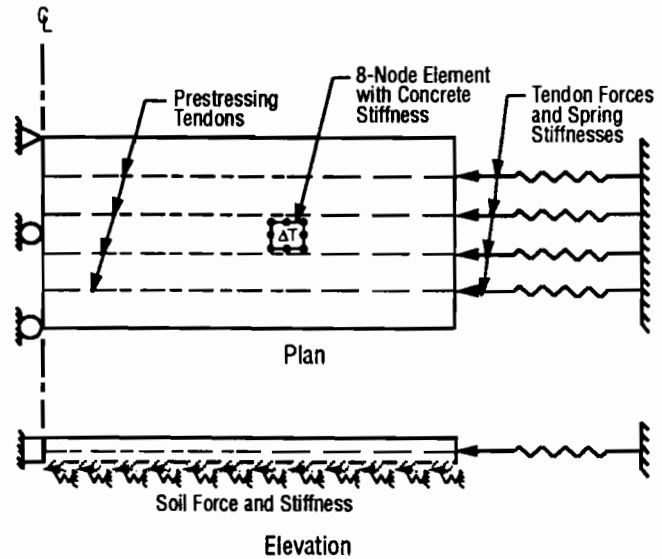


Fig 4.8. General components of the finite element model for PCP.

Program Operation

Because there is an interdependency between displacements and subbase frictional force, the computer program would normally require an iterative algorithm. However, since the elastic soil stiffness applies only to a very small amount of displacement (0.002 inch), actual soil friction is almost entirely inelastic for any practical range of slab movement. Therefore, the program operates under the assumption that all slab displacements result in inelastic friction. This assumption causes minor changes to Fig 4.5; the diagonal portions of the force-displacement curve become vertical. This simplifying assumption still allows for very close prediction of slab movements. (The results of program calibration using actual field data are presented in Chapter 5).

The basic operation of the computer program follows a linear procedure:

- (1) External forces are computed;
 $\{[P_s]_{ip}, [P_p]_n, [P_{\Delta T}]_{ip}\}$
- (2) Stiffnesses are computed;
 $\{[K_c]_{ip}, [K_s]_{ip}, [K_p]_n\}$
- (3) Displacements are determined;
- (4) Stresses are determined.

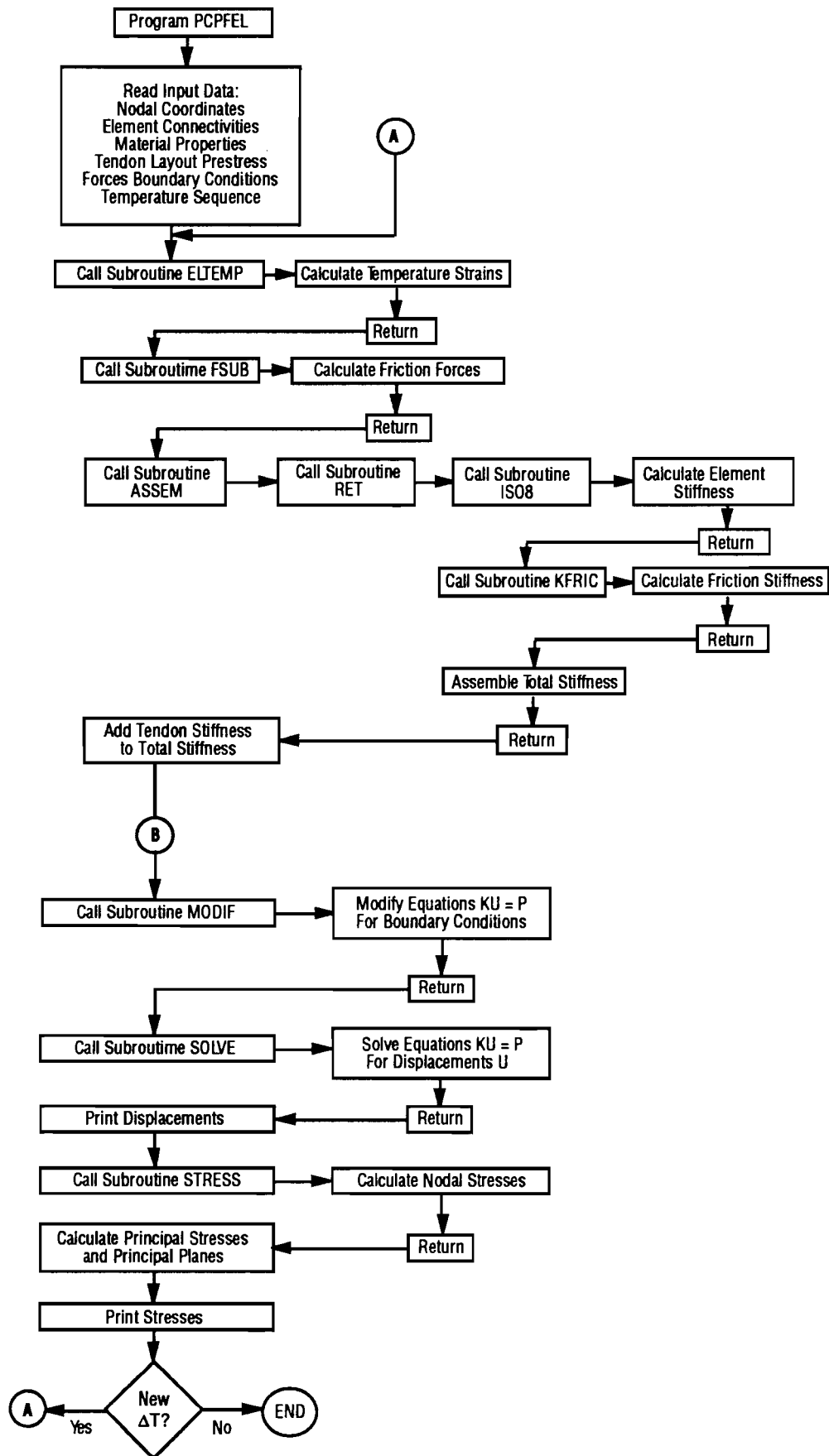


Fig 4.9. Flow chart for the program PCPFEL1.

The procedure continues for all desired increments of temperature, ΔT . The flow chart in Fig 4.9 outlines this procedure in greater detail.

The computer program solves for displacements [U]. These displacements can be compared directly with the

average measured displacements presented in Chapter 3 and Appendix A. By adjusting the components of Eq 4.1, the program can be calibrated to the measured displacements. The method of calibration for the model is described in Chapter 5.

CHAPTER 5. MODEL IMPLEMENTATION

The use of the computer model for PCP (PCPFEL1) is described in this chapter, and user guidelines are outlined. The model is implemented in three studies: a determination of finite element mesh fineness requirements, a calibration of the model to the measured response of the PCP prototypes, and an analysis of stress concentrations around central stressing blockouts. The method of analysis is presented for each study, along with the results.

PROGRAM PCPFEL1

User Interface

The input to program PCPFEL1 requires that the user specify the geometry of the investigated problem, the material properties of the components of the problem, the boundary conditions, and the sequence of concrete temperatures being considered. The geometry of the problem is defined by three input categories: nodal coordinates, element connectivities, and tendon configurations. Each node is assigned a "global" number and is given a location defined by specifying coordinates in a Cartesian plane, where the first coordinate represents the location in the longitudinal direction and the second coordinate represents the location in the transverse direction. Element connectivities are defined by correlating the element nodal numbering system (shown in Fig 4.7) to the global numbering system. For example, if two elements are connected side-by-side, element nodes 2, 6, and 3 of the left element will be assigned the same respective global number (and corresponding coordinates) as element nodes 1, 8, and 4 of the right element. The program keeps track of the element connectivities when determining nodal displacements and stresses so that these actions are compatible for adjacent elements, therefore allowing the entire array of elements to behave as a continuous mesh. The tendon layout is specified by assigning initial forces at nodes, along with the length of the tendon. The sign convention for the forces follows the convention of the Cartesian plane used for nodal coordinates.

Material properties are specified either for the entire mesh or for the individual components of the model, depending on the applicability of the property. The modulus of elasticity of the concrete is specified for each element so that concrete stiffness can be varied through the mesh (for example, at post-tensioning pockets). The Poisson's ratio and coefficient of thermal expansion of the concrete and the stiffness curve for the subbase friction are specified for the entire mesh. The modulus of elasticity and the cross-sectional area of the tendons are specified for the nodes at which the tendons are anchored. The boundary conditions are applied by specifying the nodes for which fixed or free conditions exist. Finally, the concrete temperature is applied evenly over the mesh and

is specified by listing the input temperatures in time sequence.

The program output includes an echo print of all input data and the computed results. The first cycle of output gives nodal displacements and stresses just after the prestress is applied, with no change in temperature. Subsequent cycles of output correspond to the sequence of input temperatures, where displacements do not include initial displacements from stressing operations, but stresses include both thermal and prestress effects. Displacements for all nodes are listed for every cycle, but only stresses for specified elements are listed, so that the user can focus on stresses in specific regions of the mesh if so desired. The stresses given by the program include the effect of varying prestress forces due to tensioning or relaxation of tendons as a result of slab displacements. The current status of tendon forces is included in each output cycle. More specific information regarding the program is available directly from the authors.

User Guidelines

In order to effectively model PCP using the finite element methods developed in Chapter 4, the user is

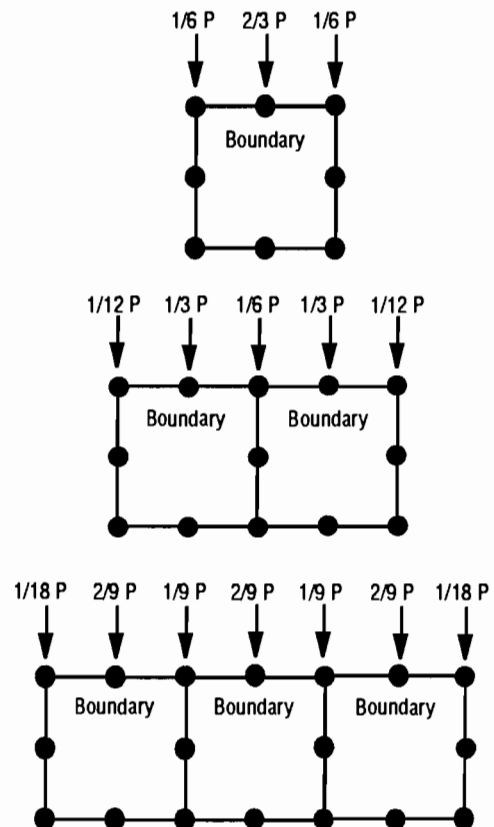


Fig 5.1. Consistent nodal forces for a total externally applied load P .

required to use engineering judgement in defining the particular aspect of PCP to be investigated, in adapting the model to that definition, and in specifying input to computer program PCPFEL1. The model provides a means for numerically representing a limitless range of problems for which the primary restriction would be the memory capacity of the computer. This versatility is inherent in the model because both geometric and material parameters are specified by the user and can be arranged to accommodate the particular situation to be investigated.

The accuracy of results depends on several conditions, which include (but are not limited to) the number of elements used to formulate a mesh of particular dimensions (i.e., the fineness or coarseness of the mesh), the method of application of tendon forces, and the sensitivity of the mesh to certain material parameters. The required fineness of a mesh for a particular investigation should be determined before the model is implemented in a formal analysis. This required fineness can be determined by formulating several trial meshes with increasing numbers of elements. As the number of elements is increased, the solutions given by the program (displacements and stresses) should become closer to the true solution; the resulting displacements for the same geometric location in the mesh should approach a constant value. In addition, since the concrete is assumed to remain linear-elastic, stresses at nodes calculated from adjacent elements should approach equality for increasingly finer meshes. The first study in the following section of this chapter shows the method for the determination of the required fineness of a mesh in greater detail.

The method of application of the tendon forces at the nodes must be consistent with the sensitivity of the nodes to which it is applied. If there are enough nodes on a boundary to accommodate all tendon forces applied on that boundary, then the actual magnitudes of the forces can be applied at the nodes, and the actual area of the tendons can be assigned to the nodes. But, if there are fewer nodes than required tendon forces on a boundary, the tendon forces must be lumped at nodes in accordance with nodal sensitivity for an 8-node isoparametric element (consistent nodal forces must be used). Figure 5.1 shows the distribution of a total applied force, P , required for an even level of stress in the elements for a one, two and

three-element boundary. Boundaries with more than three elements can be handled similarly. The distribution of the tendon cross-sectional areas should be assigned to boundary nodes in the same proportion as the distribution of tendon forces (assuming that all tendons have the same area). This will allow the tendon stiffnesses to have an even contribution to the total stiffness of the model.

The sensitivity of the mesh to material parameters can be determined only through the observation of changes in results caused by changes in material properties. For example, the effect of changes in the coefficient of thermal expansion might have varying influence on results for different subbase frictional stiffnesses or for different concrete elastic moduli. Similarly, frictional stiffness might have varying influence on results if other material parameters are varied. The material sensitivity for a particular problem can be realized only through experience with the program. It is an important effect, however, and should be considered before relying on results.

STUDIES USING PROGRAM PCPFEL1

Three studies have been conducted using PCPFEL1. The first study is a determination of required mesh fineness for modelling the McLennan County PCP. The second study is a calibration of the program using the field data collected in the instrumentation program (Chapters 2 and 3). The final study is an investigation of stress concentrations around central-stressing pockets.

Mesh Fineness

The required fineness of mesh for an accurate analysis was determined by running four trial meshes. The number of elements for each mesh was increased from 6 to 11, to 24, and finally to 44. The trial meshes are shown in Fig 5.2; they represent dimensions and boundary conditions that would be used to model the 440-foot slabs for the McLennan County PCP. A 100°F temperature change was induced for each mesh, and displacements at the right end were then compared. In addition, longitudinal stresses at nodes between the two elements furthest to the left, calculated from each of the elements, were compared. Table 5.1 summarizes the results of this study. The results show excellent consistency for all trial meshes. This is not unexpected, since an element with nine integration points

TABLE 5.1. RESULTS OF STUDY OF MESH FINENESS REQUIREMENTS

	Number of Elements			
	6	11	24	44
[Displacement at End of Slab]				
[Displacement at End of Slab for 6 Element Mesh]	1.000	1.000	1.000	1.000
[Nodal Stress from One Element]				
[Nodal Stress from Adjacent Element]	0.997	0.998	1.000	1.000

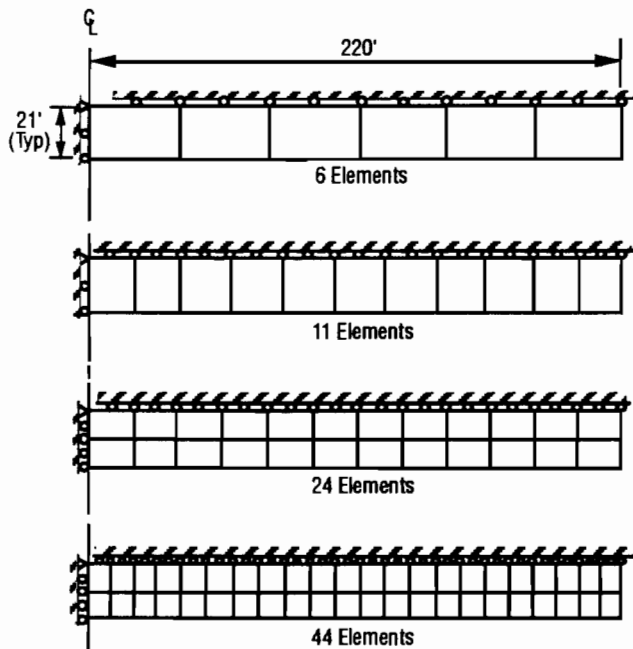


Fig 5.2. Meshes used for the determination of fineness requirements.

is quite sensitive; numerical integrations are sufficiently accurate for even a coarse mesh.

Program Calibration

The computer program has been calibrated to the field data collected from the McLennan County PCP. The calibrated model allows for the prediction of displacements and stresses for future investigations into PCP. The calibrated model also allows for the back-calculation of material properties of PCP for which displacements have been measured.

The first step in program calibration was to define which material properties were to be considered as "fixed" or "known," and which properties were "unknown." The modulus of elasticity of the concrete was considered to be known, since material tests were performed on concretes of similar mix design (Ref 10). A value of 3,958 ksi for the modulus of elasticity of concrete was used for calibration. The modulus of elasticity of the tendons was considered to be fixed at 28,000,000 psi, and the Poisson's ratio of the concrete was considered to be fixed at 0.2. The coefficient of thermal expansion had been determined to be equal to 5.44×10^{-6} inch/inch/ $^{\circ}$ F for concrete that contained a similar coarse aggregate (Ref 18), but the displacements measured in the field could not be duplicated by the model using this value. This value for the thermal coefficient requires a subbase frictional force of restraint that is not physically possible in order for the measured displacements to be matched. Therefore the coefficient of

thermal expansion was considered to be unknown and was expected to be slightly lower than the value determined in Ref 18. The subbase frictional force of restraint, although measured experimentally in Ref 7, was considered to be inherently variable and was, therefore, considered to be unknown.

Since the only two unknowns for program calibration were the coefficient of thermal expansion and the force of frictional restraint, there was a direct interdependency between these two parameters. An infinite number of combinations of these values (within bounds) could be used to achieve equality between measured and calculated values of displacements at the end of the slabs. Only one of these combinations of values, however, could give a best fit between the measured and calculated values for displacements at the third and sixth points, in addition to the ends of the slabs. The method of calibration was based on this principle.

Calibration of the model was performed on the 44-element mesh shown in Fig 5.2. Running time for one temperature change was about 9.5 TM seconds on the CDC dual cyber 370/750 computer of The University of Texas at Austin, where the TM second is calculated by adding 1.6 times CPU seconds and 0.4 times I/O seconds. Equivalent nodal forces were used at the right end of the mesh to represent longitudinal tendon forces: 11 tendons at 39.5 kips. Transverse tendon forces of 39.5 kips were applied on the lower boundary of the mesh at locations that produce the same stress as that of the prototype slabs (even though these forces were not expected to affect calibration). The regression equations calculated in Chapter 3 (Table 3.1) were used as the basis for calibration. Average slopes from these equations were used to determine the average measured changes in slab displacements for the joint, sixth point, and third point locations. The procedure followed for calibration involved solving for the values of the thermal coefficient and the frictional force that would allow the model to reproduce displacements produced by the average regression slopes.

The following steps outline the procedure that was used for calibration:

- (1) A force of frictional restraint (per unit area) was assumed.
- (2) By trial and error, the corresponding coefficient of thermal expansion that allowed the program to produce the measured displacement for a temperature change of 50° F (determined from the average slope of the regression equation) for the end of a 440-foot slab was determined.
- (3) Using the force of frictional restraint from (1) and the coefficient of thermal expansion from (2), displacement at the slab ends, sixth point, and third point were calculated for a 50, 40, 30, 20, and 10° F temperature change.

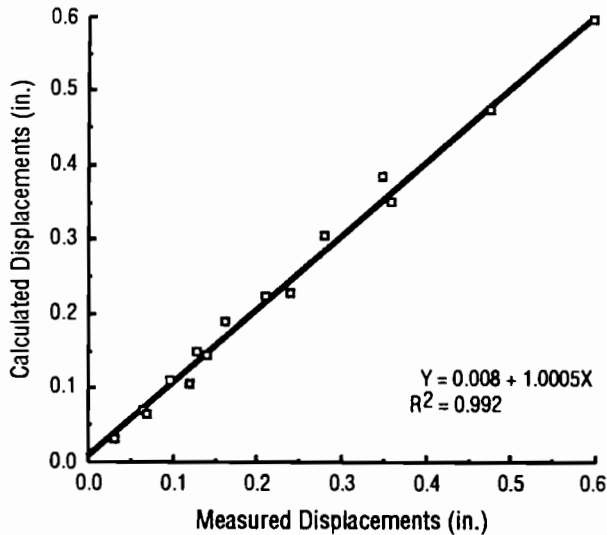


Fig 5.3. Calculated displacements produced by the calibrated model versus measured displacements.

- (4) The measured displacements were plotted versus the calculated displacements, and a regression equation was calculated.
- (5) Steps 1 through 4 were repeated for a new force of frictional restraint.

This procedure was repeated for an array of friction forces corresponding to coefficients of subbase friction that range from 0.18 to 0.5. The result was an array of regression equations from which the correct combination of friction force and thermal coefficient could be determined. The equation with a slope closest to 1.0, a Y-intercept closest to 0.0, and an R^2 value closest to 1.0 would correspond to the the correct combination. After observation of the values, there were two candidate combinations of the frictional force and thermal coefficient. Therefore, these values were tested on a mesh for the 240-foot slabs and were compared to the average measured displacements calculated from the average slope of the regression equations for the 240-foot slabs. The best fit between the two candidate values for the 240-foot slabs was considered to give the final and correct values of friction force and coefficient of thermal expansion. The final fit of the calibrated model output to the field data is shown in Fig 5.3.

The thermal coefficient of expansion that corresponds to the best data fit is 4.59×10^{-6} inch/inch/ $^{\circ}$ F, which compares well with 4.8×10^{-6} and 5×10^{-6} inch/inch/ $^{\circ}$ F determined from the data analysis in Chapter 3. The corresponding value of force of frictional restraint gives a coefficient of friction, μ , of 0.2. This value is significantly lower than the values of 0.45 and 0.4, which were determined through push-off experiments (Ref 7). However, it is exactly the same as the value determined in Ref 5

through back-calculation from previous measurements of displacements for the McLennan County PCP. A possible explanation for the lower value is that the push-off experiments in Ref 7 were conducted on small test slabs of which the only displacements occurred during the experimental procedure, whereas displacements of the actual PCP occur on a daily basis. Abrasion between the pavement and the subbase might have caused the coefficient of friction to decrease over time. For design purposes, it would be conservative to use the higher coefficient of friction for the the determination of expected stresses. The lower coefficient of friction also influences the determination of expected displacements (higher friction coefficients produce lower displacements). This should be taken into account when predicting slab displacements.

Stress Concentrations

An investigation of stress concentrations was carried out in response to cracking that was observed in the field. Cracking has occurred around the pocket locations that were used for stressing the tendons. Typical observed cracking patterns are shown in Fig 5.4, and photos of representative cracks are shown in Figs 5.5 and 5.6. The exact cause of the cracking is not immediately apparent; this study is based on the hypothesis that one cause may be that the interruptions in the tension field in the center region of the slabs caused by the pockets have created tensile stress concentrations. The computer model has been used to simulate and analyze this situation.

The method of analysis for this problem was complicated by computer memory limitations. The CDC computer mentioned earlier could not handle a mesh that both covered an entire PCP slab and was fine enough to model the comparatively small dimensions of the pockets. Therefore, a reduced mesh with a level of stress equivalent to the center region of a PCP slab had to be used. The equivalent level of stress was determined by running the program for a full-size mesh and using the resulting stresses as the initial conditions for the reduced mesh. The values of frictional restraint forces and tendon forces were adjusted on the reduced mesh until the state of stress at the center region of the full mesh and the state of stress for the entire reduced mesh were equivalent. Both meshes are shown in Fig 5.7. Consistent nodal forces were used to model the tendon forces. After the stress equivalency was established, the effect of the pockets was accomplished by adjusting the modulus of elasticity for elements that were in the pocket location; a value of 0.0 was used to simulate an empty pocket (for analysis of tendon stressing operations), and a high value was used to simulate a filled pocket (for analysis of post-construction thermal action). This technique created the disturbance to the stress field that was necessary in order to analyze stress concentrations.

The analysis had to consider the stress history of a slab since material properties were rapidly changing during the period of post-tensioning (the first three days of the life of the pavement). Therefore, the investigation was carried out in five stages, reflecting the staged stressing procedure used during construction. Table 5.2 lists and describes the stages of analysis. Tendon forces shown take into account an assumed 15 percent loss of prestress (Refs 6 and 11). Figure 5.8 shows the types of stresses that were calculated by the program (principal tensile stress shown as positive). The longitudinal and transverse stresses are labelled σ_x and σ_y , respectively, and the principal stresses are σ_1 and σ_2 . The orientation of the principal plane is θ_p , and it is also shown as positive in Fig 5.8.

Table 5.3 lists the results of the analysis. The stresses for the full mesh are for a node that is located 3.5 feet from the centerline of the pavement. The stresses for the reduced mesh are at the upper right corner of a pocket (pocket location shown in Fig 5.7). The values of the concrete modulus of elasticity (E_c) and tensile strength (f_t) are listed for their appropriate magnitudes at the particular stage of analysis (Ref 10).

The maximum principal tensile stress has not exceeded the tensile capacity of the concrete for any load stages according to this analysis. Only the second stage of the analysis exhibits tensile stress in the concrete, but the magnitude is less than half of the tensile capacity of the concrete (61.88 psi tensile stress versus 223 psi tensile capacity). Accordingly, no cracks around the pockets were reported to occur during stressing operations. The principal plane at the second stage of analysis is close to the crack orientations observed in the field (26.99° calculated versus about 30° observed in the field). The orientations of the principal plane and the observed crack angle are shown in Fig 5.9. The maximum principal stress at a location 17 inches away from the pocket corner (but located close to the principal plane of 26.99°) was +18.22 psi acting on a principal plane of 24.21° . These results seem to indicate that the stress concentrations due to the pockets might contribute to the cause of the cracks but that other factors are probably involved. These factors might be (but are not limited to) the result of a combination of the following situations:

- (1) Several pockets are closely spaced in the center region of the slabs. Actual stress concentrations may be due to a combined effect of more than one pocket.
- (2) Wheel load stresses are subject to the same stress concentrations as thermal stresses. The effect of wheel loads is not simulated by the model.
- (3) The combination of fatigue and stress concentration effects might be important. A condition survey of the experimental section (Ref 1) has revealed that the most cracking occurs in the right traffic lane - the lane with the heaviest use.

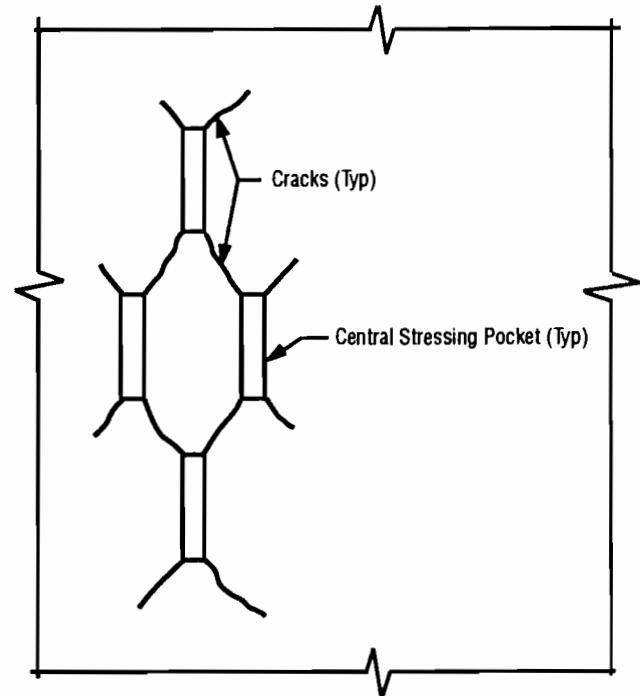


Fig 5.4. Typical observed cracking patterns around central stressing pockets.

- (4) Both the material properties of the concrete and the physical parameters in the model (frictional resistance) are variable. This model is based on average or assumed values; actual field conditions may be less favorable.

SUMMARY

A finite element model for PCP that gives stresses and displacements due to changes in temperature and prestress has been developed. User guidelines have been presented as well as input-output requirements. The model gives good precision using as few as six elements (more than six elements may be required for the modeling of special conditions in the slabs).

The model was calibrated to reflect measured conditions in the field. A coefficient of thermal expansion for the concrete was determined to be equal to 4.59×10^{-6} inch/inch/ $^\circ$ F, and the coefficient of friction of the subbase was determined to be 0.2. These values allow the model to closely predict measured displacements as indicated in Fig 5.3.

An investigation of stress concentrations caused by stressing pockets was performed. The study indicates that cracking that has been observed to propagate from the corners of the pockets has not been caused by thermal stresses alone, but rather by a combination of effects (possibly superposition of thermal stress and fatigue).

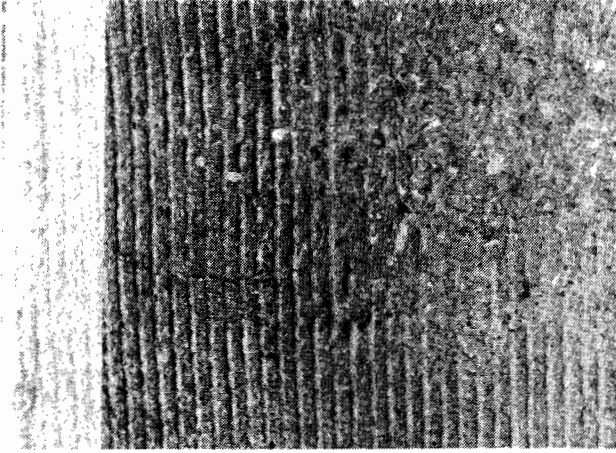


Fig 5.5. Crack propagating from the corner of a pocket.

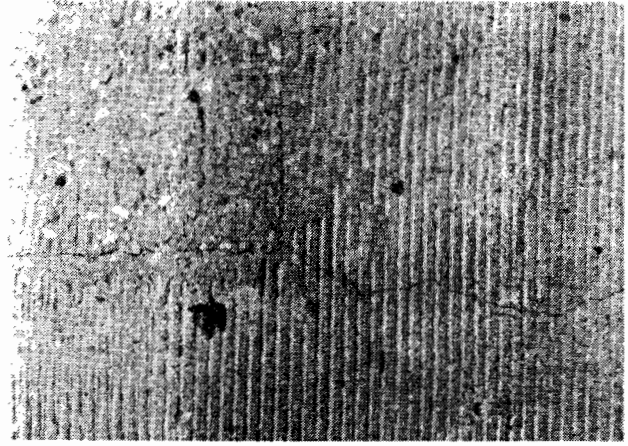


Fig 5.6. Crack propagating from the corner of a pocket.

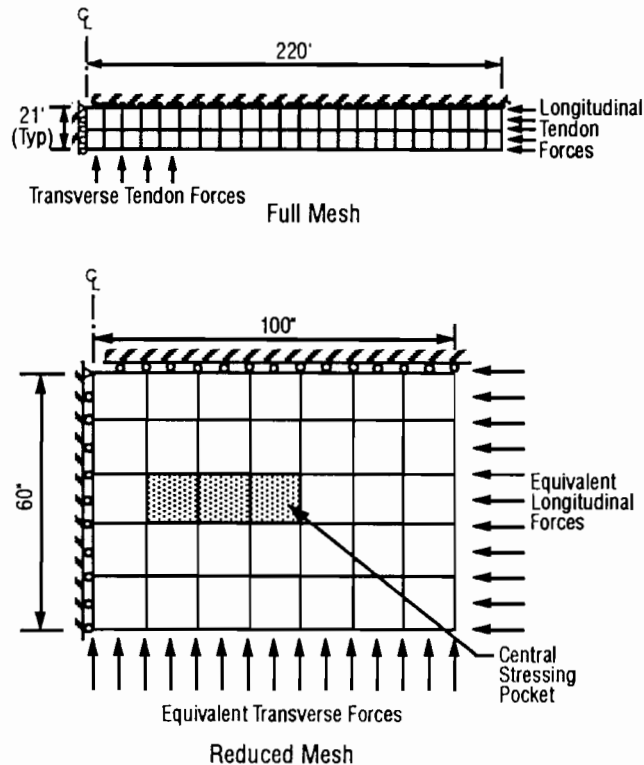


Fig 5.7. Meshes used for stress concentration analysis.

Although thermal stress alone has not caused cracking, it was determined to play a role because of the similarity between measured principal cracking plane and observed cracking plane (26.99° versus $\approx 30^\circ$).

The analysis of stress concentrations clearly shows that a higher tensile stress exists in a slab with pockets than for one without pockets (+61.88 psi with pockets vs. +1.28 psi without). This is supported by field observation; no cracking has occurred in the center region of the slabs

except at the pocket locations. Since the maximum tensile stress at the pocket corners never exceeds the tensile capacity of the concrete, the influence of fatigue and wheel loads on crack development is validated. It should be noted that the cracks are not structurally significant at this time; they have not caused any further distress and do not affect the serviceability of the pavement. Additionally, the transverse prestressing has been crucial to the control of the extent of cracking. Without the transverse tendons, the

TABLE 5.2. ANALYSIS STAGES FOR STRESS CONCENTRATION INVESTIGATION

Stage of Analysis	Description
1	Analysis of stresses for the first level of stressing: 14.0 kips per tendon (low level tensioning on 12-hour-old concrete; open pockets)
2	Analysis of stresses during the first cooling cycle: temperature decrease of 50°F (open pocket), 14.0 kips per tendon
3	Analysis of stresses for the final level of stressing: 39.5 kips per tendon (full tensioning on 60-hour-old concrete; open pockets)
4	Analysis of stresses during the third cooling cycle: temperature decrease of 50°F (open pocket), 39.5 kips per tendon
5	Analysis of stress for the current material conditions (filled pockets), 39.5 kips per tendon

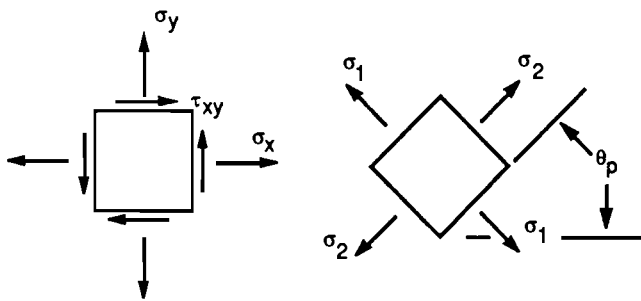


Fig 5.8. Positive stresses, principal stresses, and principal plane for program output.

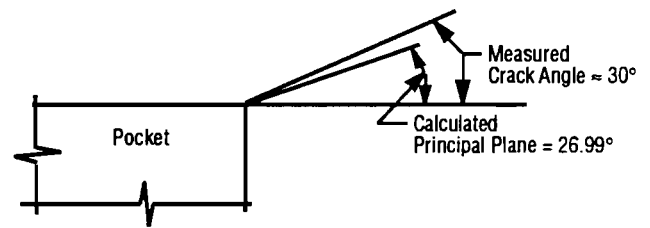


Fig 5.9. Orientation of calculated principal plane and observed crack angle.

cracks would have been wider and could have triggered further damage.

In response to the cracking observed in the field, it is recommended that steel reinforcement be used at the corners of the pockets (crossing potential crack paths) for any future PCP that uses the central stressing technique. The recommended placement of the reinforcement around the pockets is shown in Fig 5.10, where L_d is the development length of a reinforcing bar. Since an exact numerical value for the tensile stress that is causing the cracks was not determined from this analysis, the amount of steel should be based on conservative engineering judgement. Corner bars of this type are often used at the corners of openings in slabs, and they are quite effective in the control of cracks. No. 4 or No. 5 bars in the positions shown in Fig 5.10 should be satisfactory for a 6-inch slab.

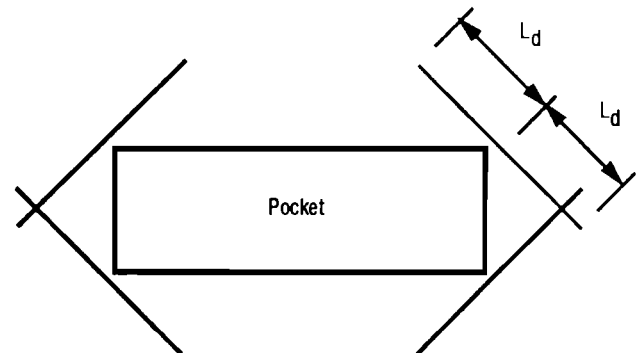


Fig 5.10. Recommended placement of reinforcement around pocket.

TABLE 5.3. RESULTS OF STRESS CONCENTRATION ANALYSIS

<u>Mesh</u> (Fig 5.7)	<u>Stage of</u> <u>Analysis</u> (Table 5.2)	<u>Time</u> (Hours)	<u>E_c</u> (psi)	<u>f_t</u> (psi)	<u>σ_x</u> (psi)	<u>σ_y</u> (psi)	<u>τ_{xy}</u> (psi)	<u>σ₁</u> (psi)	<u>σ₂</u> (psi)	<u>θ_p</u> (degrees)
Full	1	12	2590	188	-101.9	-19.4	0.0	-19.4	-101.9	0.0
Full	2	17	2785	223	+1.3	-19.6	0.0	+1.3	-19.6	0.0
Full	3	60	3645	312	-287.4	-54.9	0.0	-54.9	-287.4	0.0
Full	4	65	3690	317	-184.2	-55.0	0.0	-55.0	-184.8	0.0
Full	5	10,000	3960	484	-183.1	-55.0	0.0	-55.0	-183.1	0.0
Reduced	1	12	2590	188	-529.9	-149.7	-227.1	-43.6	-636.0	25.0
Reduced	2	17	2785	223	+6.7	-151.0	+108.4	+61.9	-206.2	27.0
Reduced	3	60	3645	312	-1494.3	-422.4	-641.0	-122.9	-1793.9	25.1
Reduced	4	65	3690	317	-957.8	-423.8	-642.7	-15.3	-1386.7	33.7
Reduced	5	10,000	3960	484	-955.9	-423.4	-642.4	-25.8	-1385.0	33.7

CHAPTER 6. CONCLUSIONS AND RECOMMENDATIONS

This chapter outlines the final conclusions of this study. The conclusions are organized into three categories: instrumentation, data analysis, and modelling. Recommendations based on field observations and analysis are proposed.

INSTRUMENTATION

The instrumentation program for this study was highly successful. The collected data indicated trends that were in direct parallel with expected results. No disturbance from extraneous sources was detected, and the final data exhibited a high degree of consistency. The outcome of the instrumentation program justifies the following conclusions:

- (1) The method of using buried anchors to support instrumentation worked well. The supports were extremely stable and therefore provided a reliable foundation for the equipment. Furthermore, the anchors provided convenience for the installation of instrumentation for each field visit. Dowels supporting the instruments could be inserted into the anchors during measurement periods and could then be removed and stored. In addition, the anchors currently remain in the field, hidden from view, but can be easily accessed if future measurements are required.
- (2) The method of measuring displacements worked well. Both the dial gages and LVDT's gave consistent and identical results. The two-hour time period between measurement readings was frequent enough to characterize movements but still allowed enough time to gather a large amount of data.
- (3) The method of measuring temperatures worked well. The thermocouples gave accurate and consistent temperatures. They currently remain inserted in the pavement and are covered with waterproof caulking compound. They can be accessed in the future if necessary.
- (4) The method of measuring joint widths worked well. Dial calipers were easy to use, and gave joint widths that closely corresponded to measured horizontal movements of the slabs. Measuring joint widths at scribe marks allowed for the direct comparison of measurements between all field visits.

The following recommendations result from experiences that were encountered either during data collection or as a result of analysis that depends on instrumentation. They are offered as guidelines for any instrumentation program that is designed to measure phenomena similar to those in the program for this study:

- (1) The exact effect of moisture level on magnitudes of displacement was not quantified in this study.

Future instrumentation programs that investigate environmental effects on pavement should consider the importance of measuring moisture level at different depths in the concrete. The acquiring of moisture level data in parallel with the measurement of temperatures and displacements could reveal effects that are currently unknown (for example, the thermal transmissivity of dry versus moist concrete, and their interactive effects on slab warping).

- (2) The construction program for experimental prototypes should include a major consideration of subsequent determination of material properties. A large sample of material specimens (cylinders, material-test beams, etc.) should be made at the time of construction so that material properties for long-term investigations can be determined directly.
- (3) The construction program for experimental prototypes should consider possible subsequent instrumentation. Installation of permanent equipment (supports, thermocouples, etc.) is a simple procedure at the time of construction but requires a significantly higher level of effort afterwards.

DATA ANALYSIS

The analysis of slab displacements for each slab length for a field visit allowed for the direct comparison of slab behavior for different seasonal conditions. The use of regression equations to characterize slab movements was helpful in comparing the behavior of all slabs for all instrumentation locations. Furthermore, the error analysis indicated that measurements were correct and quite accurate. The following points outline specific conclusions from the analysis of horizontal displacements:

- (1) The regression analysis of horizontal slab movements shows that displacements can be described by a linear equation. The slopes of the equations vary at close to a linear rate for displacements measured at the joints, the sixth points, and the third points. This indicates that almost the entire slab moves on a daily basis.
- (2) Average slopes of the regression equations can be used to predict slab movements as a function of temperature. For the 240-foot slabs, the average rate of movement was 5.89×10^{-3} inch/ $^{\circ}$ F. For the 440-foot slabs, the average rate of movement was 1.193×10^{-3} inch/ $^{\circ}$ F.
- (3) The analysis did not show a strong trend for different moisture conditions. This may have been because the slabs were not completely saturated.
- (4) Maximum and minimum measured joint widths were 1.397 inches and 0.263 inch for the 240-foot slabs, and 3.20 inches and 0.983 inch for the 440-foot slabs.

- (5) Overall seasonal behavior of the slabs indicates that daily fluctuations occur constantly, while the seasonal datum for the movements changes.
- (6) The consistency of slab movements for the entire study is quite high. Standard deviations of movements per change in temperature are 0.646×10^{-3} and 0.621×10^{-3} inch/ $^{\circ}$ F for the 240 and 440-foot slabs, respectively.
- (7) Error in joint width measurement was low. The maximum closure error between joint width measurements and horizontal displacement measurement was 0.056 inch. The average error was 0.012 inch.
- (8) The high consistency in slab movements indicates that the sample sizes for both the number of data collection field visits and the number of instrumented slabs were adequate for the characterization of slab movements.

The following recommendations result from the analysis of horizontal movements, as well as from field observations:

- (1) Although joint widths for the 240-foot slabs never reached a value of 0.0 inch at the measurement scribe marks, field observation revealed that some joints were completely closed for prolonged ambient temperatures in excess of about 100° F (no damage to the slabs or joint hardware has occurred). These joints were set closed at the time of construction so that initial shrinkage, creep, and elastic shortening of the concrete would not cause the joints widths to be excessive. In addition, the slabs were built during the afternoon hours in the mid-summer season (Ref 11) and were therefore assumed to be at a maximum seasonal datum for horizontal displacements at the time of construction. Apparently, less shortening of the slabs occurred during the early life of the slabs than was initially expected. Since maximum measurements of joint widths for the 240-foot slabs were 1.397 inches, well within serviceability limits (about 3.5 inches), there is a wide margin of safety against excessive joint widths. An initial joint width of 0.5 inch for a 240-foot slab (otherwise constructed under similar conditions) would prevent the joints from completely closing.
- (2) The joints for the 440-foot slabs always remained within serviceable limits. These joints were also set closed at the time of construction. No change is recommended for the initial setting of joints for these slabs.

MODELLING

Conclusions on modelling of PCP are based on the finite element model developed in this report, the calibration of the model to field data, and the use of the model for analysis.

- (1) The finite element method provides a two-dimensional technique for modelling PCP that can perform a detailed analysis of displacements and stresses.
- (2) The use of an eight-node isoparametric element with nine integration points gives results that are reliable, even for a relatively coarse mesh.
- (3) The assumption of linear-inelastic behavior for subbase friction between the slab and one layer of polyethylene sheeting provides a close fit for calibration of the model. This is not unexpected since previous investigations on the behavior of subbase friction show that inelastic behavior occurs after 0.002 inch of slab displacement.
- (4) The calibration of the model depended on the displacement measurements at the third and sixth points of the slabs. Several combinations of thermal coefficient of expansion and subbase force of frictional restraint could produce correct displacements at the end of a slab, but only one combination could provide the closest fit to the data for the entire length of a slab.
- (5) Calculated values of coefficient of thermal expansion and coefficient of subbase friction were 4.59×10^{-6} inch/inch/ $^{\circ}$ F (as opposed to a value of 5.44×10^{-6} inch/inch/ $^{\circ}$ F, determined from concrete with a similar coarse aggregate) and 0.2, respectively. The lower value of coefficient of subbase friction than was determined in Ref 7 (0.4 to 0.45) is likely due to the fact that movements of the slabs occur on a daily basis, whereas the movements for the investigative experiments occurred only at the time of observation. Abrasion of the slab against the subbase is likely to play a role in reducing the coefficient of friction over time.
- (6) Results of an analysis of stress concentrations around central stressing pockets indicate that cracking is not due to thermal effects alone. The calculated principal stress at all stages of construction never exceeded the tensile capacity of the concrete (accordingly, no cracking was reported at the time of construction). However, calculated principal planes were close to observed crack angles. This indicates that, even though thermal stresses are not the sole cause of the cracking, they do play a role. Other causes of the cracks are likely to be related to fatigue effects of wheel loads.

The following recommendations are offered as the result of using the finite element technique to create and simulate thermal action of PCP. In addition, some general recommendations related to modelling PCP are proposed.

- (1) Due to the inherent complexities of finite element analysis, the use of the program developed in this study, PCPFEL1, should be limited to those who

have received at least a cursory training in the use of the finite element technique. The input-output aspect of the program is not difficult to master, but the proper formation of meshes, as well as the correct interpretation of results, requires some introductory training in finite elements.

- (2) Computer program PCPFEL1 analyzes thermal effects on PCP. The model serves as a basis for other in-depth analyses. It can be modified to adapt to several phenomena, and it is recommended that the

model be considered for other types of analysis, other than just thermal action. Other possible effects that can be modelled with finite elements include slab curling and wheel loads.

- (3) In response to observed cracking around central stressing pockets, reinforcement should be placed around the pockets for any future PCP that uses the central stressing technique. This reinforcement would provide additional tensile capacity at the pocket corners and should prevent the cracking.

REFERENCES

1. Mandel, Elliott, Jose Tena-Colunga, and Kenneth Hankins, "Performance Tests on a Prestressed Concrete Pavement—Presentation of Data," Research Report 556-1, Center for Transportation Research, The University of Texas at Austin, November 1989.
2. Tena-Colunga, Jose Antonio, B. Frank McCullough, and Ned H. Burns, "Analysis of Curling Movements and Calibration of PCP Program," Research Report 556-3, Center for Transportation Research, The University of Texas at Austin, November 1989.
3. O'Brien, S. J., Ned H. Burns, and B. Frank McCullough, "Very Early Post-Tensioning of Prestressed Concrete Pavements," Research Report 401-1, Center for Transportation Research, The University of Texas at Austin, June 1985.
4. Cable, N. D., Ned H. Burns, and B. Frank McCullough, "New Concepts in Prestressed Concrete Pavement," Research Report 401-2, Center for Transportation Research, The University of Texas at Austin, December 1985.
5. Mendoza-Diaz, A., Ned H. Burns, and B. Frank McCullough, "Behavior of Long Prestressed Pavement Slabs and Design Methodology," Research Report 401-3, Center for Transportation Research, The University of Texas at Austin, September 1986.
6. Maffei, J. R., Ned H. Burns, and B. Frank McCullough, "Instrumentation and Behavior of Prestressed Concrete Pavements," Research Report 401-4, Center for Transportation Research, The University of Texas at Austin, November 1986.
7. Chia, W. S., B. Frank McCullough, and Ned H. Burns, "Field Evaluation of Subbase Friction Characteristics," Research Report 401-5, Center for Transportation Research, The University of Texas at Austin, September 1986.
8. Dunn, B. W., Ned H. Burns, and B. Frank McCullough, "Friction Losses in Unbound Post-Tensioning Tendons," Research Report 401-6, Center for Transportation Research, The University of Texas at Austin, November 1986.
9. Chia, W. S., Ned H. Burns, and B. Frank McCullough, "Effect of Prestress on the Fatigue Life of Concrete," Research Report 401-7, Center for Transportation Research, The University of Texas at Austin, November 1986.
10. Lu, J., "Recommendations of Model Based on Various Criteria," Technical Memorandum 422-40, Center for Transportation Research, The University of Texas at Austin, September 19, 1988.
11. Hankins, K., "Visit to Waco to Obtain Prestressed Paving Information," Technical Memorandum 556-8, Center for Transportation Research, The University of Texas at Austin, September 19, 1988.
12. Stott, J. P., "Tests on Materials for Use as Sliding Layers Under Concrete Road Slabs," Road Research Laboratory, *Civil Engineering*, Vol 56, 1961.
13. Zienkiewicz, O. C., *The Finite Element Method*, 3rd Edition, McGraw-Hill, Ltd., London, 1977.
14. Weaver, W., and P. R. Johnston, *Finite Elements for Structural Analysis*, Prentice-Hall, Inc., Englewood Cliffs, New Jersey, 1984.
15. Mandel, E. D., "Instrumentation Summary for the PCP Overlay," Technical Memorandum 556-17, Center for Transportation Research, The University of Texas at Austin, February 1, 1989.
16. Mandel, E. D., "Data Acquisition System Set-Up," Technical Memorandum 556-18, Center for Transportation Research, The University of Texas at Austin, February 1, 1989.
17. Mandel, E. D., "Record of Field Work," Technical Memorandum 556-19, Center for Transportation Research, The University of Texas at Austin, February 1, 1989.
18. Castedo, H., "Summary of Laboratory Test Results Phase I and II - Project 422," Technical Memorandum 422-47, Center for Transportation Research, The University of Texas at Austin, January 16, 1989.

APPENDIX A. TABLE OF AVERAGE HORIZONTAL SLAB DISPLACEMENTS

Average values of horizontal slab displacements for all field visits are listed in the following table. These values are plotted in Figs 3.1 through 3.6. The model presented in Chapter 4 is calibrated to the values in the table.

TABLE A.1. AVERAGE VALUES OF HORIZONTAL SLAB DISPLACEMENTS

Time (hr:min)	Ambient Temp. (°F)	Concrete Temp. (°F)	Horizontal Displ. of 240' slab joint (inches)	Horizontal Displ. of 240' slab 1/6 point (inches)	Horizontal Displ. of 240' slab 1/3 point (inches)	Horizontal Displ. of 440' slab joint (inches)	Horizontal Displ. of 440' slab 1/6 point (inches)	Horizontal Displ. of 440' slab 1/3 point (inches)
[Field Visit 2 - July 26, 1988]								
16:00	107.132	111.803	0.000	0.000				
18:00	106.556	110.615	-0.002	0.002				
20:00	91.472	102.758	-0.017	-0.093				
22:00	85.226	97.673	-0.049	-0.170				
0:00	80.798	93.227	-0.081	-0.236				
2:00	80.258	89.627	-0.107	-0.281				
4:00	79.106	87.305	-0.122	-0.304				
6:00	76.100	84.317	-0.139	-0.338				
8:00	87.782	83.399	-0.142	-0.350				
10:00	88.700	90.815	-0.100	-0.259				
12:00	93.650	101.057	-0.028	-0.126				
[Field Visit 3 - August 6, 1988]								
14:00	98.708	108.806	0.000	0.000				
16:00	100.904	112.577	0.010	0.036				
18:00	93.956	109.175	0.009	0.033				
20:00	88.385	102.587	-0.014	-0.110				
22:00	82.814	95.999	-0.053	-0.157				
0:00	80.474	92.201	-0.077	-0.200				
2:00	78.692	89.474	-0.098	-0.240				
4:00	77.306	87.638	-0.113	-0.268				
6:00	76.928	84.848	-0.126	-0.290				
8:00	85.496	84.515	-0.132	-0.295				
10:00	90.806	91.697	-0.086	-0.211				
12:00	100.094	101.651	-0.025	-0.087				
14:00	102.326	112.037	0.007	0.026				
[Field Visit 4 - August 26, 1988]								
15:00	106.088	108.356	0.000	0.000				
17:00	102.938	106.754	-0.003	-0.001				
19:00	94.118	102.596	-0.021	-0.059				
21:00	86.180	96.854	-0.055	-0.134				
23:00	84.146	92.984	-0.083	-0.185				
1:00	81.554	90.626	-0.102	-0.221				
3:00	80.240	88.520	-0.118	-0.252				
5:00	74.066	86.414	-0.134	-0.281				
7:00	71.744	83.228	-0.149	-0.312				
9:00	84.542	83.372	-0.150	-0.311				
11:00	94.802	91.310	-0.097	-0.221				
13:00	99.140	99.986	-0.041	-0.101				
15:00	102.614	108.608	-0.004	-0.012				

(continued)

TABLE A.1. (CONTINUED)

Time (hr:min)	Ambient Temp. (°F)	Concrete Temp. (°F)	Horizontal Displ. of 240' slab joint (inches)	Horizontal Displ. of 240' slab 1/6 point (inches)	Horizontal Displ. of 240' slab 1/3 point (inches)	Horizontal Displ. of 440' slab joint (inches)	Horizontal Displ. of 440' slab 1/6 point (inches)	Horizontal Displ. of 440' slab 1/3 point (inches)
[Field Visit 5 - November 5, 1988]								
14:00	75.686	79.331	0.000	0.000	0.000	0.000	0.000	0.000
16:00	74.984	78.341	-0.004	0.000	0.000	-0.004	0.003	0.003
18:00	57.632	73.868	-0.042	-0.023	-0.014	-0.064	-0.030	-0.009
20:00	51.404	68.477	-0.078	-0.046	-0.028	-0.135	-0.079	-0.034
22:00	49.982	62.942	-0.104	-0.061	-0.036	-0.186	-0.112	-0.050
0:00	48.164	61.988	-0.122	-0.074	-0.043	-0.219	-0.132	-0.062
2:00	44.276	59.054	-0.138	-0.085	-0.048	-0.245	-0.151	-0.070
4:00	46.940	57.614	-0.154	-0.094	-0.053	-0.274	-0.169	-0.080
6:00	41.738	54.977	-0.163	-0.100	-0.055	-0.290	-0.180	-0.084
8:00	61.934	55.427	-0.168	-0.106	-0.056	-0.300	-0.190	-0.090
10:00	74.984	62.384	-0.124	-0.081	-0.041	-0.231	-0.155	-0.078
12:00	79.358	72.329	-0.058	-0.040	-0.018	-0.111	-0.076	-0.041
14:00	72.698	77.972	-0.014	-0.011	-0.004	-0.029	-0.019	-0.013
[Field Visit 6 - January 21-22, 1989]								
14:00	53.078	58.964	0.000	0.000	0.000	0.000	0.000	0.000
16:00	56.282	60.521	0.010	0.007	0.003	0.014	0.012	0.006
18:00	46.778	55.391	-0.016	-0.008	-0.006	-0.024	-0.005	0.002
20:00	44.384	50.189	-0.048	-0.027	-0.015	-0.085	-0.044	-0.017
22:00	35.096	46.947	-0.070	-0.042	-0.023	-0.128	-0.073	-0.031
0:00	38.480	44.042	-0.087	-0.052	-0.028	-0.161	-0.096	-0.042
2:00	27.392	41.900	-0.102	-0.062	-0.032	-0.187	-0.112	-0.050
4:00	30.002	40.235	-0.113	-0.069	-0.035	-0.209	-0.126	-0.057
6:00	29.882	39.707	-0.121	-0.073	-0.037	-0.222	-0.134	-0.061
8:00	43.898	37.535	-0.129	-0.078	-0.039	-0.236	-0.143	-0.065
10:00	54.500	42.674	-0.102	-0.064	-0.032	-0.194	-0.123	-0.060
12:00	58.622	52.223	-0.046	-0.029	-0.013	-0.084	-0.051	-0.026
14:00	58.568	59.945	0.001	0.000	0.000	-0.003	0.001	-0.002
16:00	57.740	61.178	0.016	0.013	0.005	0.024	0.023	0.010
18:00	49.640	56.003	-0.008	-0.003	-0.003	-0.011	0.007	0.005
20:00	49.478	52.304	-0.035	-0.020	-0.011	-0.057	-0.026	-0.011
22:00	48.002	50.954	-0.044	-0.027	-0.015	-0.073	-0.037	-0.017
0:00	44.366	49.073	-0.056	-0.036	-0.019	-0.099	-0.054	-0.025
2:00	41.252	47.678	-0.068	-0.041	-0.022	-0.116	-0.065	-0.030
4:00	41.378	46.382	-0.074	-0.047	-0.025	-0.129	-0.076	-0.036
6:00	46.184	44.978	-0.083	-0.051	-0.027	-0.142	-0.083	-0.039
8:00	44.330	45.194	-0.083	-0.051	-0.027	-0.143	-0.084	-0.040
10:00	52.862	47.912	-0.068	-0.044	-0.024	-0.121	-0.075	-0.038
12:00	59.450	53.240	-0.041	-0.028	-0.015	-0.074	-0.047	-0.025
14:00	64.220	60.701	0.011	0.004	0.002	0.017	0.013	0.003

(continued)

TABLE A.1. (CONTINUED)

Time (hr:min)	Ambient Temp. (°F)	Concrete Temp. (°F)	Horizontal Displ. of 240' slab joint (inches)	Horizontal Displ. of 240' slab 1/6 point (inches)	Horizontal Displ. of 240' slab 1/3 point (inches)	Horizontal Displ. of 440' slab joint (inches)	Horizontal Displ. of 440' slab 1/6 point (inches)	Horizontal Displ. of 440' slab 1/3 point (inches)
[Field Visit 7...February 9, 1989]								
14:00	48.236	51.377	0.000	0.000	0.000	0.000	0.000	0.000
16:00	51.026	53.375	0.016	0.010	0.005	0.028	0.021	0.011
18:00	42.926	49.172	-0.001	0.000	0.001	0.003	0.015	0.011
20:00	38.480	45.266	-0.027	-0.017	-0.007	-0.047	-0.015	-0.004
22:00	34.052	42.305	-0.048	-0.031	-0.013	-0.087	-0.041	-0.017
0:00	35.384	40.037	-0.064	-0.041	-0.018	-0.114	-0.059	-0.025
2:00	35.348	38.471	-0.074	-0.047	-0.021	-0.134	-0.073	-0.032
4:00	31.784	37.256	-0.082	-0.052	-0.023	-0.149	-0.082	-0.037
6:00	30.902	36.095	-0.088	-0.058	-0.025	-0.163	-0.091	-0.041
8:00	45.230	35.708	-0.094	-0.061	-0.026	-0.169	-0.096	-0.045
10:00	48.506	41.945	-0.062	-0.043	-0.018	-0.116	-0.073	-0.036
12:00	59.702	51.656	-0.005	-0.006	0.000	-0.006	-0.003	-0.003
14:00	62.870	59.117	0.044	0.026	0.015	0.080	0.052	0.023

APPENDIX B. GRAPHICS OF HORIZONTAL DISPLACEMENT VERSUS CONCRETE TEMPERATURE

The graphs in Figs B.1 through B.12 show measured slab displacements versus concrete temperature at mid-depth. The plots show curves for each instrumentation

location, as described by Fig 2.5. Each graph is for measurements from one slab size (240 or 440 feet) and is presented by field visit.

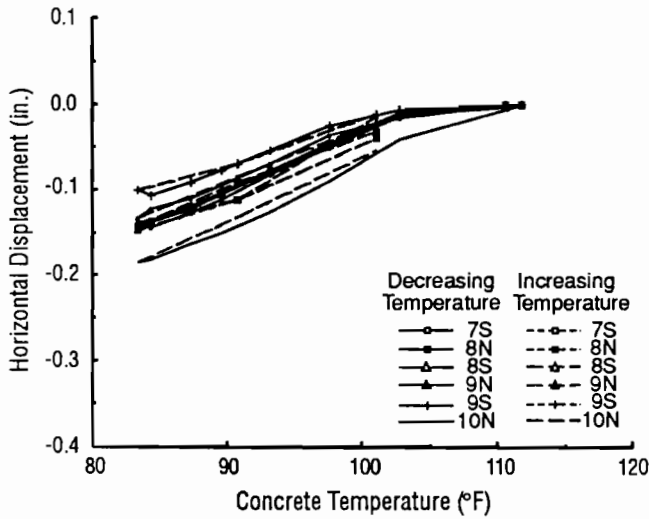


Fig B.1. Horizontal slab displacements of 240-foot slabs versus change in concrete temperature for field visit 2.

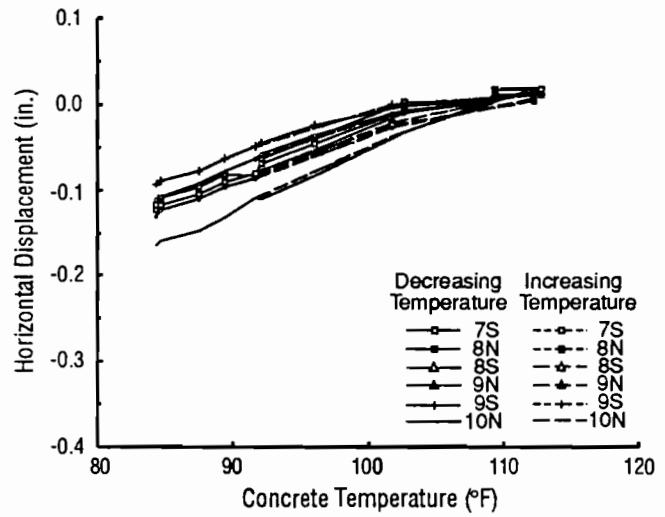


Fig B.3. Horizontal slab displacements of 240-foot slabs versus change in concrete temperature for field visit 3.

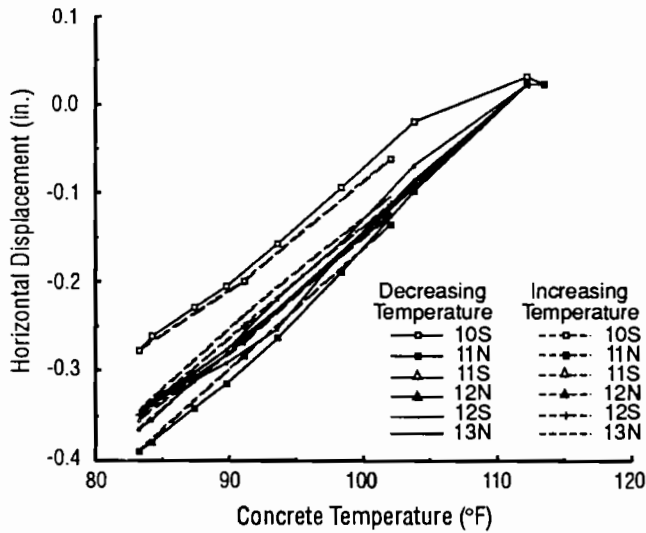


Fig B.2. Horizontal slab displacements of 440-foot slabs versus change in concrete temperature for field visit 2.

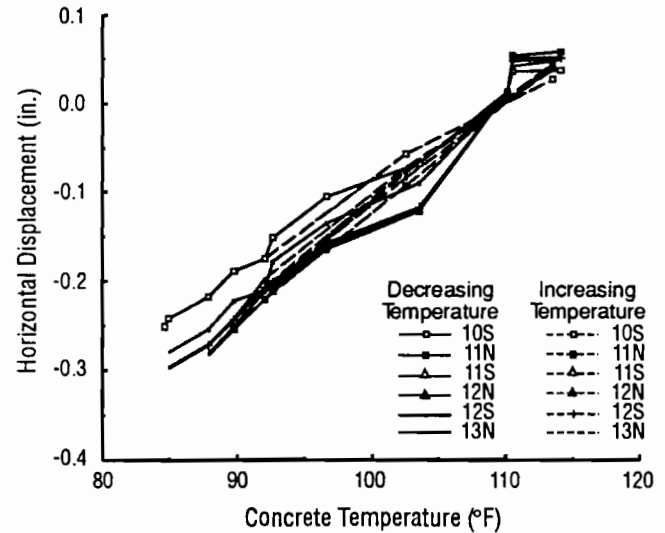


Fig B.4. Horizontal slab displacements of 440-foot slabs versus change in concrete temperature for field visit 3.

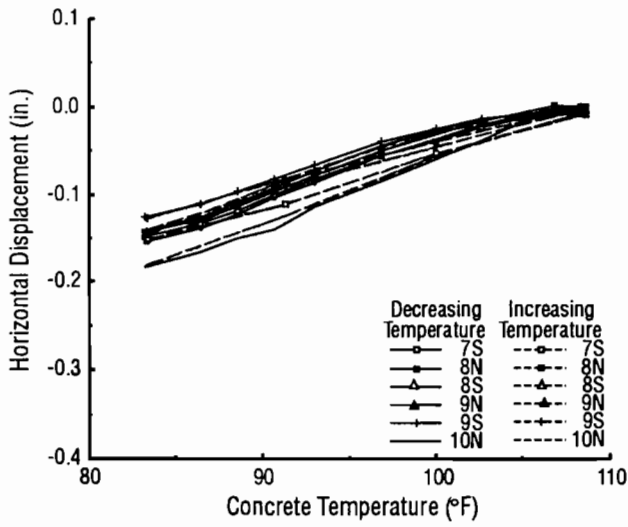


Fig B.5. Horizontal slab displacements of 240-foot slabs versus change in concrete temperature for field visit 4.

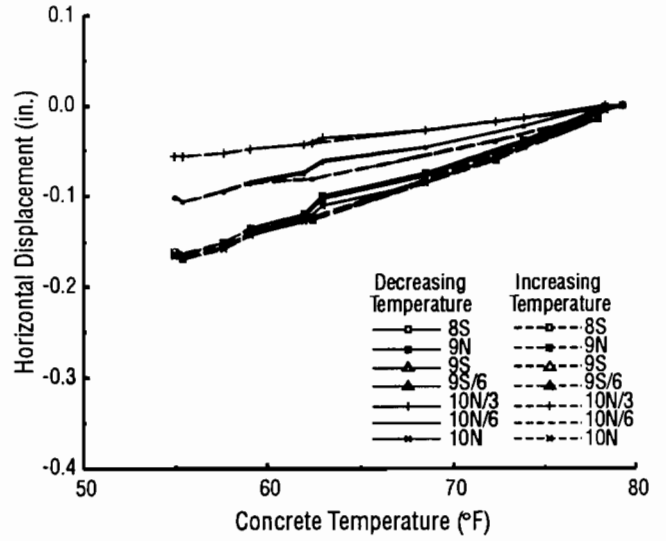


Fig B.7. Horizontal slab displacements of 240-foot slabs versus change in concrete temperature for field visit 5.

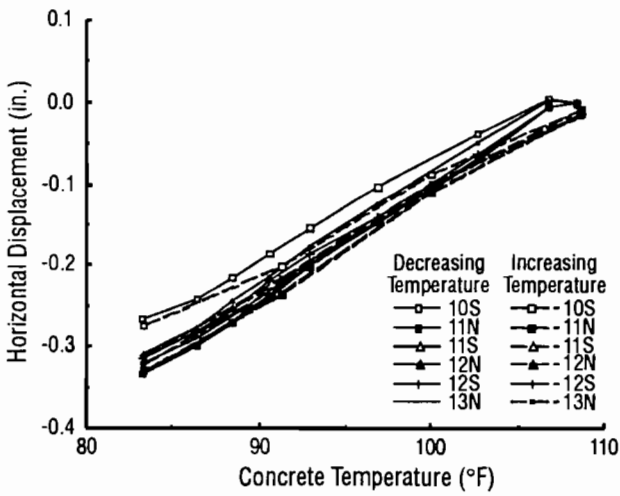


Fig B.6. Horizontal slab displacements of 440-foot slabs versus change in concrete temperature for field visit 4.

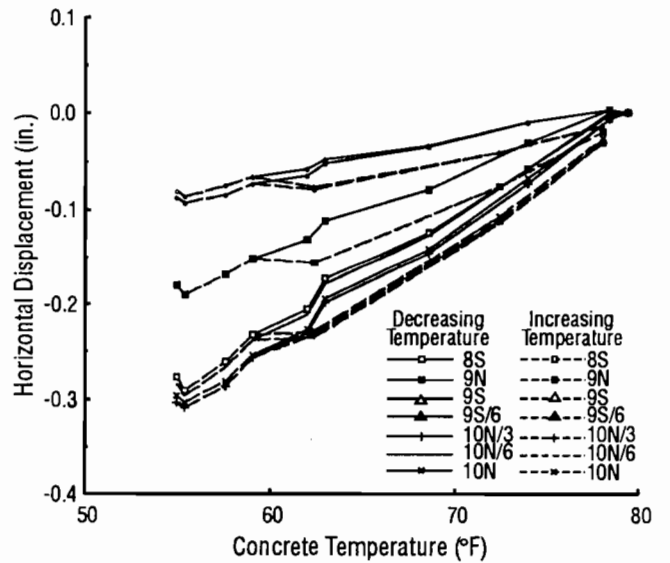


Fig B.8. Horizontal slab displacements of 440-foot slabs versus change in concrete temperature for field visit 5.

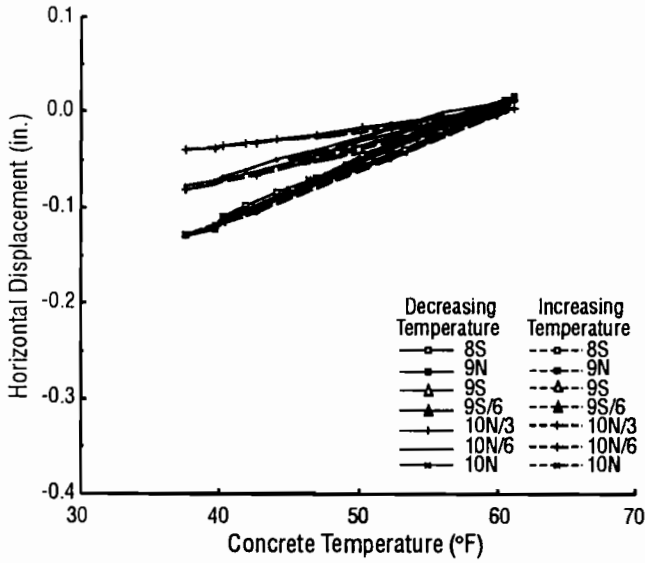


Fig B.9. Horizontal slab displacements of 240-foot slabs versus change in concrete temperature for field visit 6.

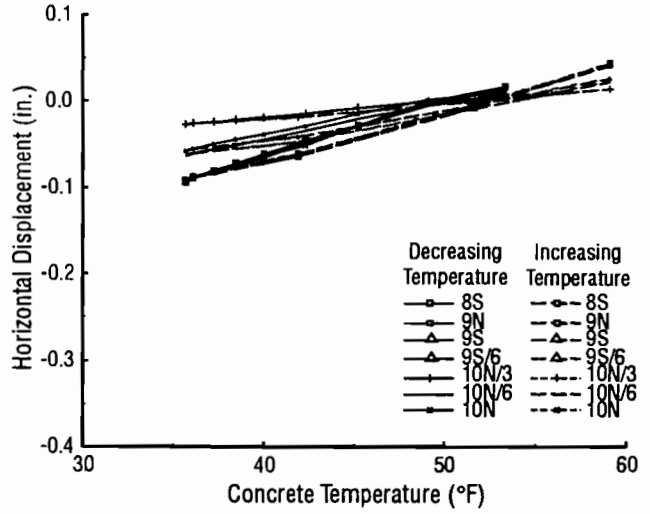


Fig B.11. Horizontal slab displacements of 240-foot slabs versus change in concrete temperature for field visit 7.

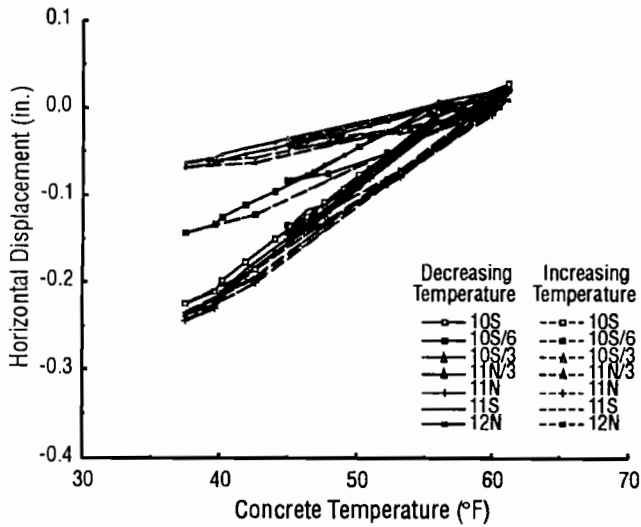


Fig B.10. Horizontal slab displacements of 440-foot slabs versus change in concrete temperature for field visit 6.

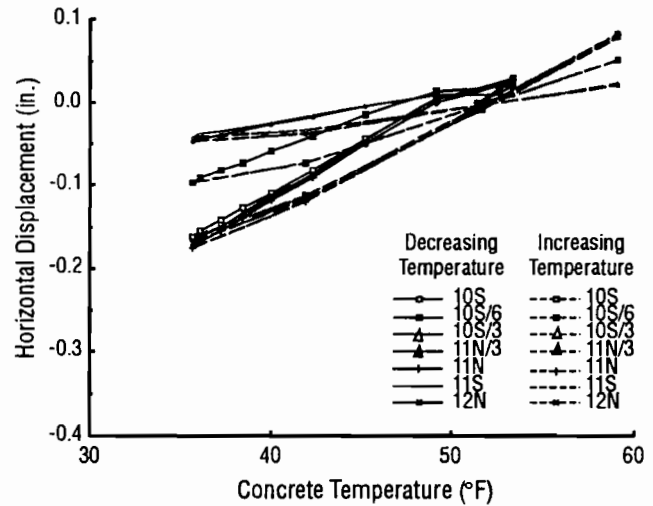


Fig B.12. Horizontal slab displacements of 440-foot slabs versus change in concrete temperature for field visit 7.

APPENDIX C. DERIVATION OF MODEL FORMULATION

The following derivation supplements the information given in Chapter 4. The basic stiffness equation for PCP is derived from basic energy principles, and the algebraic expressions used to implement the finite element method are presented.

A necessary condition for the equilibrium of a deformable continuum is that the external virtual work must equal the internal virtual work. This condition is known as the principle of virtual work and is described by

$$\int_B \delta u T dB = \int_{\Omega} \delta \underline{\varepsilon}^T \underline{\sigma} d\Omega \quad (C.1)$$

where

$$\underline{\varepsilon} = \begin{Bmatrix} \varepsilon_x \\ \varepsilon_y \\ \gamma_{xy} \end{Bmatrix} \text{ (strains)}$$

and

$$\underline{\sigma} = \begin{Bmatrix} \sigma_x \\ \sigma_y \\ \tau_{xy} \end{Bmatrix} \text{ (stresses)}$$

Displacements are denoted by u and surface tractions by T . The surface boundary is B , and the volume of the continuum is Ω .

For PCP, the principle of virtual work can be written as

$$\int_{\Omega} \delta \underline{\varepsilon}^T \underline{\sigma} d\Omega + \int_{B_1} \delta u F dB + \sum_{B_2} \delta u P = 0 \quad (C.2)$$

where F denotes surface tractions due to friction on the boundary B_1 , and P denotes surface tractions due to tendon forces on the boundary B_2 . Boundary B_1 is the pavement-subbase interface, and boundary B_2 is the edge of a PCP slab.

Defining the surface tractions due to friction as $F = k_f(u)u$, where $k_f(u)$ is the stiffness of the subbase frictional restraint as illustrated in Fig 4.5, and $P = k_p u$, where k_p is the axial stiffness of a tendon, $E_s A_s / L$, where L is the length of a tendon, Eq C.1 can be written as

$$\int_{\Omega} \delta \underline{\varepsilon}^T \underline{\sigma} d\Omega + \int_{B_1} \delta u (k_f(u)u) dB + \sum_{B_2} \delta u k_p u = 0 \quad (C.3)$$

For strains that are due to both surface tractions and temperature changes, stresses are

$$\underline{\sigma} = \underline{D} (\underline{\varepsilon} - \underline{\varepsilon}_0)$$

where

$$\underline{\varepsilon}_0 = \begin{Bmatrix} \alpha \Delta T \\ \alpha \Delta T \\ 0 \end{Bmatrix}$$

and

$$\tilde{D} = \begin{bmatrix} \frac{E_c}{1-\nu^2} & \frac{\nu E_c}{1-\nu^2} & 0 \\ \frac{\nu E_c}{1-\nu^2} & \frac{E_c}{1-\nu^2} & 0 \\ 0 & 0 & G \end{bmatrix}$$

The coefficient of thermal expansion and changes in concrete temperature are denoted by α and ΔT , respectively. Strains and displacements for an element are defined as

$$\tilde{\varepsilon} = \tilde{B} \tilde{U}$$

and

$$\tilde{u} = \tilde{N} \tilde{U}$$

where \tilde{N} represents shape functions for an element (tabulated in Ref 14) and \tilde{B} is the strain displacement matrix as defined in Ref 13. Similarly, virtual strains and virtual displacements for an element are defined as

$$\delta \tilde{u} = \delta \tilde{U}^T \tilde{N}^T$$

and

$$\delta \tilde{\varepsilon}^T = \delta \tilde{U}^T \tilde{B}^T$$

Equation C.3 can now be written as

$$\begin{aligned} & \delta \tilde{U}^T \int_{\tilde{\Omega}} \tilde{B}^T \tilde{D} \tilde{B} \tilde{U} d\tilde{\Omega} - \delta \tilde{U}^T \int_{\tilde{\Omega}} \tilde{B}^T \tilde{D} \varepsilon_o d\tilde{\Omega} \\ & + \delta \tilde{U}^T \int_{\tilde{B}_1} \tilde{N}^T k(u) \tilde{N} \tilde{U} d\tilde{B} + \delta \tilde{U}^T \sum_{\tilde{B}_2} k_p \tilde{U} = 0 \end{aligned} \quad (C.4)$$

which reduces to

$$\begin{aligned} & \int_{\tilde{\Omega}} \tilde{B}^T \tilde{D} \tilde{B} \tilde{U} d\tilde{\Omega} - \int_{\tilde{\Omega}} \tilde{B}^T \tilde{D} \varepsilon_o d\tilde{\Omega} \\ & + \int_{\tilde{B}_1} \tilde{N}^T k(u) \tilde{N} \tilde{U} d\tilde{B} + \sum_{\tilde{B}_2} k_p \tilde{U} = 0 \end{aligned} \quad (C.5)$$

where tendon forces are applied in a discrete manner on boundary \tilde{B}_2 . Therefore

$$\left[\int_{\tilde{\Omega}} \tilde{B}^T \tilde{D} \tilde{B} d\tilde{\Omega} \right] \tilde{U} + \left[\int_{\tilde{B}_1} \tilde{N}^T k(u) \tilde{N} d\tilde{B} \right] \tilde{U} \left[\sum_{\tilde{B}_2} k_p \right] \tilde{U} = \int_{\tilde{\Omega}} \tilde{B}^T \tilde{D} \varepsilon_o d\tilde{\Omega} \quad (C.6)$$

Let

$$\begin{aligned}\tilde{K} &= \int_{\tilde{\Omega}} \tilde{B}^T \tilde{D} \tilde{B} d\tilde{\Omega} \text{ (concrete stiffness),} \\ \tilde{K}_f(\tilde{U}) &= \int_{\tilde{B}_1} \tilde{N}^T k(u) \tilde{N} d\tilde{B} \text{ (subbase restraint stiffness),} \\ \tilde{K}_p &= \sum_{\tilde{B}_2} k_p \text{ (tendon stiffness), and} \\ \tilde{P}_T &= \int_{\tilde{\Omega}} \tilde{B}^T \tilde{D} \tilde{\epsilon}_o d\tilde{\Omega}.\end{aligned}$$

Therefore

$$\left[\tilde{K} + \tilde{K}_f(\tilde{U}) + \tilde{K}_p \right] \tilde{U} = \tilde{P}_T \quad (C.7)$$

If initial conditions include tendon forces and subbase friction forces, then Eq C.7 becomes

$$\left[\tilde{K} + \tilde{K}_f(\tilde{U}) + \tilde{K}_p \right] \tilde{U} = \left[\tilde{P}_s + \tilde{P}_p + \tilde{P}_T \right] \quad (C.8)$$

which corresponds to Eq 4.1.

Numerical integration is used to perform the integrals that make up the terms in Eq C.8. The algebra is performed as follows:

$$\tilde{K} = \int_{\tilde{\Omega}} \tilde{B}^T \tilde{D} \tilde{B} d\tilde{\Omega} \equiv t \sum_i \sum_j w_i w_j \tilde{B}^T \tilde{D} \tilde{B} |J| \quad (C.9)$$

$$\tilde{K}_f(\tilde{U}) = \int_{\tilde{B}_1} \tilde{N}^T k(u) \tilde{N} d\tilde{B} \equiv t \sum_i \sum_j w_i w_j \tilde{N}^T k(u) \tilde{N} |J| \quad (C.10)$$

$$\tilde{P} = \int_{\tilde{\Omega}} \tilde{B}^T \tilde{D} \tilde{\epsilon}_o d\tilde{\Omega} \equiv t \sum_i w_i \tilde{B}^T \tilde{D} \tilde{\epsilon}_o |J| \quad (C.11)$$

where

- t = pavement thickness,
- w = Gauss weights for 9 integration points (tabulated in Ref 14),
- J = the Jacobian matrix (as defined in Ref 13).

After displacements are determined for all increments of temperature change (corresponding to 2 hours of temperature change from field data) by solving Eq C.8 for \tilde{U} , stresses are calculated. The stresses for an element are

$$\tilde{\sigma} = \tilde{D} (\tilde{\epsilon} - \tilde{\epsilon}_o)$$

Finally, principal stresses, σ_1 and σ_2 , and principal planes, θ_p , are calculated using Mohr's circle relationships:

$$\sigma_{1,2} = \frac{\sigma_x + \sigma_y}{2} \pm \sqrt{\left(\frac{\sigma_x - \sigma_y}{2}\right)^2 + \tau_{xy}^2}$$

$$\theta_p = \frac{1}{2} \tan^{-1} \left(\frac{2\tau_{xy}}{\sigma_x - \sigma_y} \right)$$